Energy Efficient Large Scale Antenna Systems for 5G Communications and Beyond

A thesis submitted for the degree of Doctor of Philosophy

(PhD)

by

Pierluigi Vito Amadori

Communications and Information Systems Research Group

Department of Electronic and Electrical Engineering

University College London

January 2017

Statement of Originality

I, Pierluigi Vito Amadori confirm that the work presented in this thesis is my own. Where information has been derived from other sources, I confirm that this has been indicated in the thesis.

Signed:

Date:

Abstract

The increasing popularity of mobile devices has fueled an exponential growth in data traffic. This phenomenon has led to the development of systems that achieve higher spectral efficiencies, at the cost of higher power consumptions. Consequently, the investigation on solutions that allow to increase the maximum throughput together with the energy efficiency becomes crucial for modern wireless systems. This thesis aims to improve the trade-off between performances and power consumption with special focus toward multiuser multiple-antenna communications, due to their promising benefits in terms of spectral efficiency.

Research envisaged massive Multi-Input-Multi-Output (MIMO) systems as the main technology to meet these data traffic demands, as very large arrays lead to unprecedented data throughputs and beamforming gains. However, larger arrays lead to increased power consumption and hardware complexity, as each radiating element requires a radio frequency chain, which is accountable for the highest percentage of the total power consumption. Nonetheless, the availability of a large number of antennas unveils the possibility to wisely select a subset of radiating elements. This thesis shows that multiuser interference can be exploited to increase the received power, with significant circuit power savings at the base station.

Similarly, millimeter-wave communications experienced raising interest among the scientific community because of their multi-GHz bandwidth and their ability to place large arrays in limited physical spaces. Millimeter-wave systems inherit same benefits and weaknesses of massive MIMO communications. However, antenna selection is not viable in millimeter-wave communications because they rely on high beamforming gains. Therefore, this thesis proposes a scheme that is able to reduce the number of radio frequency chains required, while achieving close-to-optimal performances.

Analytical and numerical results show that the proposed techniques are able to improve the overall energy efficiency with respect to the state-of-the-art, hence proving to be valid candidates for practical implementations of modern communication systems.

Acknowledgements

When I look back at the years that led to this thesis, there are a few people that I believe need to be properly mentioned and thanked.

First and foremost, I would like to thank my supervisor Dr. Christos Masouros for believing in me and for giving me such a great opportunity. I truly appreciate his never-ending patience during these years, especially at the first stages of my PhD. After reading my first reports and each chapter of this thesis, I feel like I cannot thank him enough for his constructive comments and guidance. Words cannot express how thankful I am for trusting me when I asked to work in remote. I would also like to thank Prof. Izzat Darwazeh for his help and support towards my professional development.

I would like to thank my colleagues at the Communications and Information Systems group in UCL, for their help since my arrival and for creating such a friendly environment to work in. I would like to dedicate a special thanks to Dr. Adrian Garcia-Rodriguez, for always lending an ear and a hand in those moments when both were greatly needed and for our daily discussions on the way home. I would also like to thank Dr. Francesco Renna, Dr. Joao De Castro Mota, Dr. Ka Lung Law, Mr. Jure Sokolic and Mr. Ang Li.

Additionally, I would like to thank my family. Grazie a Mamma, Papà e Marina, per esserci stati in tutti questi anni, per avermi ascoltato quando rimpiangevo ogni mia decisione e per avermi rincuorato quando mi preoccupavo di ogni cosa. Vorrei ringraziarvi per essere come siete, senza mai chiedere nulla in cambio e per volermi bene, anche quando penso di non meritarlo. Non c'é giorno che non vi pensi e che non speri di rendervi tanto orgogliosi di me, quanto io lo sono di ognuno di voi. I ringraziamenti alla famiglia non possono finire senza un pensiero speciale per i miei nonni. Vorrei ringraziare Nonna Savina e Nonno Pierino, per avermi trasmesso il valore e la importanza di studio e impegno, specialmente quando da piccolo avrei preferito passare il tempo facendo altro.

Finalment, desitjo dedicar les últimes paraules d'agraïment per la Laura. Voldria dir-te gràcies per la teva paciència, quan he començat a aprendre català, per la teva ajuda i força, en tots els moments del meu doctorat, per les nostres trucades diàries a la nit, quan estàvem vivint separats, i per haver decidit de venir a Londres per viure amb mi, en aquella trucada del 18 de desembre. Gràcies per tot, per la felicitat que em dones cada dia i per haver canviat la meva vida en el millor que hagués mai pogut desitjar.

Contents

List of Figures

List of Tables

List of Abbreviations

A

AS	Antenna Selection
AWGN	Additive White Gaussian Noise

B

B-MIMO	Beamspace Multiple-Input Multiple-Output
BPSK	Binary Phase Shift Keying
BS	Base Station

C

CAS	Constructive Antenna Selection
CBF	Constructive Beamforming
CCM	Convex Capacity Maximization
CECI	Constant Envelope Constructive Interference
CEM	Cross-Entropy Method
CEO-CIO	Cross-Entropy Optimization - Constructive Interference Optimization
CEO-IR	Cross-Entropy Optimization - Interference Reduction
CEP	Constant Envelope Precoding
CI	Constructive Interference
CIB	Constructive Interference Beamforming
CIM	Constructive Interference Maximization
CM	Capacity Maximization
CM-BS	Capacity Maximization Beam Selection
CR	Correlation Rotation
CSI	Channel State Information
CVX-CIO	Convex - Constructive Interference Optimization

D

DAC	Digital-to-Analog Converter
DCM-BS	Decremental Capacity Maximization Beam Selection
DLA	Discrete Lens Array
DLP	Dynamic Linear Precoding
DPC	Dirty Paper Coding
DSP	Digital Signal Processor

E

ERM	Error-Rate Minimization
ESPAR	Electronically Steerable Parasitic Array

F

FDD	Frequency Division Duplexing
FLOP	Floating-Point Operation
FPGA	Field-Programmable Gate Array

G

GD	Gradient Descent

I

ICM-BS	Incremental Capacity Maximization Beam Selection

L

LOS	Line-Of-Sight
LR	Likelihood Ratio
LS-MIMO	Large-Scale Multiple-Input Multiple-Output
LSA	Large-Scale Array

M

M-MIMO	Massive Multiple-Input Multiple-Output
MEM	Minimum Eigenvalue Maximization
MF	Matched Filter
MIMO	Multiple-Input Multiple-Output
MIP	Mixed-Integer Programming
MIP-CASP	Mixed-Integer Programming Constructive Antenna Selection and Precoding

MISO Multiple-Input Single-Output

MM-BS Maximum Magnitude Beam Selection

mm-wave Millimeter Wave

MP Multi-Path

MU-MIMO Multiuser MIMO

N

NLS Nonlinear Least Squares

O

OFDM Orthogonal Frequency Division Multiplexing

P

PA Power Amplifier

PAPR Peak-to-Average Power Ratio

PGM Path Gain Maximization

PSK Phase Shift Keying

Q

QAM Quadrature Amplitude Modulation

QPSK Quadrature Phase Shift Keying

R

RF Radio Frequency

RZF Regularized Zero Forcing

S

SB SINR Balancing

SDR Semidefinite Relaxation

SER Symbol Error-Rate

SIMO Single-Input Multiple-Output

SINR Signal-to-Interference-plus-Noise Ratio

SISO Single-Input Single-Output

SM Spatial Modulation

SM-BS Signal-to-Interference and Noise Maximization Beam Selection

SM-MIMO Spatial Modulation Multiple-Input Multiple-Output

SO	Successive Optimization
SOCP	Second-Order Cone Programming
SSK	Space Shift Keying
SVD	Singular Value Decomposition

T

TAS	Transmit Antenna Selection
TDD	Time Division Duplexing
THP	Tomlinson-Harashima precoding
TPM	Transmitted Power Minimization

U

UHF	Ultra High Frequency
ULA	Uniform Linear Array
UWB	Ultra Wide Band

V

VLA	Very Large Array
VP	Vector Perturbation

Z

ZF	Zero Forcing

List of Symbols and Operators

$\lvert \cdot \rvert$	Absolute value of a complex number or determinant of a matrix
$(\cdot)^{\mathrm{T}}$	Transpose of a vector or matrix
$(\cdot)^{\mathrm{H}}$	Hermitian transpose of a vector or matrix
$(\cdot)^{-1}$	Inverse of a matrix
$p \bmod L$	Modulo operation for a real number p with base L
$\mathrm{diag}\,(\cdot)$	Diagonal of a matrix
$\mathrm{rank}\,(\cdot)$	Rank of a matrix
$\sim$	Indicates "distributed as"
$\mathcal{CN}\,(\cdot, \cdot)$	Complex normal statistical distribution
$E\,\{\cdot\}$	Statistical expectation
$\lfloor \cdot \rfloor$	Floor function
$\lceil \cdot \rceil$	Ceiling function
$\mathbb{C}$	Set of complex numbers
$\mathbb{R}$	Set of real numbers
$\mathbb{Z}$	Set of integer numbers
$\mathbb{B}$	Set of binary matrices
$\Re\,(\cdot)$	Real component of a complex number
$\Im\,(\cdot)$	Imaginary component of a complex number
$\mathcal{O}\,(\cdot)$	Complexity order
$\otimes$	Kronecker product
$\lVert \cdot \rVert_p$	ℓ_p norm of a vector or matrix
$\lVert \cdot \rVert_{\mathrm{F}}$	Frobenius norm of a vector or matrix
$(\cdot)!$	Factorial of a real number
$\subseteq$	Subset operator
$\subset$	Strict subset operator
$\mathbf{A} \succeq 0$	Positive semidefinite matrix $\mathbf{A}$

$\cup$	Union of sets
$\cap$	Intersection of sets
$\in$	$\mathcal{X} \in \mathcal{Y}$ indicates that $\mathcal{X}$ takes values from the set $\mathcal{Y}$
∞	Infinity
$\det(\cdot)$	Determinant of a matrix
$\mathrm{Tr}(\cdot)$	Trace of a matrix
$\binom{a}{b}$	Binomial coefficient indexed by a and b
$\triangleq$	Equality by definition
$\min(\cdot)$	Minimum entry of a vector
$\arg\min(\cdot)$	Index of the minimum entry in a vector
$\max(\cdot)$	Maximum entry of a vector
$\arg\max(\cdot)$	Index of the maximum entry in a vector
$\lambda_{\max}(\cdot)$	Maximum singular value of a matrix
$\lambda_{\min}(\cdot)$	Minimum singular value of a matrix
$\sigma_{\max}(\cdot)$	Maximum eigenvalue value of a matrix
$\sigma_{\min}(\cdot)$	Minimum eigenvalue value of a matrix
$\mathrm{var}(\cdot)$	Variance of random variables
$\forall$	"For all"

Chapter 1

Introduction

The ever-increasing popularity of mobile devices and the success of social networking have brought data traffic to experience an exponential growth over the last decade [1]. Recent studies predict that the global mobile data traffic is expected to reach a 66% annual growth rate [2] in the next years. Consequently, the growing need of higher data rates has inspired both research and academia to move towards new protocols and technologies that maximize spectral efficiency and throughput. However, research on energy consumption and hardware complexity has been often neglected in the past, affecting both battery lifetime for mobile devices and carbon emissions. In fact, information and communication technology is identified as the cause for $\sim 2\%$ of the global carbon emissions, and this value is expected to increase [3] each year. The effects of data traffic escalation are not just environmental, as the employment of data-based cellular standard is leading to higher energy costs for the base station [4] as well. Because of this, future 5G communication systems are required to be able to provide both high data rate and higher power consumption efficiency [5–7]. The need for a direct evaluation of the relationship between power consumption and achievable rates has brought the researchers to define a new performance metric that combines both, called energy efficiency [5].

Energy efficiency is a quantifiable evaluation of the trade-off between the total power consumption of a communication system and its spectral efficiency. As a consequence of the increasing importance of energy efficiency, research has witnessed the emergence of

a new trend: green communications [8, 9]. Green communications concepts, which can be summarized in the aim to maximize the energy efficiency of future wireless communication systems, have found a prolific applicability to multiple antennas technologies, generally identified as MIMO systems [10]. In fact, while MIMO technology was first introduced to maximize achievable throughputs, new power-saving strategies rapidly showed that multiple-antennas systems were also able to provide energy efficient communications [5]. Among these, large-scale or massive MIMO [11] has risen as one of the most promising technologies for future wireless communications.

Massive MIMO technology can be simply described as a multiple-antenna system, where the number of radiating elements is scaled up to the order of tens or hundreds [11]. In fact, the employment of very large arrays at the base stations is expected to offer unprecedented benefits, such as extremely high throughputs and beamforming gains [12]. Additionally, the higher spatial resolutions offered by large antenna arrays allow to greatly reduce the impact of noise and multiuser interference, while requiring lower transmission power [11]. Even though the theoretical benefits of massive MIMO systems are undoubtedly very appealing, their practical implementation are just as equally challenging for both hardware requirements and signal processing. In fact, a conventional MIMO approach to large-scale systems would require to dedicate one radio frequency (RF) chain for each radiating element, hence leading base stations equipped with very large arrays to require an equally large number of amplifiers, analog-to-digital converters and mixers. The above are detailed in Section 2.4.3.3.

Because of these considerations, research has focused on technologies that can promote both practicability and energy efficiency of massive MIMO systems, such as beamspace MIMO [13, 14], Antenna Selection (AS) [15, 16] and Constant Envelope Precoding (CEP) [17, 18]. All these techniques share the aim for higher energy efficiency, either by reducing the number of RF chains required by the transceiver, as in beamspace MIMO and AS, or by employing highly efficient power amplifiers, as for CEP. Given the importance and relevance of green communications for future wireless communication systems, this thesis focuses on the design of novel energy efficient transmission schemes and approaches.

1.1 Aim and Motivation

While energy efficiency is regarded as one of the main metrics for realistic implementations of future large-scale systems, most of the energy efficient massive MIMO technologies still present a significant number of open questions.

AS was firstly introduced as an effective tool for reducing the intrinsic hardware complexity of MIMO [15, 16, 19, 20]. In fact, even in the early stages of MIMO communications study, the need for a dedicated RF chain to each radiating element was identified as the cause of higher, and often unsustainable, power consumptions either at the transmitter or at the receiver side. However, the techniques that originated from these studies have proven not to be directly scalable to massive systems, as their computational costs are deemed prohibitive [21]. As a consequence of these considerations, the design of selection algorithms specifically tailored for very large arrays is particularly relevant, since it allows to exploit both the higher diversity offered by a large number of antennas and the power savings deriving from utilizing a lower number of RF chains.

Likewise, constant envelope transmissions [17,18] proved that a symbol-level precoding with unit peak-to-average power ratio can facilitate the implementation of massive MIMO systems by allowing the employment of efficient non-linear RF components. However, their design metrics are based on the minimization of multiuser interference, which supports the search for more efficient interference-exploiting approaches that can further increase energy efficiency. Moreover, their performances are heavily reliant on the availability of perfect channel-state information at the transmitter, which is non-realistic.

While AS and precoding are both capable to deliver interesting benefits for energy-efficient large-scale systems, they conventionally operate on a separate manner [15, 16, 19, 20] as they are based on disjointed performance metrics. This justified the search for a novel transmission scheme, where both techniques are jointly performed in order to attain the maximum combined energy efficiency benefits that each of the two approaches can offer.

Finally, the application of beamspace MIMO to millimeter wave communications has shown that near-optimal performances can be achieved even with a strongly reduced number of RF chains at the transmitter, yet early studies mostly focused on the simplistic assumption of exclusively line-of-sight scenarios [14, 22, 23], which are not realistic according to recent measurements campaigns [24]. This motivates the development of more complete techniques that include the effects of multi-path and interference among mobile stations, in order to fully leverage on the diversity effects of a multiuser scenario.

1.2 Main Contributions

This thesis aims to enhance energy efficiency and practicability of large-scale multi antenna systems through the introduction of novel transmission schemes and the improvement of existing approaches from the literature. The following list highlights and summarizes the main contributions of this thesis:

- Definition of an interference exploiting scheme for CEP and solution of the corresponding optimization problem through a cross-entropy solver and a low-complexity convex relaxation (Chapter 3). The performance of the proposed schemes are analyzed through extensive numerical simulations and show that interference exploitation can favorably affect reception and increase the received power.

- Development of a computationally efficient AS algorithm that exploits multiuser interference for increasing the received power in a massive MIMO downlink transmission (Chapter 4). Analytical and numerical results prove that the proposed metric allows to greatly reduce both hardware and computational complexity of massive MIMO, especially when compared to large-scale systems where existing AS schemes from the literature are employed.

- Introduction of a novel transmission scheme where AS and precoding are jointly and simultaneously performed according to interference exploiting metrics (Chap-

ter 5). The optimization problem is solved both optimally, via mixed integer programming solver, and heuristically, via convex optimization tools. Results show a significant increase of the performances when compared to previous interference exploiting-based AS schemes and state-of-the-art AS schemes from the literature.

- Design of several beam selection techniques that aim to maximize the received Signal-to-Interference-plus-Noise Ratio (SINR) and system capacity in beamspace MIMO for millimeter wave communications (Chapter 6). The results show that the proposed schemes are able to outperform existing techniques both in terms of capacity and energy efficiency in more realistic scenarios, where multi-path effects are considered and the number of available RF chains is fixed.

1.3 Thesis Organization

Subsequent to this introductory chapter, this thesis is organized following the structure illustrated in Fig. 1.1 and described in the sequel.

Chapter 2 provides a thorough review of multiple antenna communications systems, in their small-scale and large-scale implementation. The theoretical principles behind MIMO systems are discussed, with special focus on multiuser signal processing. Numerous state-of-the-art low-complexity and energy-efficient schemes for large-scale MIMO are examined, which include millimeter wave communications and AS schemes.

Chapter 3 introduces a precoding design for an energy efficient Constant Envelope Precoding (CEP) scheme for multiuser scenarios. Downlink precoding design is performed in order to exploit the multiuser interference at the receiver side, hence increasing the received power. Two different CEP schemes are presented: a first technique, based on the application of the cross-entropy solver, and a two-step approach, based on an initial relaxation of the power constraints and a subsequent enforcement of per-antenna power constraints.

Chapter 4 presents a low complexity AS scheme based on constructive interference. We show that the proposed AS algorithm, combined with simple matched filter pre-

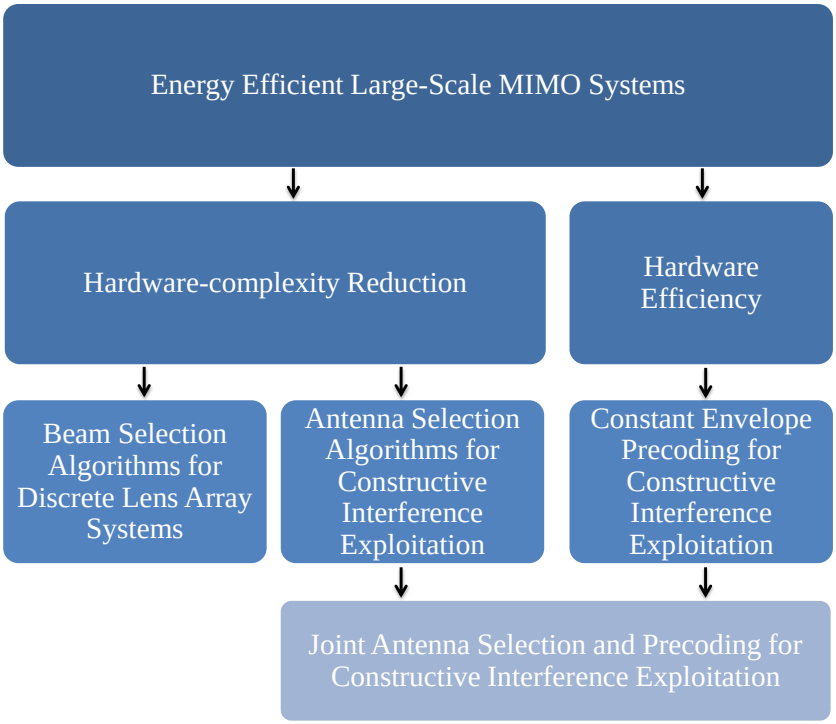

Figure 1.1: Thesis Structure.

coding, outperforms more complex and computationally expensive AS techniques that involve zero forcing linear precoding. The computational burdens of the proposed technique are discussed and its benefits are analyzed by means of an energy efficiency metric that combines throughput performance with the circuit power required.

Chapter 5 discusses several low-complexity transmission schemes for massive MIMO based on jointly performing transmit AS and convex optimization precoding. The presented schemes are analyzed in terms of running time and compared with state-of-the art algorithms. Their performances are evaluated in terms of symbol error rate, capacity and energy efficiency. Finally, the effects of imperfect channel-state information at the transmitter are studied and a methodology for designing robust joint transmit AS and precoding is derived.

Chapter 6 presents a new millimeter-wave (mm-wave) transmission scheme that combines Beamspace Multiple-Input Multiple-Output (B-MIMO) communications and beam selection techniques to achieve near-optimal performances with a low hardware-

complexity transceiver. The benefits of the proposed scheme are evaluated via performance computations, comparisons of numbers of required RF chains and a joint sum-rate and complexity metric that shows the trade-off between spectral and energy efficiency.

Chapter 7 concludes the thesis with a summary of contents and the conclusions derived throughout. Moreover, future research lines within the framework of this thesis are also presented.

1.4 Publications

The aforementioned contributions have been presented in the following list of publications:

Journals.

[J1] P.V. Amadori and C. Masouros, "Interference Exploiting Antenna Selection for Hardware-Efficient Massive MU-MIMO," *submitted to IEEE Transactions on Communications*.

[J2] P.V. Amadori and C. Masouros, "Constant Envelope Precoding by Interference Exploitation in Phase Shift Keying-Modulated Multiuser Transmission," *Accepted for publication in IEEE Transactions on Wireless Communications*.

[J3] P.V. Amadori and C. Masouros, "Interference-Driven Antenna Selection for Massive Multiuser MIMO," *IEEE Transactions on Vehicular Technology* , vol. 65, no. 8, pp. 5944 - 5958, August 2016.

[J4] P.V. Amadori and C. Masouros, "Low RF-Complexity Millimeter-Wave Beamspace-MIMO Systems by Beam Selection," *IEEE Transactions on Communications*, vol. 63, no. 6, pp. 2212 - 2223, June 2015.

Conferences.

[C1] P.V. Amadori and C. Masouros, "A Mixed-Integer Programming Approach to Interference Exploitation for Massive-MIMO," *2017 IEEE International Conference*

on Communications (ICC), Submitted.

[C2] P.V. Amadori and C. Masouros, "Constructive interference based Constant Envelope Precoding," *2016 IEEE 17th International Workshop on Signal Processing Advances in Wireless Communications (SPAWC)*, pp. 1 - 5, 2016.

[C3] P.V. Amadori and C. Masouros, "Power efficient massive MU-MIMO via antenna selection for constructive interference optimization," *2015 IEEE International Conference on Communications (ICC)*, pp. 1607 - 1612, 2015.

[C4] P.V. Amadori and C. Masouros, "Beam selection techniques in mm-wave communications," *IET Colloquium on Antennas, Wireless and Electromagnetics*, pp. 1 - 20, 2015.

[C5] P.V. Amadori and C. Masouros, "Low complexity transceivers in multiuser millimeter-wave beamspace-MIMO systems," *2014 IEEE 25th Annual International Symposium on Personal, Indoor, and Mobile Radio Communication (PIMRC)*, pp. 118 - 122, 2014.

Chapter 2

Energy Efficiency in Multiple Antenna Wireless Communications Systems

This chapter introduces the concepts that inspired the research synthesized in this thesis. These preliminary sections are used to briefly address the key benefits of multiple antenna communications and their main drawbacks. In addition, a detailed presentation of large-scale systems is provided, with special focus on the challenges they present.

2.1 MIMO Communications

Generally, the term MIMO communications is used to identify transceiver systems that involve multiple antennas at the transmitter and the receiver. Because of this, MIMO can be seen as a direct evolution of antenna array communications, with diversity being simultaneously exploited both at transmitter and receiver. The interest for MIMO applications has strengthened over the past years, thanks to the high capacity, increased diversity and interference suppression they are able to provide [25].

Wireless channels of point-to-point MIMO systems, see Fig. 2.1, with n_t antennas at the transmitter and n_r antennas at the receiver, are generally represented by a $\mathbb{C}^{n_r \times n_t}$

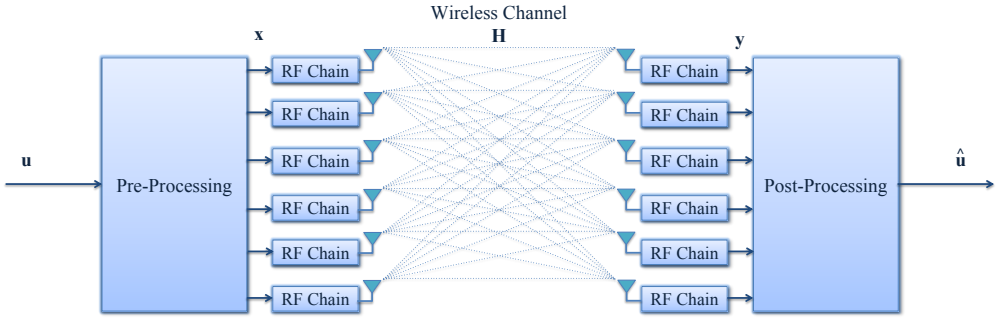

Figure 2.1: Block diagram of a point-to-point 6×6 MIMO.

matrix $\mathbf{H}$, where each element $h_{i,j}$ identifies the transfer function between the j-th transmitter and the i-th antenna of the receiver. This notation leads to a $\mathbb{C}^{n_r \times 1}$ received signal vector $\mathbf{y}$ that can be defined analytically as

$$\mathbf{y} = \mathbf{H}\mathbf{x} + \mathbf{n}, \tag{2.1}$$

where $\mathbf{x}$ is the $\mathbb{C}^{n_t \times 1}$ transmitted signal vector and $\mathbf{n}$ the $\mathbb{C}^{n_r \times 1}$ additive white Gaussian noise (AWGN), i.e., $\mathbf{n} \sim \mathcal{CN}(0, N_0)$ with N_0 being the noise variance.

If transmitter and receiver possess perfect knowledge of the channel, we can derive the capacity of such a system by decomposing the channel into a set of parallel, non-interfering, Single-Input Single-Output (SISO) channels via singular value decomposition (SVD) [26]. Accordingly, we can compute the system capacity as

$$C = \sum_{i=1}^{n_{min}} \log\left(1 + \frac{P_i^* \lambda_i^2}{N_0}\right), \tag{2.2}$$

where $P_i^* = \max\left(0, \mu - \frac{N_0}{\lambda_i^2}\right)$ is the waterfilling power allocation for the i-th *eigenmode* of the channel and μ is the waterfill level, chosen to respect the total power constraint [10].

2.2 MIMO Precoding

The use of multiple antennas at both sides of a communication link leads to increased signal processing burdens, either at the transmitter or the receiver. The techniques used to separate data streams can be differentiated between detection and precoding, whether they are applied at the receiver or at the transmitter side, respectively. In multiuser MIMO (MU-MIMO), precoding techniques are generally preferred for *downlink* communications and detection techniques for *uplink* communications. Thanks to this choice, the burdens of signal processing are always sustained by the Base Station (BS) instead of the mobile users, which are generally characterized by higher power and complexity constraints.

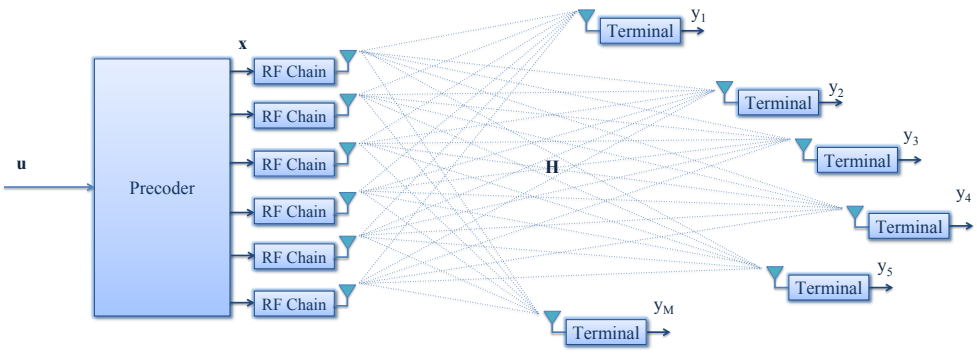

Figure 2.2: Block diagram of a 6×6 MU-MIMO.

In this section, we focus on a brief introduction to MU-MIMO downlink precoding, see Fig. 2.2, where the BS employs an array with N elements and communicates with M single-antenna users or terminals. In this scenario, the $\mathbb{C}^{M \times N}$ channel matrix $\mathbf{H}$ can be seen as a set of multi-input single-output (MISO) channels, where each row $\mathbf{h}_m^T$ of $\mathbf{H}$ represents the $\mathbb{C}^{1 \times N}$ channel vector for the m-th user, as

$$\mathbf{H} = [\mathbf{h}_1, ..., \mathbf{h}_M]^T, \tag{2.3}$$

hence leading to the following definition of the m-th user received symbol

$$y_m = \mathbf{h}_m^T \mathbf{x} + n_m = \sum_{n=1}^{N} h_{n,m} x_n + n_m. \tag{2.4}$$

Precoding techniques that help overcoming the interference between users have attracted the attention of the scientific community over the past years with several linear and non-linear approaches, as shown in Fig. 2.3. The distinction between linear and non-linear precoding is based on the operations the $\mathbb{C}^{M\times 1}$ desired symbols vector $\mathbf{u}$ experiences before transmission. In general, linear precoding approaches from the literature are characterized by low-complexity computational burdens and aim to either cancel [25,27,28] or exploit [29,30] the interference at the transmitter side, while non-linear precoding techniques require more complex signal processing but are able to achieve higher rates [29,31–33]. Finally, we include a brief description of non-linear optimization-based downlink beamforming, based on SINR optimization [34, 35]. While such approaches are characterized by high and near optimal performances, they are affected by higher computational burdens both at the transmitter and at the receiver side, where channel equalization is necessary.

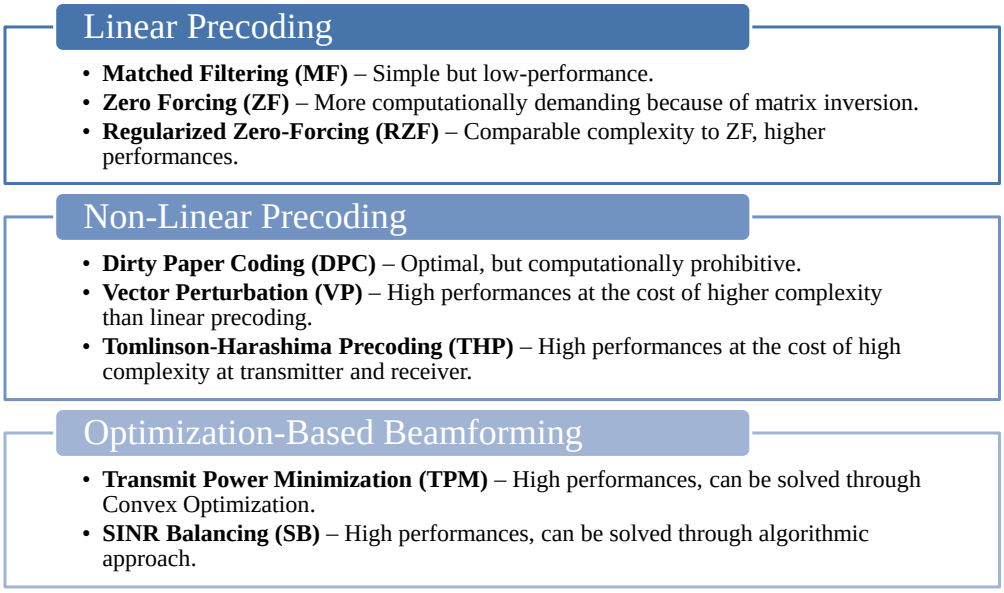

Figure 2.3: Downlink Precoding and Beamforming classification and representative techniques.

2.2.1 Linear Precoding

Linear precoding is a simple transmission approach where the transmitted signal $\mathbf{x}$ is derived as a linear combination of the data symbol $\mathbf{u}$. The operation used to derive

the transmitted signal vector $\mathbf{x}$ can be described analytically as follows

$$\mathbf{x} = \mathbf{G}\mathbf{u} = \gamma\mathbf{F}\mathbf{u}, \tag{2.5}$$

where $\mathbf{G} = \gamma\mathbf{F}$ is the $\mathbb{C}^{N\times M}$ precoding matrix and is defined as the combination of two different elements: the scaling factor $\gamma \in \mathbb{R}$, necessary to ensure that the transmitted signal $\mathbf{x}$ respects power constraints, i.e. $E\left\{||\mathbf{x}||^2\right\} = P$, and the precoding matrix without scaling $\mathbf{F}$. Here, we list the fundamental linear precoding techniques for MIMO communications:

- **Matched filtering** (MF) represents the simplest linear precoding technique from the literature and is designed to maximize the received signal-to-noise ratio (SNR). Given the scaling factor $\gamma_{_{MF}}$, the MF precoding matrix $\mathbf{F}_{MF}$ can be computed as the Hermitian of the channel matrix $\mathbf{H}$ [27]

$$\mathbf{G}_{MF} = \gamma_{_{MF}}\mathbf{H}^H = \frac{\mathbf{H}^H}{\sqrt{tr[(\mathbf{H}^H\mathbf{H})]}}. \tag{2.6}$$

- **Zero Forcing** (ZF) is a simple linear precoding technique that has been extensively studied in the past[28, 29] and is designed in order to equalize the effects of the channel at the receiver side. Given the scaling factor $\gamma_{_{ZF}}$, the ZF precoding matrix $\mathbf{F}_{ZF}$ is defined as the Moore-Penrose pseudoinverse of the channel $\mathbf{H}$ [36]

$$\mathbf{G}_{ZF} = \gamma_{_{ZF}}\mathbf{H}^H(\mathbf{H}\mathbf{H}^H)^{-1} = \frac{\mathbf{H}^H(\mathbf{H}\mathbf{H}^H)^{-1}}{\sqrt{tr[(\mathbf{H}\mathbf{H}^H)^{-1}]}}. \tag{2.7}$$

- **Regularized Zero Forcing** (RZF) identifies a modification of conventional ZF, with the aim to reduce its high susceptibility to ill-conditioned channel matrices [25]. Performance losses are identified by a decreasing SNR at the receiver and are caused by the increased scaling factor $\gamma_{_{ZF}}$ experienced by channel matrices with smaller condition number. The RZF precoding matrix aims to maximize the

SINR at the receiver [30] and is defined as

$$\begin{aligned} \mathbf{G}_{RZF} &= \gamma_{RCI}\mathbf{H}^H(\mathbf{H}\mathbf{H}^H + \alpha\mathbf{I})^{-1} \\ &= \frac{\mathbf{H}^H(\mathbf{H}\mathbf{H}^H+\alpha\mathbf{I})^{-1}}{\sqrt{tr\left[(\mathbf{H}\mathbf{H}^H+\alpha\mathbf{I})^{-1}\mathbf{H}\mathbf{H}^H(\mathbf{H}\mathbf{H}^H+\alpha\mathbf{I})^{-1}\right]}}, \end{aligned} \tag{2.8}$$

where $\alpha = N \cdot N_0$ is the optimal regularization factor for a single-cell scenario [29].

2.2.2 Non-linear Precoding

Non-linear precoding embraces all the signal processing techniques devoted to the generation of the precoded vector $\mathbf{x}$ by means of complex non-linear operations over the desired symbol vector $\mathbf{u}$. While the use of non-linear precoding techniques at the transmitter offers significant sum-rates benefits, it generally comes at the expense of very sophisticated signal processing. Due to their innate high complexity, non-linear precoding techniques are only briefly presented in this thesis, as main focus resides on systems which require low computational burdens.

- **Dirty Paper Coding** (DPC) methods are based on the concepts introduced by the seminal work in [31], which showed that DPC is able to achieve the theoretical channel capacity if the transmitter is aware of the interference. In addition, such remarkable performances can be achieved without the need of additional power in transmission nor of shared channel-state-information (CSI) with the receiver [25]. Despite offering significant benefits, DPC methods suffer from low practicability in realistic scenarios because they require complex signal processing, such as sphere-search algorithms and infinite length codewords.

- **Vector Perturbation** (VP) performs a perturbation of the user data before transmission in order to reduce the scaling factor of ZF precoding. While this allows to greatly enhance the performances of linear precoding, as for RZF, its application is affected by a significant increase in the signal processing burdens, as it requires to solve an integer-lattice least squares problem [29, 32].

- **Tomlinson Harashima Precoding** (THP) is a technique that aims to equalize

the intersymbol interference. In particular, the approach to interference followed by THP can be seen as translation of V-BLAST [33] to the transmitter side, where the channel matrix $\mathbf{H}$ is decomposed into the multiplication of a unitary matrix feedforward matrix $\mathbf{F}$ and a lower triangular matrix $\mathbf{L}$. The aim of the technique is the reduction of the channel matrix at the receiver side to a simple lower triangular matrix $\mathbf{B} = \mathbf{DHF}$ with unitary diagonal elements, where the diagonal scaling matrix $\mathbf{D}$ entries are the inverse of the diagonal elements of the matrix $\mathbf{L}$. The transmitted signal is computed as

$$\mathbf{x} = \mathbf{F}\widetilde{\mathbf{x}}, \tag{2.9}$$

where the i-th element of $\widetilde{\mathbf{x}}$ is obtained through a recursive approach at the receiver over the i-th desired symbol u_i

$$\widetilde{x}_i = \left[u_i - \sum_{j=1}^{i-1} b_{i,j}\widetilde{x}_j \right] mod_L, \tag{2.10}$$

where $b_{i,j}$ is the i-th entry of the j-th column of $\mathbf{B}$ and $[\cdot]mod_L$ is the L-base modulo operation that keeps the symbol $\widetilde{x}_i$ within its original Voronoi region [37], with L being a real number that depends on the modulation used. In opposition to the previous techniques, THP requires further signal processing at the receiver side. In fact, the i-th receiver needs to both normalize the i-th received symbol by the i-th diagonal entry of the matrix $\mathbf{D}$ and to apply an additional modulo operation in order to estimate the received symbol.

2.2.3 Optimization-based Beamforming

In addition to linear and non-linear precoding, we list the state-of-the-art on non-linear beamforming based on the optimization of the received SINR : transmitted power minimization [34] and SINR balancing [35]. When using beamforming, the transmitted signal can be defined as follows

$$\mathbf{x} = \sum_{m=1}^{M} \mathbf{p}_m u_m, \tag{2.11}$$

where $\mathbf{p}_m$ represents the $\mathbb{C}^{N\times 1}$ weight or beamforming vector for the m-th user and u_m identifies the data or constellation symbol for the m-th user. Given the definition of the beamforming vectors, it is possible to evaluate the received SINR for the m-th user as

$$\gamma_m = \frac{\left|\mathbf{h}_m^T \mathbf{p}_m\right|^2}{\sum\limits_{j\neq m} \left|\mathbf{h}_m^T \mathbf{p}_j\right|^2 + N_0} = \frac{\left|\sum\limits_{n=1}^{N} h_{n,m} p_{n,m}\right|^2}{\sum\limits_{j\neq m} \left|\sum\limits_{n=1}^{N} h_{n,m} p_{n,j}\right|^2 + N_0}, \tag{2.12}$$

where $p_{n,m}$ represents the n-th element of the m-th user beamforming vector $\mathbf{p}_m$.

- **Transmitted power minimization** (TPM) [34] represents a conventional approach to downlink beamforming, where interference is regarded as a harmful element for transmission. Because of this, the beamforming optimization problem is designed to minimize the transmitted power while respecting predefined SINR requirements $\Gamma_m, \forall m \in \{1, ..., M\}$. Analytically

$$\begin{aligned} \mathcal{P}_{TPM}: \quad & \underset{\mathbf{p}_m}{\text{minimize}} \quad \sum_{m=1}^{M} \|\mathbf{p}_m\|^2 \\ & \text{subject to} \quad \gamma_m = \frac{\left|\sum\limits_{n=1}^{N} h_{n,m} p_{n,m}\right|^2}{\sum\limits_{j\neq m} \left|\sum\limits_{n=1}^{N} h_{n,m} p_{n,j}\right|^2 + N_0} \geq \Gamma_m, \end{aligned} \tag{2.13}$$

  which can be efficiently solved by means of convex optimization with a semidefinite relaxation (SDR) approach [34].

- **SINR balancing** (SB), also known as *Max-min* beamforming, aims to identify the beamforming vectors that maximize the minimum received SINR, while respecting a predefined transmitted power constraint P_t. The optimization problem is analytically defined as

$$\begin{aligned} \mathcal{P}_{SB}: \quad & \underset{\mathbf{p}_m}{\text{maximize}} \quad \Gamma_m \\ & \text{subject to} \quad \gamma_m \geq \Gamma_m \\ & \qquad\qquad \sum_{m=1}^{M} \|\mathbf{p}_m\|^2 \leq P_t. \end{aligned} \tag{2.14}$$

  Differently from $\mathcal{P}_{TPM}$, the SINR balancing problem is non-convex and its solution

requires a more complex algorithmic approach [35].

2.3 AS Techniques

In the previous section, we described how MIMO communications provide benefits in terms of capacity and reliability for radio communication. However, the use of multiple antennas at transmitter and receiver comes with the burden of increased costs in terms of size, power and hardware, caused by the need of higher numbers of radio frequency (RF) chains [15], which comprise digital-analog converter, mixer and filter. In this scenario, AS is a possible solution for exploiting the diversity gains offered by MIMO systems, while achieving complexity reductions. Thanks to AS, multiple antenna benefits are partially preserved with low additional costs, mostly determined by the need of RF switches.

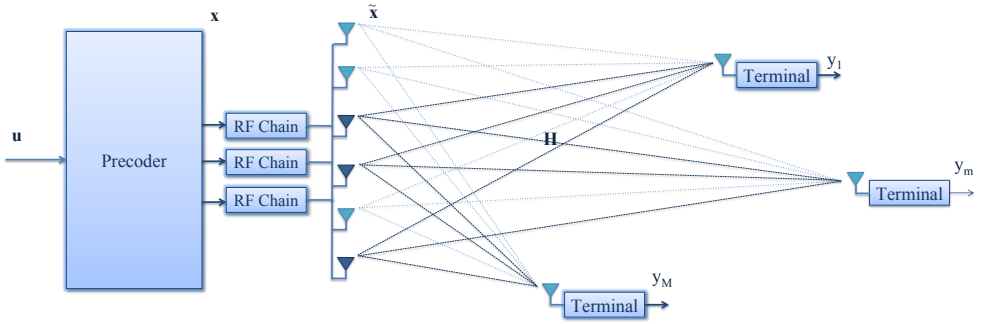

Figure 2.4: Transmitter AS for MU-MIMO

The concept behind AS, at the transmitter or at the receiver, is very simple: the system chooses, according to a specific performance metric, the best (M_{RF}, N_{RF}) antennas out of the (M, N) available antennas at the receiver or transmitter, respectively. Thanks to this selection, receiver/transmitter experiences a significant reduction in complexity, since the number of needed RF chains lowers down to (M_{RF}, N_{RF}).

Over the past years, AS has been intensively studied for both the transmitter, Fig. 2.4 for a MU-MIMO scenario, and the receiver side, showing different benefits. While subset AS at the receiver side offers interesting complexity reduction, transmit selection additionally proved to increase the capacity in comparison with an open loop MIMO

system [16].

The equation of a system that involves Transmit AS (TAS) follows the definition of a classical MU-MIMO system, as in (2.1). In particular, we have

$$\mathbf{y} = \mathbf{H}\tilde{\mathbf{x}} + \mathbf{n}, \tag{2.15}$$

where $\tilde{\mathbf{x}}$ identifies the precoded vector after TAS has been performed, whose elements are null when their index corresponds to one of the deactivated antennas, i.e., $\tilde{x}_n = 0$, $\forall n \notin \mathcal{N}$ with $\mathcal{N}$ being the subset of transmitting antennas with cardinality equal to the number of available RF chains $card\,(\mathcal{N}) = N_{RF}$.

In this section, we focus on the key TAS techniques in MU-MIMO, which have been applied according to different criteria, such as the system capacity [38], the channel matrix eigenvalues [39], the antenna path gain [40] and the error rate [41]. These techniques can be separated according to two different approaches or metrics: diversity or norm-based selection and multiplexing or capacity-based selection, as in Fig. 2.5.

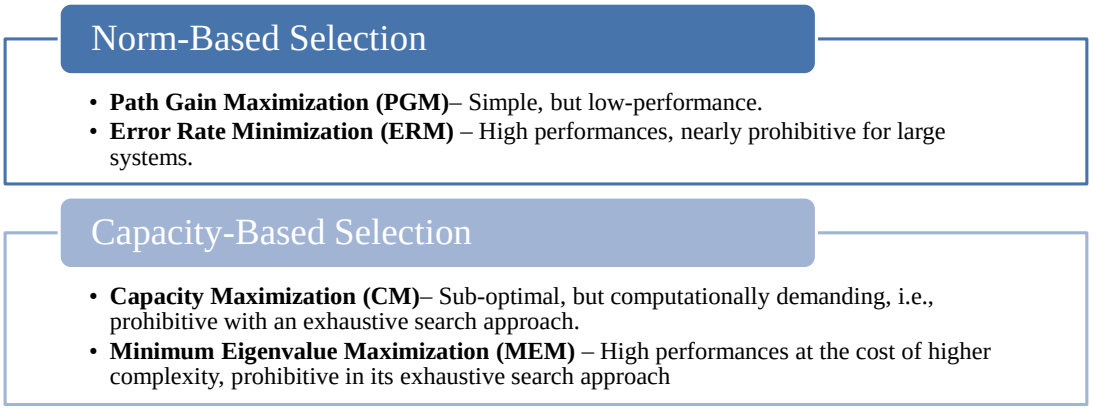

Figure 2.5: Conventional TAS classification

2.3.1 Norm-based Selection

We identify as norm-based selection, the TAS techniques that aim to capture the diversity and improve the SNR at the receiver. More specifically, we indicate as diversity the presence of multiple signal paths that fade independently.

- **Path Gain Maximization** (PGM). Path gain selection at the transmitter can be easily performed by selecting the subset of antennas with the highest path gains. The antenna subset can be analytically identified as follows

$$\mathcal{N} = \arg \max_{N_{RF}} \left\{ \|\underline{\mathbf{h}}_1\|^2, ..., \|\underline{\mathbf{h}}_n\|^2, ..., \|\underline{\mathbf{h}}_N\|^2 \right\}, \tag{2.16}$$

  where the notation $\underline{\mathbf{h}}_n$ is used to identify the channel response corresponding to the n-th antenna of the BS, i.e., the n-th column of the matrix $\mathbf{H}$, and $\max_{N_{RF}}$ identifies the N_{RF} highest values of the argument.

  While path gain selection represents a very appealing technique for its reduced complexity, performances are normally very poor when compared to more sophisticated approaches from the literature. However, early works on TAS in MISO or Single-Input Multi-Output (SIMO) systems [40,42,43] showed that PGM performs optimally when the receiver applies maximum-ratio combining.

- **Error Rate Minimization** (ERM). In [41] the authors present a TAS technique that aims to minimize the error rate at the receiver, under the assumption of a maximum likelihood detection-based receiver. While this approach is able to achieve impressive performances in terms of symbol error rate (SER), it rapidly becomes computationally prohibitive for large constellations, due to the exhaustive search over all the possible transmitted symbols and over all the possible combinations of transmitting antennas.

2.3.2 Capacity-based Selection

In addition to norm-based selection, TAS has been studied also as a technique to maximize the capacity achievable by lower dimensional systems. In fact, TAS over capacity proved to be even able to increase the capacity for systems with low-rank channels [44]. Capacity maximization techniques are based on the formulation of ergodic capacity for a system with DPC and equal power transmission between the antennas [15]

$$C = log_2 \left[\det \left(\mathbf{I}_M + SNR \cdot \mathbf{H}\mathbf{H}^H \right) \right], \tag{2.17}$$

where $\mathbf{I}_M$ is a M-dimensional identity matrix. Accordingly, we can formulate the corresponding optimization problem as follows:

$$\begin{aligned} \mathcal{P}_{CM}: \quad & \underset{\boldsymbol{\Delta}}{\text{maximize}} \quad log_2\left[\det\left(\mathbf{I}_M + SNR \cdot \mathbf{H}\boldsymbol{\Delta}\mathbf{H}^H\right)\right] \\ & \text{subject to} \quad \Delta_{n,n} \in \{0,1\}, \\ & \qquad\qquad \textstyle\sum_{n=1}^{N} \Delta_{n,n} = N_{RF}, \end{aligned} \tag{2.18}$$

where $\boldsymbol{\Delta}$ is a $N \times N$ is a binary-valued and diagonal selection matrix, whose entries can be either null, i.e., $\Delta_{n,n} = 0$ if n is a non-selected antenna, or unit, i.e., $\Delta_{n,n} = 1$ if n is an antenna selected for transmission.

First approaches in capacity maximization were based on the identification of the best antenna subset by means of an exhaustive search. While performance of such approach proved to be optimal, its application is affected by nearly prohibitive computational costs as the number of antennas at the transmitter increases. As a consequence, researchers focused on sub-optimal approaches that allowed to perform a selection over the capacity, while maintaining acceptable computational burdens.

- **Sub-optimal Capacity Maximization** (CM). This approach aims to optimize the capacity of a system with TAS by identifying the transmitting antenna subset in a recursive manner. The key concept behind this approach is that the deactivation of each transmitting antennas in a MU-MIMO system in a Rayleigh fading scenario can be related to a quantitative loss in the maximum achievable capacity. The loss δ_n caused by the n-th antenna deactivation is analytically described [38] as

$$\delta_n = \underline{\mathbf{h}}_n^H \left(\mathbf{I}_M + SNR \cdot \mathbf{H}\mathbf{H}^H\right)^{-1} \underline{\mathbf{h}}_n. \tag{2.19}$$

  The parameter δ_n is computed for each of the available antennas, allowing to identify the index d of the antenna that contributes the least to the maximum achievable capacity. The algorithm is recursively applied in order to identify the $N - N_{RF}$ antennas to deactivate, which are collected in the subset $\mathcal{D} = \left\{d_1, ..., d_l, ..., d_{N-N_{RF}}\right\}$, where d_l is the index of the antenna deactivated at the l-th step of the algorithm.

- **Minimum Eigenvalue Maximization** (MEM). Given the key role played by channel singular values in MIMO capacity performances, their optimization represented one of the main aims of TAS. In [39], the authors present a selection technique based on an exhaustive search of the antenna subset that leads to the highest minimum eigenvalue of the low dimensional channel matrix. While such approach proved to be optimal, it rapidly becomes computationally prohibitive as the sizes of the system increase.

2.3.3 Energy Efficiency

The trade-off between system performance and RF complexity introduced by TAS techniques can be analyzed via a parameter called energy efficiency, which is computed according to different metrics, such as capacity and throughput. More specifically:

- *Energy efficiency over capacity* [45] can be analytically defined as follows

$$\eta_C = \frac{C}{P_{BS}} = \frac{C}{P_t + N_{_{RF}} \cdot P_{RF}}, \tag{2.20}$$

  where $C[bits/s/Hz]$ represents the capacity, $P_{BS}[W]$ is the power consumed at the BS, according to the modelling from the literature [46], $P_t[W]$ identifies the transmitted power of the system and $P_{RF}[W]$ represents the power consumed by each RF chain, characterized by digital-analog converter, mixer and filter.

- *Energy efficiency over throughput* [45] is defined as follows

$$\eta_T = \frac{T}{P_{BS}} = \frac{T}{P_{amp} + N_{_{RF}} \cdot P_{RF} + N_{ops} \cdot P_{fpga}}, \tag{2.21}$$

  where $T = (1 - BLER) \cdot l \cdot M$ is the throughput, $BLER$ is the block error rate, l identifies the bits per symbol, i.e., $l = 1$ for 2-PSK and $l = 2$ for 4-PSK, M is the number of users, P_{amp} $[W]$ is the power required by the amplifier, P_{RF} $[W]$ is the power consumed by a single RF chain, $N_{ops}[KFLOPs]$ identifies the complexity burden of the analyzed technique in terms of 10^3 floating point operations, and P_{fpga} $[W/KFLOPs]$ is the power consumption per operation of

the field-programmable gate array (FPGA). When the information regarding the floating point operation count is not available, it is possible to evaluate η_T with a simpler model of P_{BS}, where FPGA power consumption is not accounted for, as follows

$$\eta_T = \frac{T}{P_{amp} + N_{RF} \cdot P_{RF}}. \tag{2.22}$$

While the shown metrics have been presented in order to highlight the performance-complexity trade-offs which characterize AS systems, they can be effectively employed to evaluate more generalized MIMO scenarios. For example, γ_C and γ_T could be evaluated for two separate systems as a function of the number of radiating elements N_{RF} required in order to achieve a fixed performance threshold, i.e., a minimum value of achievable capacity C or throughput T, respectively.

2.4 Large Scale MIMO

In recent years, the growing interest for MU-MIMO systems has brought to the development of the concept of large-scale MIMO (LS-MIMO) or Massive MIMO (M-MIMO). The pioneering work of [11] proposed the introduction of schemes that tackle the non-scalability of classical MU-MIMO by employing a large excess of antennas at the BS for a limited number of users, see Fig. 2.6. These schemes, namely identified as LS-MIMO or M-MIMO, rapidly experienced an increasing interest by the scientific community because of the exciting benefits they promise to provide and the new challenges they uncover [12].

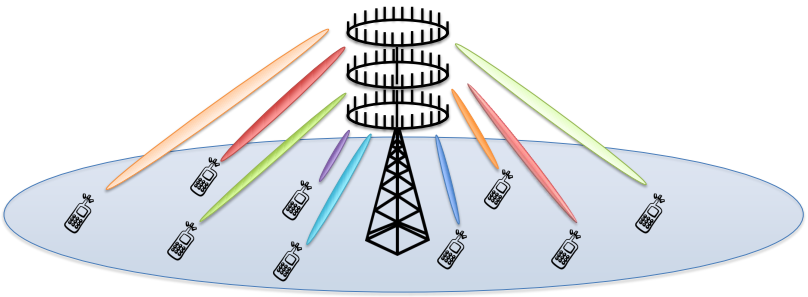

Figure 2.6: Multiuser Massive MIMO representation

In fact, the channel matrix $\mathbf{H}$ experiences significant changes in its statistical properties when the number of transmitting elements grows asymptotically to infinity, e.g., the singular values of the channel matrix approach a deterministic function [47]. While the benefits introduced by M-MIMO are not limited to the multiuser scenario, the characteristics of point-to-point M-MIMO are not addressed in this thesis for the sake of brevity. For the interested reader, the characteristics of M-MIMO for point-to-point communications are fully described in [48].

The following sections briefly describe the key elements that characterize M-MIMO, with a particular focus on the benefits and the challenges brought by this technique. More specifically, we consider a time-division duplexing (TDD) system, as it is common in M-MIMO, because of the simplifications it brings with regards to the CSI acquisition. In fact TDD systems are characterized by channel reciprocity, where both downlink/uplink transmission links exactly match, leading to the possibility to achieve CSI through the uplink. This is a particularly useful property for M-MIMO, since the time required to transmit pilots in the uplink does not depend on the number of antennas at the transmitter, while the time required for downlink pilots depends on the number of antennas at the BS [48].

2.4.1 Multiuser M-MIMO Channel Model

In a single cell scenario, when the BS is equipped with N antennas and serves M single-antenna users, the path gain between the n-th antenna and the m-th user can be defined as

$$h_{n,m} = t_{n,m}\sqrt{\beta_m}, \tag{2.23}$$

where $t_{n,m}$ represents the complex fast-small scale fading and β_m represents the real slow-large scale fading coefficients experienced by the m-th user.

Accordingly, the uplink channel matrix of a multiuser M-MIMO system can be represented as the combination of two matrices: a $\mathbb{C}^{N\times M}$ matrix $\mathbf{T}$ whose entries are different for each user and each antenna and a $\mathbb{R}^{M\times M}$ diagonal matrix $\mathbf{D}_\beta$ whose entries depend

only on the user. Analytically we have

$$\mathbf{H}_u = \mathbf{T}\mathbf{D}_\beta^{1/2}, \tag{2.24}$$

where $\mathbf{H}_u$ represents the channel matrix for the uplink scenario. Accordingly, the $\mathbb{C}^{N\times 1}$ received signal vector at the BS $\mathbf{y}_u$ for an uplink scenario can be defined as

$$\mathbf{y}_u = \sqrt{\rho_u}\mathbf{H}_u\mathbf{x}_u + \mathbf{n}_u, \tag{2.25}$$

where $\mathbf{x}_u$ is the $\mathbb{C}^{M\times 1}$ signal vector from the users to the BS, $\mathbf{n}_u$ is the $\mathbb{C}^{N\times 1}$ additive white Gaussian noise and ρ_u is the uplink transmit power. Thanks to the assumption of TDD operations, the channel model described for the uplink can be easily translated to the downlink scenario. In particular, the received signal vector $\mathbf{y}_d$ in a downlink transmission can be described analytically as

$$\mathbf{y}_d = \sqrt{\rho_d}\mathbf{H}_d\mathbf{x}_d + \mathbf{n}_d = \sqrt{\rho_d}\mathbf{H}_u^H\mathbf{x}_d + \mathbf{n}_d, \tag{2.26}$$

where $\mathbf{H}_d = \mathbf{H}_u^H$ is the reciprocal channel matrix for downlink transmission, $\mathbf{x}_d$ is the $\mathbb{C}^{N\times 1}$ signal vector transmitted by the BS, $\mathbf{n}_d$ is the $\mathbb{C}^{M\times 1}$ additive white Gaussian noise and ρ_d is the downlink transmit power.

2.4.2 Capacity and Signal Processing Benefits

The use of Large-Scale Arrays (LSA) at the transmitter leads to significant benefits in terms of achievable capacity and signal processing for both uplink and downlink. In fact, when the number of antennas at the BS N tends to infinity, the channel responses for different users become orthogonal, if the elements $t_{n,m}$ of $\mathbf{T}$ are independent [11]. This directly affects the correlation matrix as follows

$$\mathbf{R}_u = \mathbf{H}_u^H\mathbf{H}_u = \mathbf{D}_\beta^{1/2}\mathbf{T}^H\mathbf{T}\mathbf{D}_\beta^{1/2} \approx N\mathbf{D}_\beta^{1/2}\mathbf{I}_M\mathbf{D}_\beta^{1/2} = N\mathbf{D}_\beta, \tag{2.27}$$

hence simplifying the computation of the capacity for the uplink to

$$C_u = \log_2 \det\left(\mathbf{I}_M + \rho_u \mathbf{H}_u^H \mathbf{H}_u\right) \approx \log_2 \det\left(\mathbf{I}_M + N\rho_u \mathbf{D}_\beta\right) = \sum_{m=1}^{M} \log_2\left(1 + N\rho_u \beta_m\right). \tag{2.28}$$

Accordingly, the uplink transmission under M-MIMO experiences both a dramatic increase in the achievable rate and additional simplifications in the signal processing, as the MF detector becomes asymptotically optimal and is sufficient to obtain the rates shown in (2.28). Given the complex data symbols vector in uplink $\mathbf{u}_u$, the estimated received symbol vector of a BS with MF detection is

$$\hat{\mathbf{s}} = \mathbf{H}_u^H \mathbf{y}_u = \mathbf{H}_u^H \left(\sqrt{\rho_u}\mathbf{H}_u \mathbf{u}_u + \mathbf{n}_u\right) \approx N\sqrt{\rho_u}\mathbf{D}_\beta \mathbf{u}_u + \mathbf{H}_u^H \mathbf{n}_u. \tag{2.29}$$

Clearly, MF detection in M-MIMO greatly benefits from the asymptotic orthogonality of the channel vectors, as it becomes asymptotically optimal. In fact, multiuser interference is nullified and signals from different users over different streams are efficiently and perfectly separated, each transmission can be considered as a SISO channel with $SNR = N\rho_2\beta_m$ and, finally, noise whiteness is preserved.

In a downlink transmission, the sum capacity of a M-MIMO system with power allocations is defined as

$$C_d = \max_{\mathbf{P}} \log_2 \det\left(\mathbf{I}_N + \rho_d \mathbf{H}_d^H \mathbf{P} \mathbf{H}_d\right) \approx \max_{\mathbf{P}} \log_2 \det\left(\mathbf{I}_N + \rho_d N \mathbf{P} \mathbf{D}_\beta\right), \tag{2.30}$$

where $\mathbf{P}$ is a diagonal matrix whose real entries $(p_1, ..., p_M)$ represent the power allocations for each user, bound to the power constraint $\sum_{m=1}^{M} p_m = P_t$. As shown for the uplink transmission, a simple MF precoder can be proven to be asymptotically optimal. In fact, given the complex data symbols vector in downlink $\mathbf{u}_d$, the received signal vector at the user side is defined as

$$\mathbf{y}_d = \sqrt{\rho_d}\mathbf{H}_d \mathbf{H}_d^H \mathbf{P}^{1/2} \mathbf{u}_d + \mathbf{n}_d \approx \rho_d N \mathbf{D}_\beta \mathbf{P}^{1/2} \mathbf{u}_d + \mathbf{n}_d, \tag{2.31}$$

which, following a similar analysis to the one for (2.29), proves the optimality of the MF

precoder in a downlink transmission with $N \to \infty$ when power allocation is optimized.

2.4.3 Challenges

While M-MIMO is able to achieve terrific benefits, the employment of LSAs unveils a series of challenges, which are addressed in this subsection. In particular, main focus will reside on the channel estimation challenges, briefly introduced at the beginning of the section, followed by a description of the phenomenon called *pilot contamination* and, finally, a concise presentation of the practical limitations of M-MIMO.

2.4.3.1 Channel State Information Acquisition

In the previous section, TDD operations were regarded almost as a requirement for realistic implementations of M-MIMO, because of the benefits channel reciprocity introduces in terms of CSI acquisition complexity. In fact, under frequency-division duplexing (FDD), i.e., where downlink and uplink transmissions operate at different frequencies, channel reciprocity does not apply and downlink/uplink are characterized by two separate channel matrices. Because of this, channel training in FDD requires two separate steps: one for the uplink channel and one for the downlink channel. Under these conditions, downlink training might require the whole coherence time for channel estimation, leaving no time for data symbol transmission. The challenges and feasibility of FDD in M-MIMO are presented and discussed in [11], which shows the significant constraints frequency-division introduces over the number of antennas at the BS N. However, recent works [49] are trying to justify the use of FDD in M-MIMO, depicting its feasibility when specific conditions apply, such as the knowledge of the channel covariance matrix.

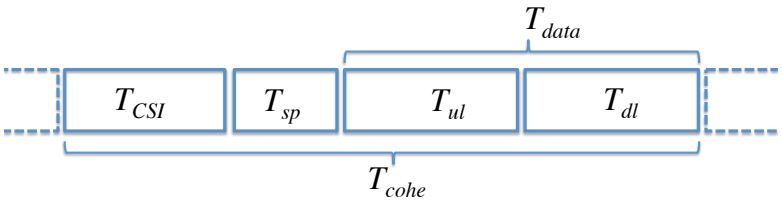

Figure 2.7: TDD protocol

While the application of M-MIMO technology to FDD transmission represents a very interesting approach, the CSI acquisition complexity can be readily tackled via TDD operations [50]. With this regard, [51] introduced a simple TDD protocol where the coherence time T_{cohe} is divided between the time for CSI acquisition T_{CSI}, the time for data transmission T_{data} and the time for BS processing T_{sp}. As shown in Fig. 2.7, the time for data is further divided between the time for downlink transmission T_{dl} and uplink transmission T_{ul}.

2.4.3.2 Pilot Contamination

As shown, TDD transmissions in a single-cell scenario allow to exploit channel reciprocity to estimate the channel response in uplink and use the information during downlink transmission. However, more realistic multi-cell M-MIMO scenarios, i.e., where terminals are distributed among different cells as in Fig. 2.8, are known to be affected by a phenomenon called pilot contamination.

In an ideal multi-cell scenario, the m-th terminal can transmit a pilot sequence of length τ to the l-th cell BS, i.e., $\boldsymbol{\psi}_{m,l} = \left\{\psi_{m,l}^{1}, ..., \psi_{m,l}^{\tau}\right\}$, without interfering with other cells and BSs. Here, non-interference between terminals is achieved by transmitting pilot sequences that are orthogonal within the same cell and between neighboring cells, as

$$\boldsymbol{\psi}_{m,l}^{H}\boldsymbol{\psi}_{n,p} = \delta\left[m-n\right]\delta\left[l-p\right], \tag{2.32}$$

where $\delta\left[\cdot\right]$ represents the Dirac delta, i.e., $\delta\left[x\right]$ is unitary if $x = 0$ and null if $x \neq 0$.

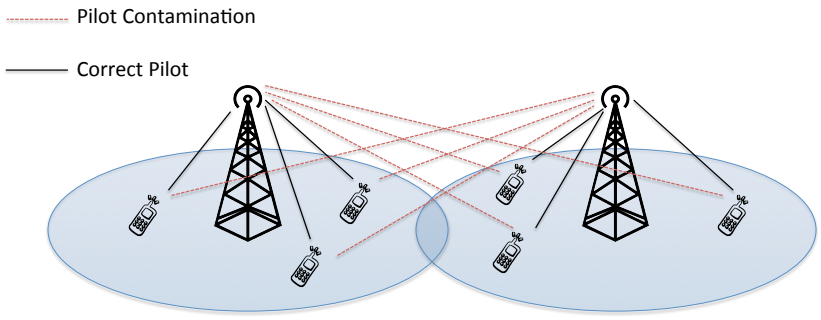

Figure 2.8: Visual representation of Pilot Contamination

However, the orthogonality for all the sequences of all terminals on different cells requires to strongly limit the number of users that can be served by a multi-cell multiuser M-MIMO system [11]. Accordingly, terminals are expected to use non-orthogonal pilot sequences, i.e., $\boldsymbol{\psi}_{m,l}^H \boldsymbol{\psi}_{n,p} \neq 0$, which causes BSs to possess a CSI that is affected by imperfections, often referred to as pilot contamination.

Recent works are trying to mitigate the pilot contamination phenomenon through different approaches, such as protocol-based techniques [11, 52–54], precoding methods [55–57] and blind transmissions [58].

2.4.3.3 Practical Limitations

Because of its key elements, M-MIMO inherits and amplifies most of the practical limitations that affect MU-MIMO systems. In particular, the use of hundreds of antennas at the transmitter comes with the necessity to use hundreds of RF chains, which corresponds to hundreds of power amplifiers, digital-to-analog converters and filters. It was already pointed out in previous sections how these components affect the hardware, power and complexity costs of a classic MU-MIMO system. The need for cheaper and low power hardware becomes a key for M-MIMO, since the dimensions of the system increase drastically [12]. As a consequence, recent works approached the implementation of M-MIMO with more efficient hardware, at the cost of increased distortions [59, 60], or increased signal processing [17, 18].

In addition to this, while the transmission through a large number of antennas allows to reduce the radiated power, the deployment of such a large number of elements will have to face new challenges. In fact, even though arrays in M-MIMO can have many different configurations and geometries, such as cylindrical or uniform-linear arrays (ULAs), they are expected to be characterized by small active units [12] in order to respect more stringent cost and space constraints. Toward this end, recent works [36, 61] have investigated the possibility of exploiting transmit mutual coupling at the BS, allowing the dimensions of antenna arrays in fixed physical spaces to further increase.

Finally, the computational costs and complexity of precoding increase together with

the number of antennas at the BS. As a consequence, the use of low complexity precoding becomes critical in M-MIMO, since the precoding at the BS reduces the time dedicated to data transmission, as shown in Fig. 2.7. This, together with the increasing circuit power consumption experienced by baseband signal processing, leads to the need for highly parallel and efficient signal processing hardware [12].

2.5 Millimeter Wave MIMO

Most of the mobile communications use the Ultra High Frequency (UHF) spectrum, i.e., in the range between 300 $MHz - 3$ GHz, see Table 2.1. Since the number of mobile devices is experiencing an unprecedented growth, wireless service providers need to face the forthcoming bandwidth shortage [62]. Accordingly, recent studies [62] envisage millimeter-wave (mm-wave) spectrum, i.e. $30 - 300$ GHz, as a promising approach, because of the high bandwidth it provides and because of its license free nature.

Nevertheless, the use of higher frequencies in wireless communications comes with the burden of less favorable propagation characteristics [63], which represent one of the main challenges of mm-wave systems. Given the peculiar propagation characteristics of mm-wave communications, the following sections introduce both channel models and transceiver architectures used in the literature to study the performances of systems that exploit the $30 - 300$ GHz bandwidth.

Band	**Uplink**	**Downlink**
700 MHz	746-763 MHz	776-793 MHz
AWS	1710-1755 MHz	2110-2155 MHz
IMT Extension	2500-2570 MHz	2620-2690 MHz
GSM 900	880-915 MHz	925-960 MHz
UMTS Core	1920-1980 MHz	2110-2170 MHz
GSM 1800	1710-1785 MHz	1805-1880 MHz
PCS 1900	1850-1910 MHz	1930-1990 MHz
Cellular 850	824-859 MHz	869-894 MHz

Table 2.1: Spectrum usage - Spectrum usage in modern mobile communications. [64]

2.5.1 Propagation Characteristics

One of the main critiques moved toward the use of mm-wave resides in the high values of free space loss experienced during propagation. In fact, according to Friis equation, we have

$$\frac{P_r}{P_t} = G_t G_r \left(\frac{f}{4\pi R c}\right)^2, \tag{2.33}$$

where P_t and P_r are transmitted and received power, respectively, G_t and G_r are the antenna gains at transmitter and receiver, f is the signal frequency, c is the speed of light in the medium and R is the distance between transmitter and receiver, described visually in Fig. 2.9. The free space loss in (2.33) is represented by the $\left(\frac{f}{4\pi R c}\right)^2$ term, describing how attenuation experiences a quadratic growth with the frequency. Accordingly, from (2.33) it is clear that if we compare two separate systems, operating at two different frequencies with same transmitter/receiver gain, the system with a higher frequency will achieve worse performances.

Nonetheless, this is not a fair comparison, as the use of shorter wavelengths λ in mm-wave systems, leads to a tremendous increase in the number of antenna elements within the same aperture. Consider a simple ULA of length L, the number of elements N that can be deployed with critical spacing $\lambda/2$ can be easily evaluated as

$$N = \frac{2 \cdot L}{\lambda}, \tag{2.34}$$

hence leading to higher antenna gains as the frequency grows. Consequently, high frequencies/short wavelengths do not necessarily experience a significant disadvantage in terms of free space attenuation in comparison with longer wavelengths [65].

The study of mm-wave communications propagation characteristics has experienced a significant increase in interest over the past years, supported by numerous measurement campaigns [66] that aim to a better understanding of the channel for high frequency systems. More specifically, recent works by [24, 67] proved the feasibility of mm-wave system in outdoor urban environments.

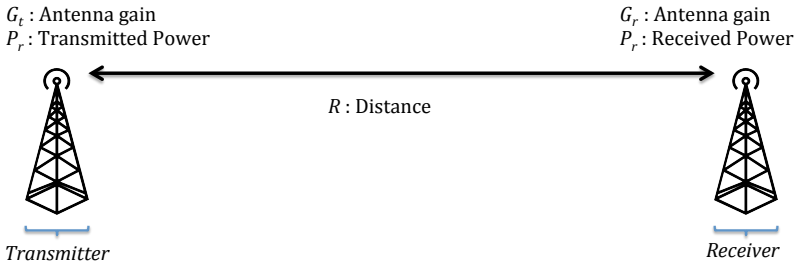

Figure 2.9: Visual representation of Friis equation

2.5.2 Channel Model

When describing the channel model for a multiuser mm-wave system (BS equipped with an N dimensional ULA), we generally refer to multiple steering-response vectors of the array for each user. This represents the most prominent model for mm-wave systems, as it allows to directly discriminate between multi-path and line-of-sight propagation, both of which greatly characterize systems that operate at these frequencies [24]. Analytically, for ULAs we have [10, 13]

$$\mathbf{a}(\theta) = \left[e^{-j2\pi\theta i}\right]_{i\in\mathcal{I}(N)}, \tag{2.35}$$

where $\mathbf{a}(\theta)$ is the $\mathbb{C}^{N\times 1}$ steering vector, $\theta = \frac{d}{\lambda}\sin(\phi)$ is the spatial frequency, whose value ranges between $-0.5 \leq \theta \leq 0.5$ for a critically spaced array, ϕ represents the physical directions $-\pi/2 \leq \phi \leq \pi/2$ and $\mathcal{I}(N) = \{i - (N-1)/2 : i = 0, 1, ...N-1\}$ is a symmetric set of indices centered around 0.

Hence the channel model for the m-th terminal can then be defined as

$$\mathbf{h}_m^{(MP)} = \sum_{i=1}^{N_p} \beta_i^{(m)} \mathbf{a}(\theta_i^{(m)}), \tag{2.36}$$

where N_p is the total number of paths, $\beta_i^{(m)}$ and $\theta_i^{(m)}$ are respectively the gain and the direction of the i-th path of the m-th user. In particular, $\theta_i^{(m)}$ can be evaluated in terms of spatial frequencies.

This model however does not take into account the line-of-sight (LOS) component

of the propagation, which strongly characterizes the channel in mm-wave frequencies communications. In fact, small wavelengths λ allow to pack hundreds of antennas at the BS, which lead to narrow and high gain beams with reduced angular spreads. Thanks to this, in a mm-wave frequencies scenario we can consider the presence of LOS paths for all the users.

The channel model for the LOS path can then be defined as

$$\mathbf{h}_m^{(LoS)} = \beta_0^{(m)} \mathbf{a}(\theta_0^{(m)}), \tag{2.37}$$

where $\theta_0^{(m)}$ represents the direction or position of the m-th user and $\beta_0^{(m)}$ is the complex gain for the LOS path.

We can define the channel for the single user as a sum of the two terms. Analytically

$$\mathbf{h}_m = \mathbf{h}_m^{(LoS)} + \mathbf{h}_m^{(MP)} = \beta_0^{(m)} \mathbf{a}(\theta_0^{(m)}) + \sum_{i=1}^{N_p} \beta_i^{(m)} \mathbf{a}(\theta_i^{(m)}), \tag{2.38}$$

where $\mathbf{h}_m^{(MP)}$ represents the multi-path (MP) component of the channel vector and the ratio between β_0^2 and $\sum_{i=1}^{N_p} \beta_i^2$ is called Rice factor.

2.5.3 Beamspace mm-wave MIMO

Thanks to the wider bandwidths they are able to provide [68], mm-wave communications have experienced a continuous increase in relevance for short-range, high-capacity wireless link. However, a large-scale MIMO approach in mm-wave frequencies is still prohibitive because of the number of antennas and the high transceiver complexity. In order to tackle transceiver complexity, the combination of beamspace MIMO (B-MIMO) [13], where data is multiplexed onto orthogonal beams, together with hybrid transceivers [69], where analog beamformers in the RF domain are combined with a smaller number of digital beamformers in baseband, has been identified as a promising candidate for future mm-wave MIMO applications [70]. In fact, systems based on such combination allow to achieve near-optimal performance with low-hardware complexity, which operates on the dimension of the communication subspace.

The study on practical implementation of the combination of hybrid transceivers and B-MIMO has mainly focused on two aspects: precoding optimization [71–76], where analog processing is performed through phase shifters, and antenna design [14,23,77–79], where analog processing is performed through lenses. More specifically:

- The use of *hybrid analog/digital precoding* for mm-wave B-MIMO transmissions is motivated by the fact that it allows to preserve beamforming gain and diversity order achieved by the large number of antennas, while the number of RF chains is lower-limited by the number of data streams to be transmitted. Several approaches have been introduced in both the single-user [71,72] and multiuser scenario [73–75], mostly focusing on the analog/digital precoding design and the impact of imperfect CSI. However, these approaches generally disregard the practical implications of signal processing in the RF domain, which have been thoroughly addressed in [76].

- With regards to antenna design, *discrete lens arrays* (DLA)-based hybrid transceiver architectures have found increasing interest in the research community [14,77]. Differently from classical MIMO, DLA-based systems are characterized by a direct correspondence between the number of transmitting beams and RF chains, since the array behaves as a convex lens, directing the signals towards different points of the focal surface [22]. Accordingly, DLAs preserve narrow beam-widths in reduced RF-chain operations, allowing to reduce both the power required per stream and the interference between the streams. In fact, DLA-based B-MIMO systems, where analog spatial beamforming is performed through DLAs, proved to be able to achieve near-optimal performance when combined with beam selection concepts [23,78]. More specifically, [23] considers a line-of-sight only scenario, while the selection algorithm presented in [78] leverages on the diversity effects in a multiuser scenario in order to increase system energy efficiency. Additionally, recent studies [79] have proven that DLA-based systems can benefit from energy efficient CSI estimation in point-to-point mm-wave MIMO.

2.6 Constructive Interference

In addition to the conventional signal processing approaches from the literature that focus on interference minimization, this section introduces a different line of research that aims at exploiting multiuser interference as a means for increasing the received SINR. In fact, early works on linear precoding [30, 32, 80] showed that interference minimization does not necessarily lead to the best performances in a communication system. Since interference is data dependent, the transmitter can predict the multiuser interference at the receiver and use this knowledge to influence it and benefit from it.

While the seminal works in [81, 82] focused on reducing the negative effects of interference while preserving its positive components, [83] finally showed that the transmitted signal can be precoded in order to rotate the destructive component of interference into constructive or beneficial interference. Therefore, future research is focusing onto identifying new optimization metrics that exploit CSI and data knowledge at the transmitter side to maximize the SINR of each user by capitalizing on the power contained within multiuser interference. More recently, works on Phase-Shift Keying (PSK) modulated signals [84–88] have introduced different metrics that prove how known interference can be effectively used as a source of green signal power for downlink transmissions. In fact, the symbol error probability in a L-PSK modulation is a function of the received SINR ξ, as expressed in the following equation [83]:

$$P_{\epsilon} = \left(\frac{L-1}{L}\right)\left\{1 - \left(\frac{l \cdot L}{L\pi - \pi}\right)\sqrt{\frac{\sin^2\left(\frac{\pi}{L}\right)\cdot\xi}{1+\xi\sin^2\left(\frac{\pi}{L}\right)}}\right\}, \tag{2.39}$$

where

$$l = \frac{\pi}{2} + \tan^{-1}\left\{\cot\left(\frac{\pi}{L}\right)\sqrt{\frac{\sin^2\left(\frac{\pi}{L}\right)\cdot\xi}{1+\xi\sin^2\left(\frac{\pi}{L}\right)}}\right\}. \tag{2.40}$$

While in this thesis the main focus resides in the application of constructive interference to downlink precoding and transmission, the same concepts can be applied to different scenarios. In this regard, [89] has investigated the applicability of symbol-level precoding based on relaxed receive constellations to increase the security of MU-MIMO communication systems by means of Directional Modulation [90].

2.6.1 Constructive Interference Regions for PSK modulated transmissions

When considering PSK-modulated signals, interference can be classified as constructive or destructive according to simple geometrical concepts [81–85]. In fact, interference can be considered beneficial for system performances when it leads the received symbol further away from the decision thresholds of the desired constellation symbol. A visual representation of constructive and destructive interference regions is presented in Fig. 2.10. Here, the received symbol benefits from interference when it falls in the constructive region (i.e., the blue shaded area) and is instead affected by its negative effects when it lies in the destructive region (i.e., the red shaded area). As we can see, when received symbols fall in the destructive region they reside closer to the decision thresholds, represented by the bold lines, when compared to the desired symbol. On the other hand, all the points lying in the constructive region are characterized by a larger distance from the decision thresholds. The analytical conditions that split interference between

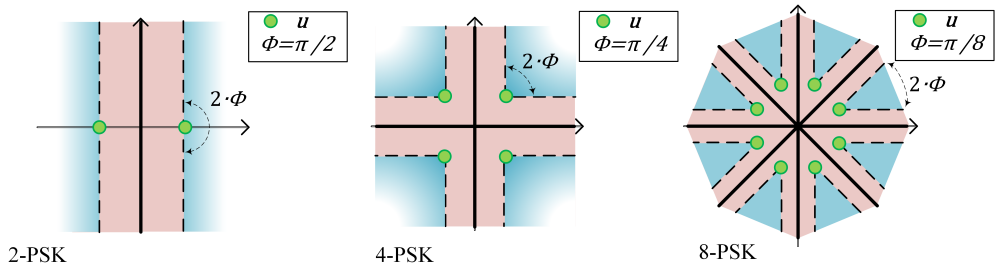

Figure 2.10: Constructive regions for different constellations

constructive and destructive can be defined according to two separate approaches: low-complexity metrics, which are specifically tailored for a modulation order, and convex optimization-based metrics, which are generalized for any-order PSK modulations. Both approaches, including their applications, are presented in the following.

2.6.1.1 Low-Complexity metrics and their applications

Low-complexity metrics propose to identify constructive and destructive interference according to the cross-correlation matrix $\mathbf{R} = \mathbf{H}\mathbf{H}^H$. Under such assumption, the

received signal for the m-th user is equivalent to the one of a MF precoded multiuser systems

$$r_m = \rho_{m,m}u_m + \sum_{m \neq k} \rho_{m,k}u_k = \rho_{m,m}u_m + ICI_m, \tag{2.41}$$

where $\rho_{m,k}$ is the m-th element of the k-th column of the cross-correlation matrix $\mathbf{R}$ and ICI_m is the inter-channel interference experienced by the m-th user. Given the set of constructive and destructive interferers for the m-th user $\mathcal{C}$ and $\mathcal{D}$, the set membership conditions for 2-PSK, 4-PSK and 8-PSK modulations are defined as follows.

- *2*-PSK or Binary Phase-Shift Keying (BPSK) conditions:

$$\mathcal{C} : \{k | sign(u_m) = sign\left(\Re\left[\rho_{m,k}u_k\right]\right)\}, \tag{2.42}$$

$$\mathcal{D} : \{k | sign(u_m) \neq sign\left(\Re\left[\rho_{m,k}u_k\right]\right)\}, \tag{2.43}$$

  where $sign(\cdot)$ and $\Re[\cdot]$ identify the sign and the real part of the argument respectively.

- *4*-PSK or Quadrature Phase-Shift Keying (QPSK) conditions:

$$\mathcal{C} : \{k | sign(\Re[u_m]) = sign\left(\Re\left[\rho_{m,k}u_k\right]\right) \cap sign(\Im[u_m]) = sign\left(\Im\left[\rho_{m,k}u_k\right]\right)\}, \tag{2.44}$$

$$\mathcal{D} : \{k | sign(\Re[u_m]) \neq sign\left(\Re\left[\rho_{m,k}u_k\right]\right) \cup sign(\Im[u_m]) \neq sign\left(\Im\left[\rho_{m,k}u_k\right]\right)\}, \tag{2.45}$$

  which represent a bi-dimensional version of (2.42) and (2.43), as 4-PSK constellation symbols require both real and imaginary part.

- *8*-PSK conditions:

$$\mathcal{C} : \left\{k | (\sqrt{2}-1)\Re\left[\frac{\rho_{m,k}u_k}{u_m}\right] \leq \Im\left[\frac{\rho_{m,k}u_k}{u_m}\right] \cap \Im\left[\frac{\rho_{m,k}u_k}{u_m}\right] \leq \left[\frac{1}{(\sqrt{2}-1)}\right]\Re\left[\frac{\rho_{m,k}u_k}{u_m}\right]\right\}, \tag{2.46}$$

$$\mathcal{D} : \left\{k | (\sqrt{2}-1)\Re\left[\frac{\rho_{m,k}u_k}{u_m}\right] \geq \Im\left[\frac{\rho_{m,k}u_k}{u_m}\right] \cup \Im\left[\frac{\rho_{m,k}u_k}{u_m}\right] \geq \left[\frac{1}{(\sqrt{2}-1)}\right]\Re\left[\frac{\rho_{m,k}u_k}{u_m}\right]\right\}. \tag{2.47}$$

While these metrics were initially used to remove destructive interference components, as in dynamic linear precoding [91], successive studies proved that they could be efficiently applied to exploit the energy of destructive components, as in correlation rotation linear precoding [83]. More specifically:

- **Dynamic Linear Precoding** (DLP) is a linear technique based on the assumption that destructive ICI can be predicted at the transmitter side and its effects nullified at the receiver side. Given the conditions over interference listed above, the m-th element of the k-th column of the constructive only correlation matrix $\mathbf{R}_c$ is analytically defined as

$$\dot{\rho}_{m,k} = \begin{cases} \rho_{m,k}, & \forall\ k \in \mathcal{C} \\ 0, & \forall\ k \in \mathcal{D}. \end{cases} \tag{2.48}$$

  Once the modified correlation matrix $\mathbf{R}_c$ has been derived, the precoding matrix $\mathbf{G}_{DLP}$is defined as follows

$$\mathbf{G}_{DLP} = \gamma_{DLP}\mathbf{H}^H \left(\mathbf{H}\mathbf{H}^H\right)^{-1} \mathbf{R}_c = \frac{\mathbf{H}\left(\mathbf{H}\mathbf{H}^H\right)^{-1}\mathbf{R}_c}{\sqrt{tr\left[\mathbf{R}_c \left(\mathbf{H}\mathbf{H}^H\right)^{-1}\mathbf{R}_c^H\right]}}. \tag{2.49}$$

- **Correlation Rotation** (CR) is a linear precoding technique based on the assumption that ICI can be predicted at the transmitter side [83] and exploited to enhance the received SINR. More specifically, the relative phase-shift between the desired symbol u_m and the interference symbol u_k can be defined as

$$\phi_{m,k} = e^{j\left(\mathfrak{U}\{u_m\} - \mathfrak{U}\{\rho_{m,k}u_k\}\right)} = u_m \frac{\rho_{m,k}\left(u_k\right)^*}{|\rho_{m,k}|}, \tag{2.50}$$

  where operator $\mathfrak{U}\{\cdot\}$ identifies the phase extraction of the argument and $\phi_{m,k}$ is the m-th element of the k-th column of the matrix $\mathbf{\Phi}$.

  In CR precoding, the information over the interference relative phase-shift is used to rotate the ICI in order to have constructive interference. The phase rotation is

obtained via the precoding matrix $\mathbf{G}_{CR}$

$$\mathbf{G}_{CR} = \gamma_{CR}\mathbf{H}^H \left(\mathbf{H}\mathbf{H}^H\right)^{-1} \mathbf{R}_\phi = \frac{\mathbf{H}^H \left(\mathbf{H}\mathbf{H}^H\right)^{-1} \mathbf{R}_\phi}{\sqrt{tr\left[\mathbf{R}_\phi \left(\mathbf{H}\mathbf{H}^H\right)^{-1} \mathbf{R}_\phi^H\right]}}, \tag{2.51}$$

where the phase-correcting correlation matrix $\mathbf{R}_\phi = \mathbf{R} \circ \mathbf{\Phi}$ is defined as the Hadamard product between the correlation matrix and the relative phase-shift matrix [83].

2.6.1.2 Convex metrics and their applications

Convex constructive interference exploitation metrics are derived for a generalized downlink transmission where the transmitter sends a precoded vector $\mathbf{x}$ and conditions are imposed directly over the received signal in a noiseless scenario $\mathbf{r} = \mathbf{H}\mathbf{x}$ instead of the cross-correlation matrix. Additionally, convex metrics for constructive interference exploitation offer a particularly important property, which is modulation order independence. In fact, these metrics operate a phase-shift on the received signal r_m according to the phase of the symbol of interest for the m-th user $\phi_m = \mathfrak{U}\{u_m\}$. The phase-shift is a fundamental operation, as it allows to isolate the received amplitude and phase-shift over the desired symbol u_m caused by the interference t_m.

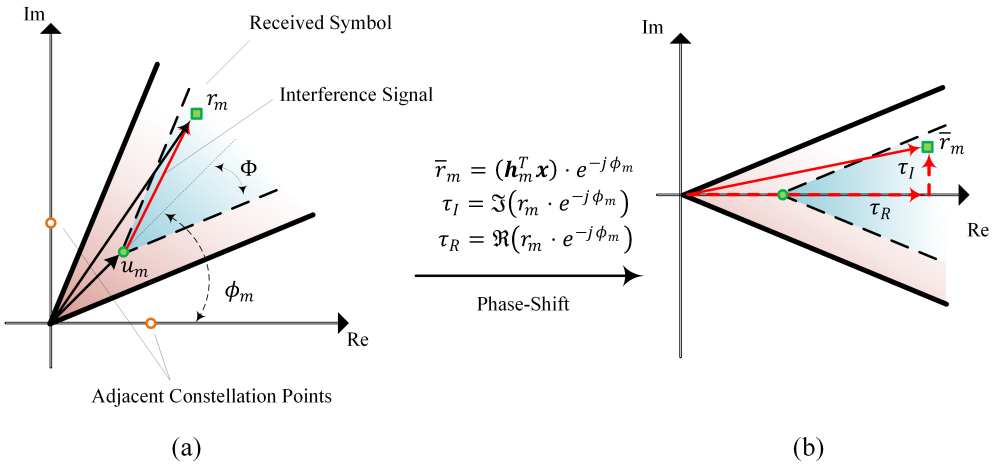

Figure 2.11: Visual representation of phase-shift in Convex metrics for 8-PSK

In [84], constructive interference conditions are analytically expressed for the m-th

received signal for the case where the received signal fully aligns with the desired symbol u_m:

$$\Re\left(r_m \cdot e^{-j\phi_m}\right) = \Re\left(r_m \cdot e^{-j\mathfrak{U}\{u_m\}}\right) = \Re\left(\sum_{n=1}^{N} h_{m,n} x_n e^{-j\mathfrak{U}\{u_m\}}\right) \geq \eta\sqrt{N_0}, \quad (2.52)$$

$$\Im\left(r_m \cdot e^{-j\phi_m}\right) = \Im\left(r_m \cdot e^{-j\mathfrak{U}\{u_m\}}\right) = \Im\left(\sum_{n=1}^{N} h_{m,n} x_n e^{-j\mathfrak{U}\{u_m\}}\right) = 0, \quad (2.53)$$

where $\eta \in \mathbb{R}^+$ is a direct proportionality coefficient used to set a threshold for constructive interference over the real part of t_m and determines the resulting SINR. Note that the conditions in (2.52) and (2.53) are imposed over the phase-shifted received signal $r_m \cdot e^{-j\mathfrak{U}\{u_m\}}$, according to the phase of the symbol of interest for the m-th user $\mathfrak{U}\{u_m\}$, as shown in Fig. 2.11b.

The condition in (2.53) can be further relaxed, as the phase of the received symbol r_m does not need to be strictly aligned with the phase of the desired symbol u_m. In fact, interference is to be considered constructive and beneficial for the transmission as long as the received symbol r_m is contained in the constructive area of the constellation, as in the 8-PSK example of Fig. 2.11.

From basic geometry properties and from the conditions (2.52) and (2.53), the constructive interference region for the m-th user can be defined as

$$\left|\Im\left(r_m \cdot e^{-j\mathfrak{U}\{u_m\}}\right)\right| \leq \left(\Re\left(r_m \cdot e^{-j\mathfrak{U}\{u_m\}}\right) - \eta\sqrt{N_0}\right)\tan\Phi, \quad (2.54)$$

where Φ is the central angle of the constructive interference sectors, which depends on the constellation order L and can be readily computed as $\Phi = \pm\pi/L$.

The constructive interference constraint definition in (2.54) allows the identification of a new precoding optimization region that exploits the interfering signal power, instead of reducing it. In fact, as shown in Fig. 2.11, the constructive interference regions can be defined as sectors with infinite radii whose central angle depends on the constellation order. This definition allows to relax classical optimization metrics based on interference minimization, as the constructive interference region is only constrained by the proximity

to the decision thresholds and extends infinitely in the directions away from them. Optimization region constraints are visually represented in Fig. 2.11 by the dashed lines.

Convex metrics for interference exploitation led to the formulation of a generalized beamforming, called *Constructive Interference Beamforming* (CIB). As described in [84], CIB is a convex optimization-based beamforming scheme, where the downlink beamforming problem is formulated in order to exploit the multiuser interference experienced at the receiver side as

$$\begin{aligned} \mathcal{P}_{CIB}: \quad & \underset{\mathbf{x}}{\text{minimize}} \quad \|\mathbf{x}\|^2 \\ & \text{subject to} \quad \left|\Im\left(\dot{\mathbf{h}}_m^T\mathbf{x}\right)\right| \leq \left[\Re\left(\dot{\mathbf{h}}_m^T\mathbf{x}\right) - \Gamma_m\right]\tan\Phi, \ \forall m, \end{aligned} \tag{2.55}$$

where $\dot{\mathbf{h}}_m = \mathbf{h}_m e^{-j\mathfrak{U}\{u_m\}}$ and the SINR requirements are identified as $\Gamma_m, \forall m$. In [84] it was shown that $\mathcal{P}_{CIB}$ is a Second-Order Cone Programming (SOCP) problem and can be efficiently solved by means of standard convex optimization tools.

In addition, Constructive Interference exploitation concepts can also be applied to the SINR balancing problem in (2.14) as follows

$$\begin{aligned} \mathcal{P}_{SCIB}: \quad & \underset{\mathbf{x}}{\text{maximize}} \quad \Gamma_t \\ & \text{subject to} \quad \left|\Im\left(\dot{\mathbf{h}}_m^T\mathbf{x}\right)\right| \leq \left[\Re\left(\dot{\mathbf{h}}_m^T\mathbf{x}\right) - \Gamma_m\sqrt{N_0}\right]\tan\Phi, \ \forall m, \\ & \qquad\quad \|\mathbf{x}\|^2 \leq P_t. \end{aligned} \tag{2.56}$$

Similarly to its power minimization formulation, the optimization problem $\mathcal{P}_{SCIB}$ is a SOCP problem that can be solved by means of convex optimization tools.

Chapter 3

Interference Exploiting Constant Envelope Precoding in Massive MIMO

In linear precoding-based MIMO communications, the average or instantaneous total transmitted power is generally constrained to a specific value by sum-power constraints [28, 29]. This is mostly supported by the fact that sum-power constraints are easy to model and study. However, in a realistic scenario, each antenna of the base station is typically connected to its own power amplifier (PA), which has to meet specific power constraints. This is particularly relevant in M-MIMO, because the benefits of using a large number of antennas at the transmitter side are followed by heavy burdens in terms of hardware costs and power consumption, which strongly affect its feasibility for future communication systems. In fact, the role of amplifiers is particularly critical for M-MIMO practicability, as inefficient PAs are accountable for $\sim 40 - 50\%$ of the total power consumption [92].

Toward this end, the employment of non-linear RF components in conjunction with low peak-to-average power-ratio (PAPR) precoding techniques [93] are expected to positively affect the energy efficiency of M-MIMO [17,18,94]. More specifically, [94] presents a transmission scheme for orthogonal frequency-division multiplexing (OFDM) modu-

lations based on low PAPR precoding, while [17, 18] propose a CEP technique where the transmitted signal amplitude corresponding to each antenna is constant and independent from the channel realization, i.e., leading to a unitary PAPR and therefore facilitating low cost PAs. In [17] the precoding technique is designed by minimizing the error norm function of the received signal for a single user scenario, while in [18] the transmitted symbols vector is designed for multiuser MIMO with the aim to reduce the interference caused by other users. CEP was further analyzed in [95], where the precoding design for frequency-selective MIMO channels is presented. Still, the performances of CEP with interference reduction are strongly affected by the number of iterations used and by the array size at the transmitter side [18]. In addition, the study in [96] investigated the effects of phase constraints at the transmitter, since additional restrictions to the change in transmitted phases at different symbol times can increase the energy efficiency of the system. Finally, the authors in [97] further improved the performances of interference reduction CEP, by employing cross-entropy optimization instead of gradient descent-based algorithms.

While the above approaches focus on interference minimization, several works on linear precoding [30,32,80] have proven that interference minimization does not necessarily lead to the best performances in a communication system. In fact, since interference is data dependent, the transmitter is able to predict the MUI at the receiver and can use this knowledge to influence it and benefit from it. Accordingly, this chapter introduces two novel CEP techniques which exploit concepts of constructive interference for PSK-modulated signals. In the proposed techniques, conditions over interference are relaxed, allowing the transmitter to use the interfering signal as a green source of power to increase the SINR at the receiver side. It is important to highlight that the proposed schemes are particularly suitable for high-interference and low-SNR scenarios, where low order modulations such as 2-PSK and 4-PSK are often preferred to ensure reliable communications [98]. Nevertheless, the benefits of constructive interference could also be extended to Quadrature Amplitude Modulation (QAM) signals, e.g., over the outer constellation points of a 16-QAM or to the whole constellation by means of adaptive decision thresholds [80].

The main contributions presented in this chapter are synthesized in the following:

- Definition of a new optimization region for CEP, based on the concepts of constructive interference.
- Introduction of two different CEP approaches, where both equality and inequality power constraints are considered.
- Study of the computational costs of the proposed techniques in comparison with the classical CEP approach in the literature.
- Introduction of a CSI-robust precoding scheme based on a relaxation of the interference optimization region.
- Evaluation of the performances of the proposed schemes for different PSK modulation orders and in scenarios where the transmitter holds perfect and imperfect CSI.

3.1 System Model

Consider a downlink multiuser scenario where the BS employs an N dimensional antenna array to communicate with a population of M single-antenna users. The received signal $\mathbf{y}$ is a $\mathbb{C}^{M\times 1}$ vector that collects the M user received signals y_m and is analytically defined in accordance with eq. (2.26), without the subindex $\{\cdot\}_d$ to ease the notation. While complex channel gains $h_{m,n}$ in M-MIMO are modeled to include both the complex small scale fading $g_{m,n}$ between the n-th antenna and the m-th user and the real large scale fading coefficient β_m experienced by the m-th user [11], our focus resides on a single-cell scenario where channel gains are commonly modeled as independent Rayleigh fading [99]. Accordingly, small scale fading $g_{m,n}$ are zero mean i.i.d. Gaussian variables and large scale coefficients are considered unitary $\beta_m = 1$, $\forall m \in \{1, ..., M\}$.

Given the total transmitted power by the antenna array P_t, the n-th element of the

transmitted signal $\mathbf{x}$ in a CEP-based system is defined as [18]

$$x_n = \sqrt{P_n} e^{j\theta_n}, \tag{3.1}$$

where P_n is the power transmitted from the n-th antenna, so that $\sum_{n=1}^{N} P_n = P_t$, and θ_n represents the precoding phase of the CEP signal. Similarly, the received signal at the m-th user can be defined as

$$y_m = \sum_{n=1}^{N} h_{m,n} \sqrt{P_n} e^{j\theta_n} + n_m. \tag{3.2}$$

For simplicity and to ease the notation, throughout the chapter we assume unitary transmitted power $P_t = 1$ and equally distributed power among the N antennas at the BS, i.e., $P_n = 1/N, \forall n \in \{1, ..., N\}$, hence leading to

$$y_m = \sum_{n=1}^{N} \frac{1}{\sqrt{N}} h_{m,n} e^{j\theta_n} + n_m. \tag{3.3}$$

The first term of the received signal y_m can be rearranged in order to explicitly discriminate between the desired signal and the interference. Analytically we have

$$y_m = u_m + t_m + n_m, \tag{3.4}$$

where $u_m = d_m e^{j\phi_m}$ is the PSK desired symbol for the m-th user, with magnitude d_m and phase ϕ_m, and t_m represents the interfering signal for the m-th user

$$t_m = \left(\sum_{n=1}^{N} \frac{1}{\sqrt{N}} h_{m,n} e^{j\theta_n} - d_m e^{j\phi_m} \right). \tag{3.5}$$

Accordingly, we can identify the total MUI energy as

$$E_{MUI} = \sum_{m=1}^{M} \left| \left(\sum_{n=1}^{N} \frac{1}{\sqrt{N}} h_{m,n} e^{j\theta_n} - d_m e^{j\phi_m} \right) \right|^2. \tag{3.6}$$

3.1.1 Benchmark

First approaches to CEP were based on the minimization of the MUI energy [18]. In order to minimize (3.6), the base station proceeds to identify the N dimensional transmit phase angle vector $\boldsymbol{\theta} = [\theta_1, ..., \theta_N]$ that leads to the lowest MUI energy. Accordingly, the CEP algorithm can be formulated as follows [18, 97]

$$\begin{aligned} \mathcal{P}_{CEIR}: \quad & \underset{\boldsymbol{\theta}}{\text{minimize}} \quad \sum_{m=1}^{M} \left| \left(\sum_{n=1}^{N} \tfrac{1}{\sqrt{N}} h_{m,n} e^{j\theta_n} - d_m e^{j\phi_m} \right) \right|^2 \\ & \text{subject to} \quad |\theta_n| \leq \pi, \forall n \in \{1, ..., N\}, \end{aligned} \tag{3.7}$$

which represents a non-convex non-linear least squares (NLS) problem, affected by local minima. The optimization problem (3.7) was first solved in [18] with a gradient descent (GD) based approach, and further improved in [97] with a direct application of cross-entropy method [100]. Once the transmit phase vector $\boldsymbol{\theta}$ is computed, the system proceeds to compute the transmitted signal according to (3.1).

3.2 Constructive Interference Optimization Region

In Chapter 2, it was shown that for PSK-modulated signals, interference can be classified as constructive and destructive according to simple geometrical concepts. In fact, the interference signal t_m can be considered beneficial for system performances when it leads the noise free received symbol $r_m = y_m - n_m$ further away from the decision thresholds of the desired constellation symbol u_m.

Previously, constructive interference conditions were expressed for the received signal in a noiseless scenario, however, they can be explicitly imposed over the interfering signal by substituting t_m into r_m as

$$\left| \Im \left(t_m \cdot e^{-j\phi_m} \right) \right| \leq \Re \left(t_m \cdot e^{-j\phi_m} \right) \tan \Phi. \tag{3.8}$$

A visual representation of the distinction between constructive and destructive interference is presented in Fig. 3.1a, where the desired symbol u_m is considered to be the

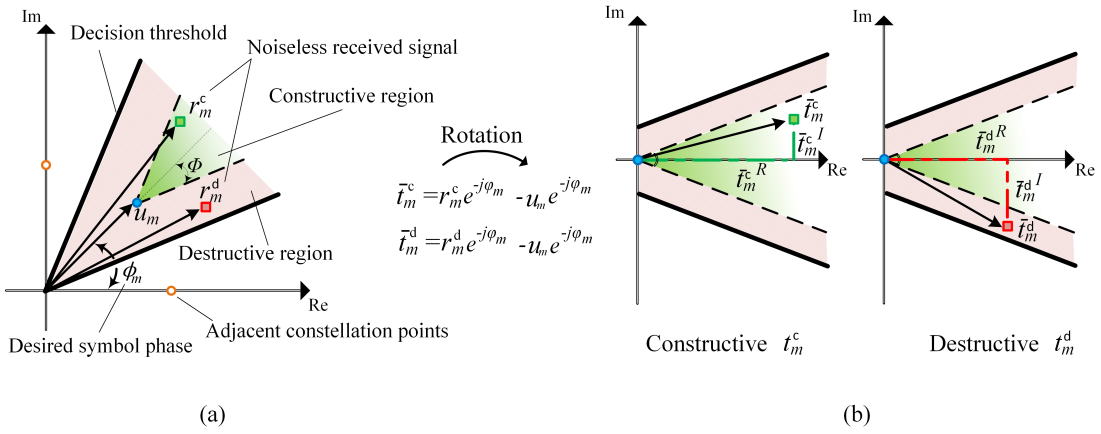

Figure 3.1: Optimization region for constructive interference exploitation, 8PSK example: (a)Interference regions for 8-PSK symbol, (b) Interference signal after rotation.

$\left(1/\sqrt{2}+j1/\sqrt{2}\right)$ point of the 8-PSK constellation. Here the superscripts $\{\cdot\}^c$ and $\{\cdot\}^d$ are used to differentiate between two different cases, where the received symbol falls in the constructive region (i.e., the green shaded area) or in destructive region (i.e., the red area), respectively. As per above, we can see that when the received symbol falls in the destructive region it resides closer to the decision thresholds, represented by the bold lines, when compared to the desired symbol. On the other hand, when $\bar{t}_m$ lays in the constructive region, its distance from the decision thresholds is greater than the one which characterizes u_m.

The condition (3.8) is visually described in Fig. 3.1b for the 8-PSK case, where $\bar{t}_m = t_m \cdot e^{-j\phi_m}$ represents the rotated interfering signal for the m-th user and $\bar{t}_m^R = \Re(\bar{t}_m)$ and $\bar{t}_m^I = \Im(\bar{t}_m)$ identify the shift from u_m suffered by the received symbol by means of interference. More specifically, $\bar{t}_m^R$ is an analytical measure of the amplification of the received constellation point along the axis of u_m, while $\bar{t}_m^I$ represents a linear measure of the angle shift from the original constellation point with phase ϕ_m [1]. The reader is referred to [82–84] for more details on the definition of the constructive interference region.

[1] It is important to stress that $\bar{t}_m^R$ and $\bar{t}_m^I$ can grow infinitely, as long as they respect the condition in (3.8).

3.3 Constant Envelope Precoding with Constructive Interference Optimization

Existing studies in M-MIMO systems mostly consider precoding techniques with sum-power constraints at the transmitter side. However, this is not a realistic assumption, since each transmitting antenna is typically characterized by its own amplifier and is hence affected by specific power constraints. Moreover, the use of precoding techniques where the power at each antenna is fixed also allows the employment of highly efficient amplifiers, hence reducing the total operational power consumption of the system. Since CEP provides a solution to the above challenges, its joint application with interference exploitation concepts is proposed, in order to improve the performance of classical CEP approaches.

Toward this end, two different CEP approaches are introduced, both based on constructive interference exploitation concepts: one with CEP equality constraints, i.e., $|x_n| = p, \forall n \in \{1, ..., N\}$, and a two-stage approach where the constraints are initially relaxed to inequality conditions, i.e., $|x_n| \leq p, \forall n \in \{1, ..., N\}$, to be successively reapplied by means of normalization in order to perform CEP.

Following the concepts of constructive interference in (3.8), it is possible to define a new optimization metric that maximizes the interference power, while imposing constraints over the phase of t_m. Thanks to simple analytical operations, we can rearrange (3.8) as

$$\Re\left(t_m \cdot e^{-j\phi_m}\right) \tan\Phi - \left|\Im\left(t_m \cdot e^{-j\phi_m}\right)\right| \geq 0. \tag{3.9}$$

The difference on the left side of the inequality can be used as an indicator of how constructive or destructive the interfering signal t_m is. In fact, if (3.9) is negative, the interfering signal lies in the destructive region of interference, while if (3.9) is positive it implies that the interfering signal is constructive. In addition, since the real part of (3.8) represents the power of the interfering signal, we can infer that higher and positive values of (3.9) lead to stronger forms of constructive interference. Accordingly, the Constant Envelope Constructive Interference (CECI) optimization problem $\mathcal{P}_{CECI}$ is defined as

follows:

$$\begin{aligned} \mathcal{P}_{CECI}: \quad & \underset{\boldsymbol{\theta}}{\text{maximize}} \quad \min_{m} \left\{ \Re\left(t_m e^{-j\phi_m}\right) \tan\Phi - \left|\Im\left(t_m e^{-j\phi_m}\right)\right| \right\} \\ & \text{subject to} \quad |\theta_n| \leq \pi, \forall n \in \{1, ..., N\}, \end{aligned} \tag{3.10}$$

where $m \in \{1, ..., M\}$ and the operator $\min_{m} \{\cdot\}$ represents the minimum value of the argument among each of the M values. In $\mathcal{P}_{CECI}$ the minimum value of the constructive interference metric is maximized. With this approach, when the minimum value of the metric is positive, we can automatically infer that the constructive interference condition is verified and maximized for all the M users. In cases where the solution to $\mathcal{P}_{CECI}$ leads to negative values of the minimum, instead, it implies that the precoding phases minimize the destructive interference as its least constructive component is maximized, as visually described for the 8-PSK case in Fig. 3.1b. The formulation in $\mathcal{P}_{CECI}$ is clearly non-convex, however it can be efficiently solved via the cross-entropy method (CEM).

3.3.1 A CEM Solver for Constructive Interference Optimization

The cross-entropy method can be described as an adaptive algorithm that aims to the identification of rare events by means of variance reduction. The algorithm is characterized by an iterative approach [100], where each iteration presents two main steps:

- Generation of random samples based on a specific distribution $f(\boldsymbol{\theta}, \mathbf{u})$.
- Update distribution parameters $\mathbf{u} \in \mathbb{R}$, according to the computed values of a chosen cost function, in order to improve the random samples generation in the following iterations.

The use of cross-entropy method to perform combinatorial optimization can be described as follows. Consider the maximization problem described in $\mathcal{P}_{CECI}$, the global optimum

γ^* is defined as

$$\begin{aligned}\gamma^* &= \min_m \left\{\Re\left(\bar{t}_m^*\right)\tan\Phi - \left|\Im\left(\bar{t}_m^*\right)\right|\right\} \\ &= \max_{\boldsymbol{\theta}\in\Theta}\left[\min_m \left\{\Re\left(\bar{t}_m\right)\tan\Phi - \left|\Im\left(\bar{t}_m\right)\right|\right\}\right],\end{aligned} \tag{3.11}$$

where $\bar{t}_m^*$ represents the m-th element of the normalized interfering signal, analytically expressed as

$$\bar{t}_m^* = \left(\sum_{n=1}^{N}\frac{1}{\sqrt{N}}h_{m,n}e^{j\theta_n^*} - d_m e^{j\phi_m}\right)e^{-j\phi_m}, \tag{3.12}$$

with θ_n^* being the n-th element of the optimal solution $\boldsymbol{\theta}^*$ to the optimization problem. The application of CEM to optimization problems is based on the association of the maximization problem with the probability estimation of a rare event. Given a performance threshold γ, we can evaluate the probability of the rare event $\min_m \left\{\Re\left(\bar{t}_m\right)\tan\Phi - \left|\Im\left(\bar{t}_m\right)\right|\right\} \geq \gamma$ as

$$\begin{aligned}\mathcal{L}(\gamma) &= \mathbb{P}_{\mathbf{u}}\left(\min_m \left\{\Re\left(\bar{t}_m\right)\tan\Phi - \left|\Im\left(\bar{t}_m\right)\right|\right\} \geq \gamma\right) \\ &= E_{\mathbf{u}}\left\{\mathcal{I}\left\{\min_m \left\{\Re\left(\bar{t}_m\right)\tan\Phi - \left|\Im\left(\bar{t}_m\right)\right|\right\} \geq \gamma\right\}\right\} \\ &= \int \mathcal{I}\left\{\min_m \left\{\Re\left(\bar{t}_m\right)\tan\Phi - \left|\Im\left(\bar{t}_m\right)\right|\right\} \geq \gamma\right\} f\left(\boldsymbol{\theta},\mathbf{u}\right) d\boldsymbol{\theta}\end{aligned} \tag{3.13}$$

where the operator $\mathbb{P}_{\mathbf{u}}\left(\cdot\right)$ evaluates the probability of the event in argument, the operator $E_{\mathbf{u}}\left\{\cdot\right\}$ represents the expectation of the argument with respect to the distribution $f(\boldsymbol{\theta},\mathbf{u})$ and $\mathcal{I}\left\{\cdot\right\}$ is a Boolean indicator function that returns 1 or 0 values when its argument it true or false, respectively. The estimation of $\mathcal{L}(\gamma)$ can be performed through Monte Carlo simulations [2], by drawing a set of K random states $\boldsymbol{\Theta}_1, ..., \boldsymbol{\Theta}_K$ from $f\left(\boldsymbol{\theta},\mathbf{u}\right)$ and by computing

$$\widehat{\mathcal{L}}\left(\gamma\right) = \frac{1}{K}\sum_{k=1}^{K}\mathcal{I}\left\{\min_m \left\{\Re\left(\bar{t}_m^k\right)\tan\Phi - \left|\Im\left(\bar{t}_m^k\right)\right|\right\} \geq \gamma\right\}, \tag{3.14}$$

[2] While analytical estimations of $\mathcal{L}(\gamma)$ can also be performed, Monte-Carlo estimation represents the standard procedure for applications of the Cross-Entropy solver, as described in [100, 101] and as performed in [97].

where $\bar{t}_m^k$ is the m-th element of the interfering signal for the k-th state $\boldsymbol{\Theta}_k = \left[\Theta_1^k, ..., \Theta_n^k, ..., \Theta_N^k\right]$

$$\bar{t}_m^k = \left(\sum_{n=1}^{N} \frac{1}{\sqrt{N}} h_{m,n} e^{j\Theta_n^k} - d_m e^{j\phi_m}\right) e^{-j\phi_m}. \tag{3.15}$$

A direct application of (3.14) becomes rapidly prohibitive when the probability of the event is very small, i.e., on the order of $\sim 10^{-5}$. This can be addressed by means of *importance sampling*, which estimates a different probability density function $g(\boldsymbol{\theta})$ that more frequently generates such rare events. Under importance sampling, the estimation problem becomes

$$\widehat{\mathcal{L}}(\gamma) = \frac{1}{K} \sum_{k=1}^{K} \mathcal{I}\left\{\min_m \left\{\Re\left(\bar{t}_m^k\right) \tan\Phi - \left|\Im\left(\bar{t}_m^k\right)\right|\right\} \geq \gamma\right\} \frac{f(\boldsymbol{\Theta}_k, \mathbf{u})}{g(\boldsymbol{\Theta}_k)}, \tag{3.16}$$

where $g(\boldsymbol{\Theta}_k)$ represents the importance sampling distribution and $\frac{f(\boldsymbol{\Theta}_k, \mathbf{u})}{g(\boldsymbol{\Theta}_k)}$ is defined as the *likelihood ratio* (LR) estimator.

The importance sampling function is commonly chosen as a probability density function from the same family of $f(\boldsymbol{\theta}, \mathbf{u})$, as

$$g(\boldsymbol{\theta}) = f(\boldsymbol{\theta}, \mathbf{v}), \tag{3.17}$$

where $\mathbf{v} \in \mathbb{R}$ is the tilting parameters vector and is obtained by computing the function with the minimum Kullback-Leiber distance from the ideal solution $g^*(\boldsymbol{\theta}) = \frac{\mathcal{I}\{\mathcal{S}(\boldsymbol{\theta}) \geq \gamma\} f(\boldsymbol{\theta}, \mathbf{u})}{\mathcal{L}(\gamma)}$, where $\mathcal{S}(\boldsymbol{\theta})$ is a real valued function of the optimization parameter $\boldsymbol{\theta}$. The Kullback-Leiber distance or cross-entropy between two densities $s(\mathbf{x})$ and $t(\mathbf{x})$ is analytically defined as

$$\mathcal{D}(s,t) = \int s(\mathbf{x}) \ln s(\mathbf{x}) d\mathbf{x} - \int s(\mathbf{x}) \ln t(\mathbf{x}) d\mathbf{x} \tag{3.18}$$

and its minimization can be achieved through the maximization of the second term in the equation. The tilting parameters $\mathbf{v}$ deriving from the minimization of the Kullback-

Leiber distance between $g^{*}\left(\boldsymbol{\theta}\right)$ and $f\left(\boldsymbol{\theta},\mathbf{u}\right)$ can be obtained as

$$\mathbf{v}^{*}=\arg\max_{\mathbf{v}}\int\frac{\mathcal{I}\left\{\mathcal{S}\left(\boldsymbol{\theta}\right)\geq\gamma\right\}f\left(\boldsymbol{\theta},\mathbf{u}\right)}{\mathcal{L}\left(\gamma\right)}\ln f(\boldsymbol{\theta},\mathbf{v})d\boldsymbol{\theta}, \tag{3.19}$$

which, for the proposed optimization problem, is equivalent to the maximization [100] :

$$\mathbf{v}^{*}=\arg\max_{\mathbf{v}}E_{\mathbf{u}}\left\{\mathcal{I}\left\{\min_{m}\left\{\Re\left(\bar{t}_{m}\right)\tan\Phi-\left|\Im\left(\bar{t}_{m}\right)\right|\right\}\geq\gamma\right\}\ln f(\boldsymbol{\Theta},\mathbf{v})\right\}. \tag{3.20}$$

A solution to (3.20) can be numerically estimated as

$$\widehat{\mathbf{v}}^{*}=\frac{1}{K}\sum_{k=1}^{K}\mathcal{I}\left\{\min_{m}\left\{\Re\left(\bar{t}_{m}^{k}\right)\tan\Phi-\left|\Im\left(\bar{t}_{m}^{k}\right)\right|\right\}\geq\gamma\right\}\ln f(\boldsymbol{\Theta}_{k},\mathbf{v}). \tag{3.21}$$

Here, $f\left(\boldsymbol{\theta},\mathbf{v}\right)$ is considered to be a Gaussian distribution, i.e., $f\left(\boldsymbol{\theta},\mathbf{v}\right)=f\left(\boldsymbol{\theta},[\mu,\sigma]\right)$, which allows to analytically estimate (3.20) as

$$\widehat{\mu}=\frac{\sum_{k=1}^{K}\mathcal{I}\left\{\min_{m}\left\{\Re\left(\bar{t}_{m}^{k}\right)\tan\Phi-\left|\Im\left(\bar{t}_{m}^{k}\right)\right|\right\}\geq\gamma\right\}\boldsymbol{\Theta}_{k}}{\sum_{k=1}^{K}\mathcal{I}\left\{\min_{m}\left\{\Re\left(\bar{t}_{m}^{k}\right)\tan\Phi-\left|\Im\left(\bar{t}_{m}^{k}\right)\right|\right\}\geq\gamma\right\}} \tag{3.22}$$

$$\widehat{\sigma}=\sqrt{\left[\frac{\sum_{k=1}^{K}\mathcal{I}\left\{\min_{m}\left\{\Re\left(\bar{t}_{m}^{k}\right)\tan\Phi-\left|\Im\left(\bar{t}_{m}^{k}\right)\right|\right\}\geq\gamma\right\}\left(\boldsymbol{\Theta}_{k}-\widehat{\mu}\right)^{2}}{\sum_{k=1}^{K}\mathcal{I}\left\{\min_{m}\left\{\Re\left(\bar{t}_{m}^{k}\right)\tan\Phi-\left|\Im\left(\bar{t}_{m}^{k}\right)\right|\right\}\geq\gamma\right\}}\right]}, \tag{3.23}$$

where $\widehat{\mu}$ and $\widehat{\sigma}$ respectively represent mean and standard deviation of the importance sampling distribution, i.e., $\widehat{\mathbf{v}}^{*}=[\widehat{\mu},\widehat{\sigma}]$. This assumption is not uncommon for continuous optimization problems [97] and leads to efficient solutions. As previously mentioned, CEM is based on an iterative approach and requires the tilting parameters to be updated at each iteration. However, a direct update from (3.21) is often undesirable, as it might rapidly converge to suboptimal solutions [100]. The occurrence of these events can be reduced by using smooth updating procedures, as follows

$$\mu^{(l)}=\alpha\widehat{\mu}^{(l)}+\left(1-\alpha\right)\mu^{(l-1)} \tag{3.24}$$

$$\sigma^{(l)} = \alpha\widehat{\sigma}^{(l)} + (1-\alpha)\,\sigma^{(l-1)}, \tag{3.25}$$

where the superscript $(\cdot)^{(l)}$ represents the l-th iteration of the value in argument.

An analytical description of the constructive interference optimization precoding based on cross-entropy optimization (CEO-CIO) technique is presented in Algorithm 3.1. Here, T represents the number of iterations, K identifies the random sample size and ρ is direct proportionality coefficient used to compute the intermediate threshold $\gamma^{(l)}$. More specifically, the intermediate threshold $\gamma^{(l)}$ is identified by the cost function evaluation $\mathcal{C}_k$ whose index is the smallest integer to be greater or equal to ρK and is evaluated in Algorithm 3.1 as $\mathcal{C}_{\lceil \rho K \rceil}$.

Algorithm 3.1 CEO-CIO Precoding

Input: $\mathbf{H}$, $\mathbf{u}$, T, L , K

Output: $\mathbf{x}$

Initialize $\boldsymbol{\mu}^{(0)}$ and $\boldsymbol{\sigma}^{(0)}$

for $l = 1 \rightarrow T$

$\boldsymbol{\Theta}^{(l)} = \left[\boldsymbol{\theta}_1^{(l)}, ..., \boldsymbol{\theta}_k^{(l)}, ..., \boldsymbol{\theta}_K^{(l)}\right]$ where the columns $\boldsymbol{\theta}_k^{(l)} \sim \mathcal{N}\left(\boldsymbol{\mu}^{(l-1)}, \left(\boldsymbol{\sigma}^{(l-1)}\right)^2\right)$

for $k = 1 \rightarrow K$

$\mathbf{x}_k^{(l)} = \frac{1}{\sqrt{N}} e^{j\boldsymbol{\theta}_k^{(l)}}$

$\mathbf{t}_k^{(l)} = \mathbf{H} \cdot \mathbf{x}_k^{(l)} - \mathbf{u}$

$\mathcal{C}_k = \min_m \left\{ \Re\left(t_{m,k}^{(l)} e^{-j\phi_m}\right) \tan\Phi - \left| \Im\left(t_{m,k}^{(l)} e^{-j\phi_m}\right) \right| \right\}$

end

Sort $\mathcal{C}_1 \geq \mathcal{C}_2 \geq ... \geq \mathcal{C}_K$

$\gamma^{(l)} = \mathcal{C}_{\lceil \rho K \rceil}$

$\widehat{\mu}^{(l)}$ and $\widehat{\sigma}^{(l)}$ from (3.22) and (3.23)

$\mu^{(l)}$ and $\sigma^{(l)}$ from (3.24) and (3.25)

end

Return $\mathbf{x} = \mathbf{x}_1^{(T)}$

The application of the proposed algorithm leads to received symbols $\mathbf{r}$ which prevalently reside in the constructive interference region. To illustrate this effect, Fig. 3.2 shows the received constellation of CEP precoded signals for the example of 8-PSK constellation in a noise free transmission over 100 different channel realizations, in a

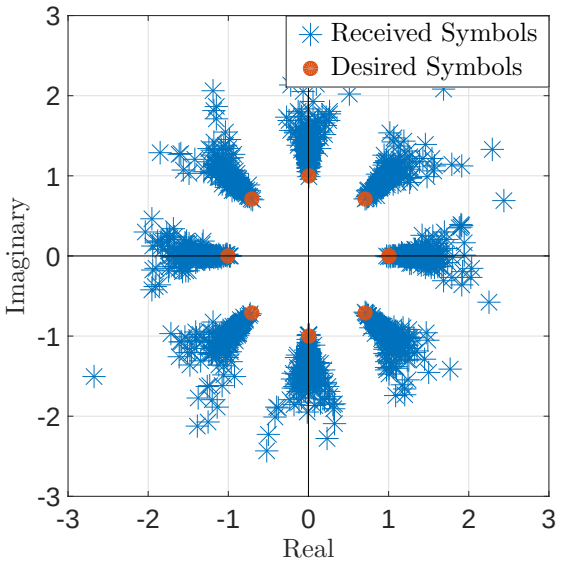

Figure 3.2: Received symbols for a noiseless scenario with $N = 100$ antennas for $M = 20$ users when using 8-PSK.

scenario where the BS is equipped with $N = 100$ antennas and communicates with $M = 20$ single-antenna users.

3.3.2 Two-Step Convex CEP

In addition to the previous approach, an additional technique for constant envelope transmissions is presented where power constraints are initially relaxed into inequality, allowing to use standard convex optimization techniques, and subsequently enforced to equality via normalization at a later stage (i.e., by dividing the antenna outputs that do not respect power constraints by their absolute value). In order to relax the conditions in $\mathcal{P}_{CECI}$, we reformulate the optimization problem in its equivalent form where the cost function is dependent on the transmitted signal $\mathbf{x} = [x_1, ..., x_n, ..., x_N]^T$:

$$\begin{aligned} \mathcal{P}_{eCECI}: \quad & \underset{\boldsymbol{x}}{\text{maximize}} \quad \min_m \left\{ \Re\left(t_m e^{-j\phi_m}\right) \tan\Phi - \left|\Im\left(t_m e^{-j\phi_m}\right)\right| \right\} \\ & \text{subject to} \quad |x_n| = 1/\sqrt{N}, \forall n \in \{1, ..., N\}. \\ & \qquad\qquad t_m = \sum_{n=1}^{N} h_{m,n} x_n - u_m. \end{aligned} \tag{3.26}$$

Similarly to the optimization in $\mathcal{P}_{CECI}$, the above problem is non-convex, because

of the equality constraint over a convex set. In order to tackle this, the problem can be convexified by imposing relaxed conditions to the transmitted signal $x_n \in \mathbb{C}, \forall n \in \{1, ..., N\}$ and its absolute value $|x_n| \leq 1/\sqrt{N}, \forall n \in \{1, ..., N\}$. Thanks to this, the optimization problem $\mathcal{P}_{eCECI}$ can be reformulated into its relaxation $\mathcal{P}'_{eCECI}$ as

$$\begin{aligned} \mathcal{P}'_{eCECI}: \quad & \underset{\boldsymbol{x}'}{\text{maximize}} \quad \min_{m} \left\{ \Re\left(t_m e^{-j\phi_m}\right) \tan\Phi - \left|\Im\left(t_m e^{-j\phi_m}\right)\right| \right\} \\ & \text{subject to} \quad |x'_n| \leq 1/\sqrt{N}, \forall n \in \{1, ..., N\}. \\ & \qquad\qquad t_m = \sum_{n=1}^{N} h_{m,n} x'_n - u_m. \end{aligned} \tag{3.27}$$

where the superscript $\{\cdot\}'$ is used to identify the solution achieved through relaxation. Different from $\mathcal{P}_{eCECI}$, the newly formulated problem is a standard second-order cone program (SOCP) [3] and can be effectively solved by means of standard convex optimization techniques [84]. Since the constraints over the amplitude of the precoded signal $|x'_n| \leq 1/\sqrt{N}, \forall n \in \{1, ..., N\}$ cannot guarantee a strict constant envelope condition, in order to achieve a full CEP transmission for all the antennas at the BS we need to force the equality constrained before transmission. More specifically, in the second and final stage of the algorithm, we can proceed by normalizing the elements where $|x'_n| \neq 1/\sqrt{N}, \forall n \in \{1, ..., N\}$ as follows

$$x_n = \begin{cases} x'_n / \left(\sqrt{N}|x'_n|\right) & \forall n \text{ where } |x'_n| \neq 1/\sqrt{N} \\ x'_n & \forall n \text{ where } |x'_n| = 1/\sqrt{N}. \end{cases} \tag{3.28}$$

The precoding scheme, namely identified as Convex Constructive Interference Optimization (CVX-CIO), is analytically described in Algorithm 3.2, where $\mathbf{x}' \preceq 1/\sqrt{N}$ is used to represent that $x'_n \leq 1/\sqrt{N}, \forall n \in \{1, ..., N\}$.

[3] More specifically, the problem can be cast as a standard SOCP [102], as its objective function is concave [84] as it can be decomposed into the combination of a linear function $\Re\left(t_m e^{-j\phi_m}\right)$ and a concave function $-\left|\Im\left(t_m e^{-j\phi_m}\right)\right|$. In fact, in [84] it was shown that the extraction of the imaginary and real of a linear function preserves its linearity.

Algorithm 3.2 CVX-CIO Precoding
Input: H, **u**
Output: x

$$\mathbf{x}' = \underset{\boldsymbol{x}' \in \mathbb{C}, |\mathbf{x}'| \preceq 1/\sqrt{N}}{\arg\max} \left\{ \min_{m} \left[\Re\left(\bar{t}_m\right) \tan\Phi - \left|\Im\left(\bar{t}_m\right)\right| \right] \right\}$$

$$\text{Return } \mathbf{x} = [x_1, ..., x_N]^T = \left[\frac{x'_1}{|x'_1|\sqrt{N}}, ..., \frac{x'_N}{|x'_N|\sqrt{N}} \right]^T$$

3.4 Computational Complexity

This section computes and analyzes the complexity of the proposed CEO-CIO in comparison with the CEO approach to interference reduction (CEO-IR) precoding from [97] in terms of floating-point operations (FLOPs), following the operational costs listed in the literature [102]. More specifically, addition, subtraction and multiplication between two floating-point numbers are considered as a FLOP. Since both approaches are characterized by the same number of iterations T, the analysis focuses on the computational burdens of the two different cost functions.

In line with Chapter 2, a simple time-division duplexing (TDD) scenario [51] is considered, as it allows to exploit the reciprocity of the channel, enabling the CSI acquisition for downlink via uplink pilots. This property is fundamental in M-MIMO systems, as the time required by CSI acquisition T_{CSI} becomes proportional to the number of users M instead of the number of antennas N. In our analysis, we consider a simple TDD case where $T_{CSI} = \mu M$, with $\mu \geq 1$ being the number of pilot slots. Finally, a symmetrical transmission case is assumed, where the time for data transmission $T_{data} = T_{cohe} - T_{CSI}$ is divided between downlink and uplink transmissions according to a parameter $0 \leq \epsilon_{_{DL}} \leq 1$. The parameter $\epsilon_{_{DL}}$ explicitly represents the portion of T_{data} devoted to downlink symbol transmission. Analytically, we have

$$T_{DL} = \epsilon_{_{DL}} \left(T_{cohe} - T_{CSI}\right) = \epsilon_{_{DL}} \left(T_{cohe} - \mu M\right). \tag{3.29}$$

3.4.1 CEO-CIO Costs

As previously mentioned, main costs of the proposed CEO-CIO algorithm reside in the need to compute the cost function for each of the randomly generated samples. Cost function computation can be synthesized in the following main operations:

- Computation of the received vector in a noise free scenario $\mathbf{r} = \mathbf{H}\mathbf{x}$,
- Identification of the interfering signal vector $\mathbf{t} = \mathbf{r} - \mathbf{u}$,
- Projection of the interfering signal $\bar{\mathbf{t}} = \mathbf{t} \circ \mathbf{u}^*$,
- Identification of $\min \{\Re(\bar{\mathbf{t}}) \tan \Phi - |\Im(\bar{\mathbf{t}})|\}$,

where $\circ$ represents the Hadamard product.

From the literature [102], the costs of each of the aforementioned operations is known: the multiplication between a $M \times N$ matrix and an $N \times 1$ vector requires $M(2N-1)$ FLOPs, while the computation of the interfering signal and its rotation can be performed with M FLOPs each, since they can be achieved by M subtractions and multiplications, respectively. Finally, we can compute the costs of the identification of the minimum as a search through an M-sized vector, hence leading to M FLOPs. It follows that the proposed approach is characterized by a total FLOP count of $M(2N-1)+4M$ FLOPs, which includes the cost of the separation between the real and imaginary part of the rotated interfering signal. Computational costs for the derivation and transmission of a CEO-CIO signal are listed in Table 3.1.

3.4.2 CEO-IR Costs

The application of the conventional CEO-IR follows a similar pattern to CEO-CIO, due to the fact that they both require the computation of the interfering signal for all the randomly generated samples. More specifically, the computational costs of CEO-IR can be highlighted in the following operations:

- Computation of the received vector in a noise free scenario $\mathbf{r} = \mathbf{H}\mathbf{x}$,

- Identification of the interfering signal vector $\mathbf{t} = \mathbf{r} - \mathbf{u}$,
- Computation of the interference energy $\sum_{1}^{M} |t_m|^2$,

Following a similar approach to the previous section, we identify the multiplication costs in $M(2N-1)$ FLOPs and the computation of the interfering signal as M FLOPs. Since the interfering energy can be computed as the inner product of two M-sized vectors, i.e., by a cost of $2M-1$ FLOPs, the total cost of the CEO-IR algorithm is $M(2N-1)+3M-1$ FLOPs.

As we can see, the computational costs of the proposed technique CEO-CIO are comparable to the ones of the CEO-IR approach from the literature, as the FLOP count difference is almost negligible. The total costs of the application of the precoding techniques in a coherence time are listed in Table 3.1, which includes the effects deriving by both the number of iterations T and the sample size K.

Table 3.1: Computational costs in FLOPs.

CEO-CIO	
$\mathbf{r} = \mathbf{H}\mathbf{x}$	$T \cdot K \cdot M(2N-1)$
$\mathbf{t} = \mathbf{r} - \mathbf{u}$	$T \cdot K \cdot M$
$\bar{\mathbf{t}} = \mathbf{t} \circ \mathbf{u}^*$	$T \cdot K \cdot M$
$\min\{\Re(\bar{\mathbf{t}}) \tan\Phi - \lvert\Im(\bar{\mathbf{t}})\rvert\}$	$T \cdot K \cdot 2M$
Total	$T_{DL} \cdot T \cdot K\,[M(2N-1)+4M]$
CEO-IR	
$\mathbf{r} = \mathbf{H}\mathbf{x}$	$T \cdot K \cdot M(2N-1)$
$\mathbf{t} = \mathbf{r} - \mathbf{u}$	$T \cdot K \cdot M$
$\mathbf{t}^H\mathbf{t}$	$T \cdot K \cdot 2M-1$
Total	$T_{DL} \cdot T \cdot K\,[M(2N-1)+3M-1]$

3.5 CSI-Robust CEP

In the previous sections we assumed the transmitter to possess a perfect knowledge over the channel, allowing the definition of the constructive and destructive regions of interference in absence of uncertainty. When the CSI acquisition is imperfect, however, the received signal region extends according to the CSI error. The BS is assumed to be

aware of an estimated channel matrix, defined analytically as follows [84]

$$\widehat{\mathbf{H}} = \mathbf{H} + \mathbf{S}, \tag{3.30}$$

where the error matrix $\mathbf{S}$ represents the CSI uncertainty at the BS, statistically independent from $\mathbf{H}$, and characterized as a constrained spherical error, i.e., each element $s_{m,n} : \left\{ |s_{m,n}|^2 \leq \delta_{m,n}^2 \right\}$[84]. As in [84], the following analysis considers a scenario where the base station is aware of the error bounds $\delta_{m,n}^2$ but has no knowledge over the error matrix $\mathbf{S}$. Different from classical robust precoding approaches from the literature [84, 103, 104], where the transmitted power is increased in order to overcome the effects of CSI estimation errors, this section introduces a worst-case approach where the optimization region is redefined according to the CSI uncertainty, while preserving CEP constraints. The estimated interfering signal for the m-th user, in case of imperfect CSI, can be defined as follows

$$\begin{aligned} \widehat{t}_m &= \left(\sum_{n=1}^{N} \tfrac{1}{\sqrt{N}} \widehat{h}_{m,n} e^{j\theta_n} - d_m e^{j\phi_m} \right) \\ &= \left[\sum_{n=1}^{N} \tfrac{1}{\sqrt{N}} \left(h_{m,n} + s_{m,n} \right) e^{j\theta_n} - d_m e^{j\phi_m} \right] \\ &= \left(\sum_{n=1}^{N} \tfrac{1}{\sqrt{N}} h_{m,n} e^{j\theta_n} - d_m e^{j\phi_m} \right) + \sum_{n=1}^{N} \tfrac{s_{m,n}}{\sqrt{N}} e^{j\theta_n}, \end{aligned} \tag{3.31}$$

where $s_{m,n}$ represents the n-th element of the m-th row of the CSI uncertainty matrix $\mathbf{S}$. As we can see in the last step of (3.31), the estimated interference signal $\widehat{t}_m$ is characterized by two different components: the actual interference signal t_m, i.e., when considering perfect CSI, and the uncertainty error signal $z_m = \sum_{n=1}^{N} s_{m,n} e^{j\theta_n}$. It follows that the estimated interfering signal can be defined as the sum of the two terms

$$\widehat{t}_m = t_m + z_m. \tag{3.32}$$

In (3.8), the interfering signal is rotated according to the desired symbol, with the aim to have a region definition that is independent from the specific phase of the symbol of interest u_m. In a similar manner, the rotated interfering signal for the m-th user in

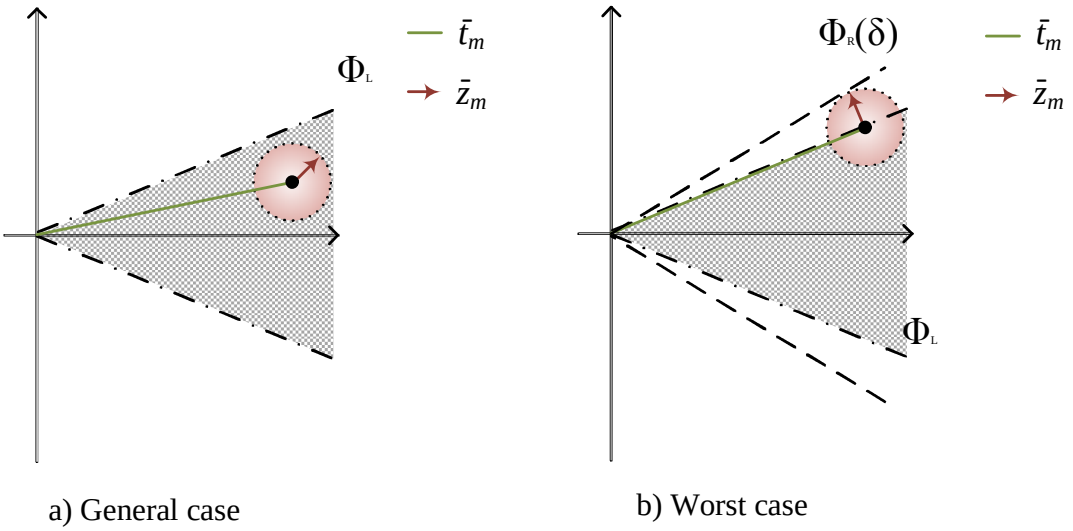

Figure 3.3: Imperfect CSI effects on the phase-shifted interfering signal $\bar{t}_m$.

presence of CSI errors $\hat{\bar{t}}_m$ is defined as

$$\hat{\bar{t}}_m = \hat{t}_m \cdot e^{-j\phi_m} = \bar{t}_m + \bar{z}_m. \tag{3.33}$$

The second term in (3.33) can be described as the shift from the ideal interfering signal $\bar{t}_m$ caused by the CSI errors and can be represented as a circular constrained region of uncertainty, as visually presented in Fig. 3.3a. Accordingly, we can identify the worst-case scenario in the event where the actual interfering signal $\bar{t}_m$ is within the constructive interference region, but the uncertainty error signal $\bar{z}_m$ moves the estimated $\hat{\bar{t}}_m$ away from it, as shown in Fig. 3.3b. Given the assumption of CSI errors to be constrained within a spherical region, it is possible to analytically derive amplitude and phase of the worst-case scenario uncertainty error signal $\bar{z}_m$.

Lemma 3.5.1 *The amplitude of $\bar{z}_m$ is characterized by the following analytical upper-bound*

$$|\bar{z}_m| \leq \frac{\sum_{n=1}^{N} \delta_{m,n}}{\sqrt{N}} \tag{3.34}$$

Proof of Lemma 3.5.1 Following the definition of $\bar{z}_m$ we have

$$\begin{aligned} |\bar{z}_m| &= \left| \sum_{n=1}^{N} \frac{1}{\sqrt{N}} s_{m,n} e^{j\theta_n} e^{-j\phi_m} \right| \\ &= \left| \sum_{n=1}^{N} \frac{1}{\sqrt{N}} |s_{m,n}| \, e^{j(\mathfrak{U}\{s_{m,n}\}+\theta_n-\phi_m)} \right|, \end{aligned} \tag{3.35}$$

where $s_{m,n}$ has been represented in order to show amplitude and phase and the operator $\mathfrak{U}\{\cdot\}$ identifies the phase extraction of the argument. The absolute value of z_m is evaluated as the absolute value of the sum of complex values. According to the triangle inequality (i.e., given two complex numbers $a, b \in \mathbb{C}$ they satisfy the property $|a+b| \leq |a| + |b|$) we have

$$\left| \sum_{n=1}^{N} \frac{1}{\sqrt{N}} |s_{m,n}| \, e^{j(\mathfrak{U}\{s_{m,n}\}+\theta_n-\phi_m)} \right| \leq \sum_{n=1}^{N} \frac{1}{\sqrt{N}} |s_{m,n}| \,. \tag{3.36}$$

Given the assumption of a spherical constrained error during CSI estimation, we have

$$\sum_{n=1}^{N} \frac{1}{\sqrt{N}} |s_{m,n}| \leq \sum_{n=1}^{N} \frac{1}{\sqrt{N}} \delta_{m,n}. \tag{3.37}$$

which ends the proof.

Finally, the worst-case scenario phase of $\bar{z}_m$ can be readily identified as the phase that is orthogonal to the constructive interference threshold identified by Φ.

The knowledge of the worst-case effects of CSI errors at the transmitter can be used to relax the optimization region, in order to include the events that would be affected by the uncertainty error signal. Thanks to this relaxation, a CSI errors robust precoding can be derived, without the need to increase the transmitted power.

More specifically, according to simple geometrical analysis, the phase threshold Φ is relaxed as

$$\Phi_R(\delta_m) = \Phi_L + \arctan \left\{ \frac{\sum_{n=1}^{N} \delta_{m,n}}{E\{|t_m|\}\sqrt{N}} \right\}, \tag{3.38}$$

where $\Phi_L = \pi/L$ identifies the threshold angle for the L order PSK modulation used

in transmission. Accordingly, we can define a new optimization problem, specifically designed for the imperfect CSI case.

$$\begin{aligned} \mathcal{P}_{CECIR}: \quad & \underset{\boldsymbol{\theta}}{\text{maximize}} \quad \min_{m} \left\{ \Re\left(\bar{t}_m\right) \tan \Phi_R\left(\delta_m\right) - \left|\Im\left(\bar{t}_m\right)\right| \right\} \\ & \text{subject to} \quad \left|\theta_n\right| \leq \pi, \forall n \in \{1, ..., N\}, \end{aligned} \tag{3.39}$$

Without loss of generality, this study considers a case where $\delta_{m,n} = \delta, \forall m \in \{1, ..., M\}, \forall n \in \{1, ..., N\}$, which leads to a simplified definition of the robust relaxation

$$\Phi_R\left(\delta\right) = \begin{cases} \Phi_L + \arctan\left\{\frac{\delta\sqrt{N}}{E\{|t_m|\}}\right\} & \text{if} \arctan\left\{\frac{\delta\sqrt{N}}{E\{|t_m|\}}\right\} \leq \frac{\pi}{L} \\ \Phi_{L-1} - \epsilon & \text{otherwise,} \end{cases} \tag{3.40}$$

where ϵ is an arbitrarily small positive quantity, which imposes an upperbound to the growth of Φ_R for high values of δ, and $L-1$ identifies the modulation order which is immediately lower than the one used during data transmission. The defined upperbound is particularly important, given the fact that very high values of δ could cause ambiguity with lower modulation orders, i.e., when their values lead the robust region $\Phi_R(\delta)$ to coincide with or exceed Φ_{L-1}.

3.6 Results

This section shows the performances of the proposed precoding techniques through Monte Carlo simulations over 50000 channel realizations. The downlink transmission described in the previous sections is assumed, where the BS employs $N = 64$ antennas to communicate with a population of $M = 12$ mobile users. While the proposed techniques can be directly applied to any modulation order, results are presented for both 4-PSK and 8-PSK. Legends are characterized by the following notation: CEO-CIO identifies constructive interference driven precoding based on CEM, CEO-IR is used to represent interference minimization CEO precoding and finally, CVX-CIO represents the two-step convex CEP approach to constructive interference optimization. Both CEO techniques are applied while considering the same parameter settings: $T = 1000$, $\rho = 0.05$ and

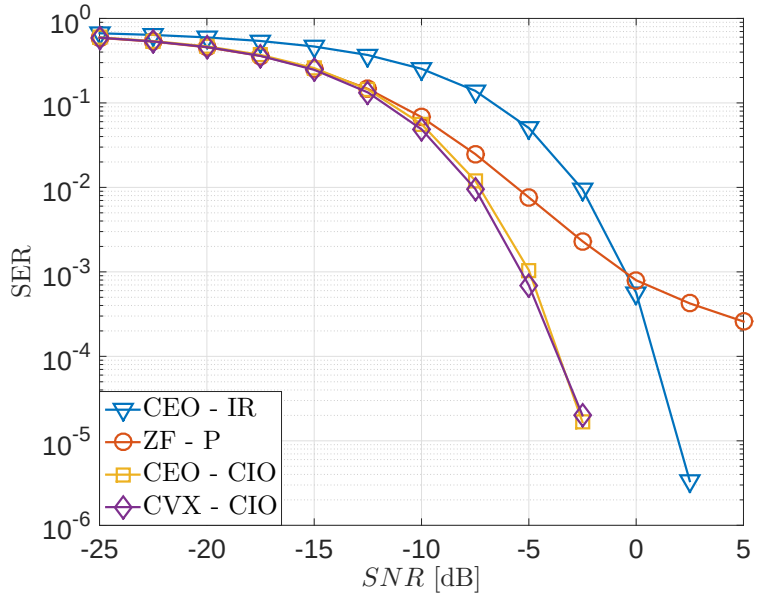

Figure 3.4: 4-PSK Symbol Error Rate when $M = 12$, $N = 64$ with perfect CSI.

$\alpha = 0.08$ [97]. CEM solver parameter values have been studied in [101], where the used settings are recommended for achieving good performances in terms of both convergence speed and quality of the solution. In addition to CEO-IR and in line with the literature, the proposed techniques are compared with a CEP approach to linear zero-forcing(ZF) precoding [18], ZF-P in the legends, which can be analytically defined as

$$\mathbf{x}_{ZF-P} = \frac{e^{j\mathcal{U}\{\mathbf{G}_{ZF}\mathbf{u}\}}}{\sqrt{N}}, \tag{3.41}$$

where $\mathbf{G}_{ZF}$ is the ZF precoding matrix, as defined in Chapter 2.

Figures 3.4 and 3.5 present the SER as a function of the transmitted SNR for 4-PSK and 8-PSK modulation respectively when considering a BS with $N = 64$ and $M = 12$ users. As we can see from Fig. 3.4 and Fig. 3.5, the proposed approaches greatly outperform the classical CEO-IR and ZF-P. This is due to the fact that CEO-CIO wisely exploits the interference signal $t_m, \forall m \in \{1, ..., M\}$ to increase the received signal power, while CEO-IR aims to a direct minimization of the interference energy. Regarding the ZF-P approach, we can see that a direct normalization of the precoded signal leads to a significant decrease in performances, due to its sub-obtimal approach. In addition, Fig. 3.6 shows the SER as a function of the transmitted SNR when a

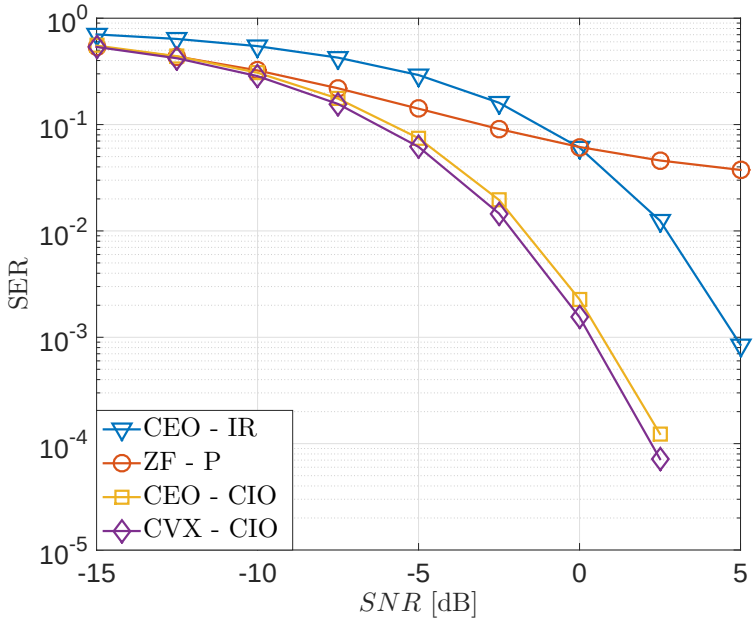

Figure 3.5: 8-PSK Symbol Error Rate when $M = 12$, $N = 64$ with perfect CSI.

different topology is considered, where $N = 32$ and $M = 6$, for both the 4-PSK and 8-PSK case. Even in this different topology, the same performance trend is preserved for all the described techniques, with the proposed schemes outperforming the CEP approaches from the literature. It is interesting to notice that in Fig. 3.6, CEO-CIO is able to achieve slightly better performances than CVX-CIO, differently from what happens in Fig.s 3.4-3.5. This is due to the fact that the second-step normalization of CVX-CIO, enforced in order to achieve a CEP transmission, has a stronger impact over the performances achievable by systems with a lower number of transmitting antennas and users, such as the scenario shown in Fig. 3.6. It was empirically observed that on average both scenarios are characterized by the same number of elements where $|x'_n| \neq 1/\sqrt{N}, \forall n \in \{1, ..., N\}$. This means that for scenarios with a larger number of transmitting antennas, the percentage of elements where the normalization is necessary is lower, hence reducing the degradation in performances caused by the second-step normalization of CVX-CIO.

In Fig. 3.7 we further characterize the proposed schemes when the base station possesses imperfect CSI in the scenario where $\delta^2_{m,n} = \delta^2 = 0.1$, $\forall m \in \{1, ..., M\}, \forall n \in \{1, ..., N\}$. Here, we set the value of $\epsilon = 0.1$ and consider a simplified derivation of

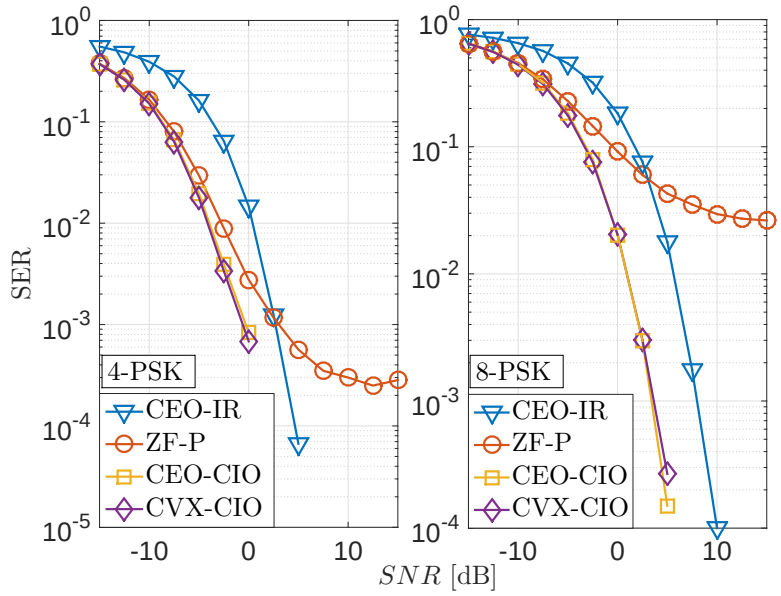

Figure 3.6: Symbol Error Rate as a function of the transmitted SNR when $M = 6$, $N = 32$ with perfect CSI.

the relaxation $\Phi_R(\delta)$ where $E\{|t_m|\}$ is unitary. While more complex derivations of $E\{|t_m|\}$ are expected to give a finer evaluation of $\Phi_R(\delta)$, it was empirically shown that such approximation has a negligible impact in the overall system performance. More specifically, Fig. 3.7 shows that for a system with imperfect CSI, the performances of classical CEO-IR are strongly affected by the errors in the channel estimation, while the performance gap with the proposed schemes is strongly accentuated. This phenomenon is caused by the fact that CEO-IR aims to minimize the MUI over desired symbols with unitary energy, hence leading to received points that are more prone to noise and CSI errors. More specifically, CEP-IR leads to received symbols that more susceptible to the imperfect CSI shift $\bar{z}_m$ because of their shorter distance from the decision threshold when compared to the proposed schemes. On the other hand, it is important to notice how the performance trend of the proposed CEO-CIO scheme follows the one of the system where perfect CSI is available at the transmitter. This is due to the interference energy exploitation in the CIO scheme, which allows a certain robustness against noise in the channel estimation. In addition, we can see that the robust relaxation of CEO-CIO, identified as CEO-CIO R in the legend, is able to increase the performances achieved by its non-robust counterpart, due to the proposed error-based optimization region, which

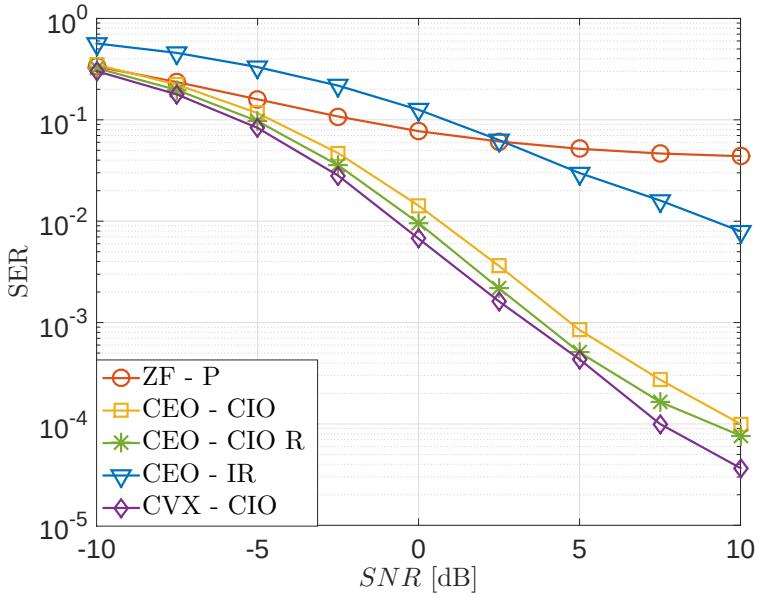

Figure 3.7: Symbol Error Rate for 8-PSK modulation when $M = 12$, $N = 64$ with imperfect CSI and $\delta^2 = 0.1$.

allows to partially reduce the deteriorating effects of imperfect CSI at the transmitter side. Finally, it can be noticed how the CVX-CIO is inherently more robust to imperfect estimations of the CSI when compared to the approach based on the CEM-solver. This behavior is caused by the fact that CVX-CIO received signals tend be more aligned to the corresponding desired constellation points, hence allowing a innate robustness against noisy channels.

Fig. 3.8 studies the behavior of the proposed robust relaxation of CEO-CIO with increasing values of the error bound δ^2 and fixed $SNR = 10dB$. As we can see, all the techniques achieve lower SER performances as the error bound δ^2 grows. However, it is interesting to notice how the CSI error-based region relaxation allows CEO-CIO R to outperform the non-robust approach over all the spectrum of δ^2 values. Moreover, we can see that the performance gap between the robust and non-robust version of CEO-CIO becomes more significant as the uncertainty over the CSI grows, while the gap between CEO-CIO R and CVX-CIO reduces as δ^2 grows. This is explained by the fact that, when the error bound δ^2 is very low, the deriving relaxation is less appreciable, hence leading CEO-CIO R to achieve similar performances to its non-robust counterpart. On the other hand, for higher values of δ^2, the CEO-CIO R is characterized by a more

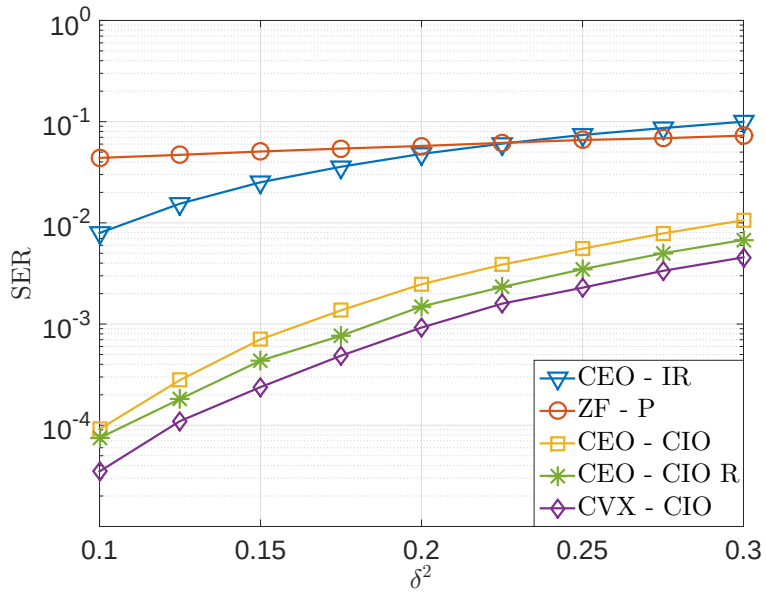

Figure 3.8: Symbol Error Rate for 8-PSK modulation when $M = 12$, $N = 64$ and $SNR = 10dB$ with imperfect CSI.

noticeable relaxation which leads to higher benefits, when compared to CEO-CIO.

In order to better represent the trade-off between complexity and performances offered by the proposed scheme CEO-CIO, the achievable SER is shown in Fig. 3.9 as a function of the per frame FLOPs count when considering an $SNR = 0dB$ and perfect CSI at the transmitter. More specifically, the size of the set of random states K is considered to gradually increase, as it directly affects the FLOPs count per frame shown in Table 3.1. When computing the FLOPs per-frame, for the sake of simplicity, we consider the frame length to be equal to the coherence time for downlink transmission $T_{DL} = 70$, in line with the LTE standard [98]. It is extremely important to highlight that, while the proposed scheme is required to evaluate the precoded signal at a symbol-rate, such need is shared by all the other CEP precoding schemes from the literature, for both single [17] and multiuser scenarios[18, 95–97]. As a consequence, we can see that for similar complexities, the proposed CEO scheme is able to greatly outperform its interference reduction counterpart, hence showing a very positive and interesting trade-off between complexity and performances.

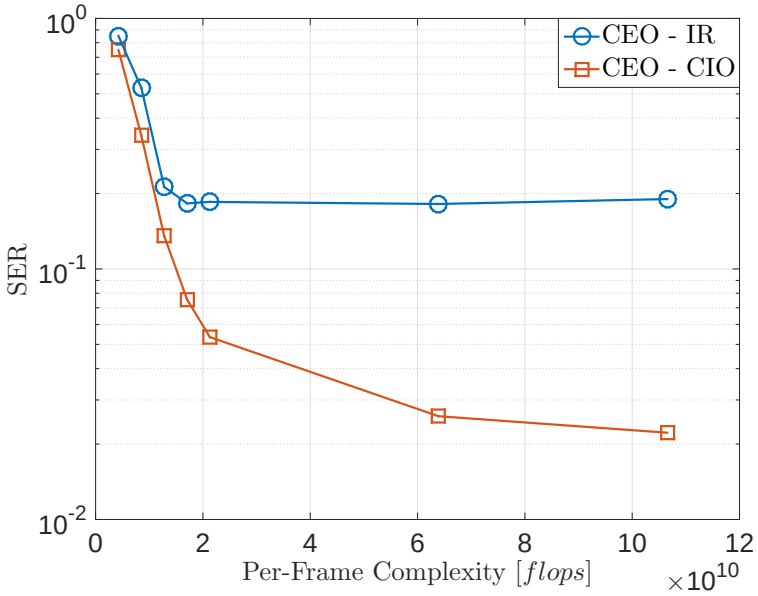

Figure 3.9: Symbol Error Rate for 8-PSK modulation when $M = 6$ and $N = 32$ and $SNR = 0dB$ as a function of FLOPs per-frame.

3.6.1 Constellation Energy

In previous simulations, the desired symbols are assumed to have unitary energy constellation, i.e., $d_m = d = 1, \forall m \in \{1, ..., M\}$. While this assumption is not uncommon in CEP literature [17, 18, 95, 97], the constellation energy can be increased to improve CEP-IR performances. This represents one of the key drawbacks of the CEP-IR approach, as its performances are strongly dependent on the constellation energy $E = d^2$. In fact, since the expected value of the MUI is a function of both topology (i.e., number of antennas at the BS and number of users) and modulation used in transmission [18], it is not possible to know a priori the optimal constellation amplitude d^*. More specifically, the identification of the optimal energy would require to dynamically estimate the SER at the transmitter side as a function of the constellation energy E, hence increasing the computational complexity of the system. Otherwise, the search for a sub-optimal constellation energy for CEO-IR could be performed at the transmitter side via an additional topology-dependent optimization problem [18]. The optimization

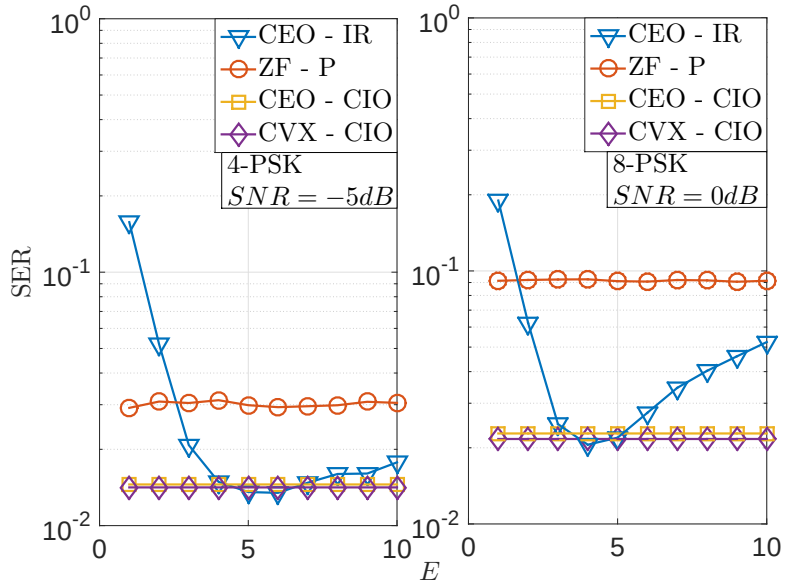

Figure 3.10: Symbol Error Rate as a function of the constellation energy $E = d_m^2 = d^2, \forall m \in \{1, ..., M\}$ when $M = 6$ and $N = 32$.

problem that identifies the optimal constellation amplitude d^* is defined as follows [18]

$$\begin{aligned} &\text{maximize} \quad d \\ &\text{subject to} \quad E\left\{\sum_{m=1}^{M}\left|\left(\sum_{n=1}^{N}\frac{h_{m,n}}{\sqrt{N}}e^{j\theta_n} - d_m e^{j\phi_m}\right)\right|^2\right\} \leq \gamma \\ &\qquad\qquad d_m = d, \forall m \in \{1, ..., M\} \end{aligned} \tag{3.42}$$

where $\gamma \geq 0 \in \mathbb{R}^+$ is a chosen threshold parameter to the MUI energy. The optimization problem aims to identify the maximum constellation energy that preserves the expected MUI energy within a desired threshold.

It is important to stress that the constellation energy is critical parameter for classic CEO-IR. These considerations are visually presented in Fig. 3.10 and Fig. 3.11, for the $M = 6, N = 32$ and $M = 12, N = 64$ scenario respectively. Both figures consider the perfect-CSI case, while similar results can be seen for the imperfect-CSI case. In fact, the aforementioned figures show that the performances of CEO-IR worsen as we incautiously increase the constellation energy d, with this effect being particularly visible for higher modulation orders such as 8-PSK. This is due to the fact that the MUI-based metric used for CEO-IR aims to minimize the energy of the interference signal (i.e.,

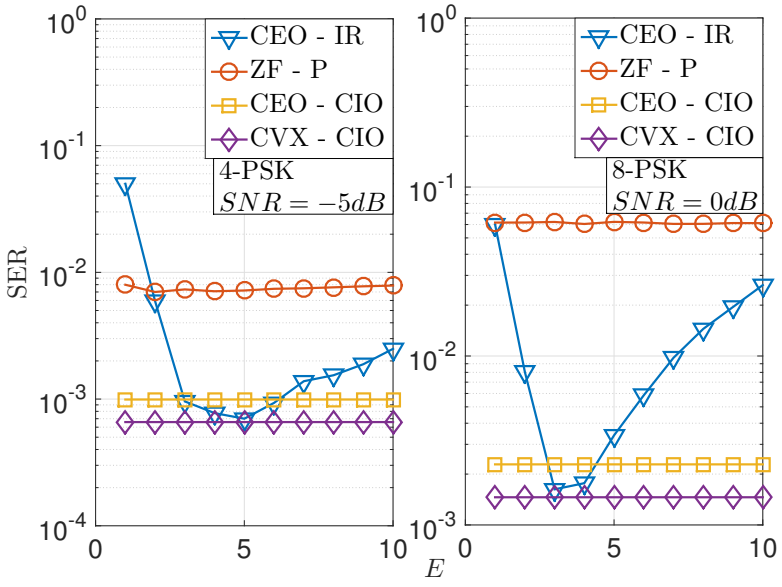

Figure 3.11: Symbol Error Rate as a function of the constellation energy $E = d_m^2 = d^2, \forall m \in \{1, ..., M\}$ when $M = 12$ and $N = 64$.

the distance between the received symbol and the corresponding desired constellation point), but fails to have any control over its phase $\mathfrak{U}\{t_m\}$. More specifically, CEO-IR metric is not affected by the phase of the received signal, which is particularly important for PSK modulated signals, as information is carried through the phases of the received signals, while their amplitude identifies their robustness against noise. Moreover, we can see that the optimal d^* changes when considering different scenarios and different modulations, supporting how it is not possible to identify d^* before transmitting.

On the other hand, the performances of the proposed techniques are not affected by the desired symbol energy, as they aim to maximize the constructive effects of interference over the received signal. Therefore, a critical benefit of the proposed scheme is that the additional optimization of E can be avoided, along with the significant associated computational costs. In fact, as shown in Fig. 3.10 and Fig. 3.11 the proposed techniques are able to outperform the classical CEO-IR for most of the energy spectrum. This is supported by the fact that the performances of the proposed metric are independent from the desired symbol energy as they allow a constrained portion of the interference at the user side. In other words, the proposed metric adaptively increases the received constellation in function of the current CSI, without the need to addition-

ally identify the optimal transmitted constellation energy, hence showing a very positive complexity-performance trade-off. Additionally, we can notice that the performance gap between CVX-CIO and CEO-CIO is larger for Fig. 3.11. This phenomenon is caused by the aforementioned different impact of the second-step normalization of CVX-CIO, which causes the performance gap to be more significant and beneficial for CVX-CIO when considering systems with larger arrays at the BS.

3.7 Conclusions

This chapter proposed two CEP schemes for downlink multiuser transmissions where interference is effectively exploited to greatly increase the received signal to interference and noise. The proposed techniques showed that a relaxation of the optimization region in function of the constructive interference can be beneficial to achieve reliable communications. The computational burdens of the proposed techniques have been analyzed in terms of FLOPs, and compared with the approaches from the literature, showing negligible differences. In addition, a precoding approach robust to bounded channel-state information errors that does not require to increase the transmitted power has been analytically derived and applied to scenarios where the base station possesses imperfect channel-state information. Finally, performances have been shown in terms of symbol error rate for different modulation orders, proving the benefits introduced by the proposed schemes when compared to classical CEP approaches with interference reduction.

Chapter 4

Low-Complexity Interference Exploiting Antenna Selection for Massive MIMO

In Massive MIMO technology, the number of radiating elements can increase up to few hundreds, performing secure, robust and energy-efficient communications [12]. However, the use of very large arrays leads to an increased and almost prohibitive hardware complexity in terms of RF chains, as they are accountable for 50-80% of the total transceiving power consumption [105]. Beside the application of CEP at the downlink transmission from the previous Chapter, antenna selection can be seen as an interesting approach to tackle the inherent hardware complexity of M-MIMO and, at the same time, exploit the higher degrees of freedom provided by the excess of antennas at the base station.

As described in Chapter 2, antenna selection (AS) in conventional MIMO system has been a key topic of research in the past years [15, 20], showing the benefits in terms of energy efficiency and performances of the use of a subset of antennas in transmission or reception[106]. These works, among many others, proved that AS can reduce the RF complexity at the transmitter/receiver. However, their computational costs increase together with the system size, limiting their direct applicability in multiuser M-MIMO

scenarios. Toward this end, recent works are studying the energy efficiency benefits offered by AS for large scale MIMO systems [107–109]. More specifically, the study in [110] proposes an energy efficiency approach toward AS, but the energy costs caused by the algorithms are not included in the analysis. In addition, the authors in [111] analyze the effects of AS with a random approach, while [112] proposes an AS algorithm based on Convex Optimization for a massively distributed antenna system.

This chapter introduces a novel low-complexity AS algorithm, specifically designed to operate in a multiuser M-MIMO scenario and to exploit constructive interference [80–83, 113]. In fact, the interference between the links of a MIMO system can be beneficial for the transmission and improve the performances in terms of signal detection by increasing the power of the desired signal. In the proposed scheme, the transmitter is able to predict multiuser interference and can use this knowledge to identify the subset of transmitting antennas for which interference is most constructive. The developed algorithm makes full use of the high antenna diversity offered by very large arrays and selects the subset that optimizes inter-channel interference, greatly reducing the number of RF chains required for transmission and increasing the energy efficiency of the system with a favorable trade-off between performance and complexity. The proposed technique is characterized by a reduced digital signal processing complexity, having overall computational burdens that are comparable or even lower than the ones of a full M-MIMO system with a simple MF or ZF precoding.

The contributions presented in the chapter can be listed in the following:

- Introduction of a novel and low-complexity AS algorithm for multiuser M-MIMO scenarios based on the concept of constructive interference;
- Analytical study of the computational complexity of the proposed scheme in comparison with previous approaches from the literature;
- Analytical derivation of the upper bound of the received SINR for each user, for the proposed AS algorithm;
- Performance evaluation of the proposed technique in terms of SER and an energy

efficiency metric that combines throughput with system power requirements.

4.1 System Model

In this chapter, we focus on the downlink transmission of a transmit AS-based multiuser scenario where the BS equips a very large array of N antennas with $N_{RF} \leq N$ RF chains to communicate with M single-antenna users. In accordance with the previous chapter, the channel response is modeled by a $\mathbb{C}^{M\times N}$ matrix, whose channel entries $h_{m,n}$ can be simply modeled as independent Rayleigh fading for a single-cell scenario [99]. Additionally, in an effort to achieve the highest efficiency and lowest computational complexity, the BS is assumed to perform only linear MF and ZF. Accordingly, in line with (2.15), the linearly precoded transmitted vector for a transmit AS-based system can be analytically defined as

$$\tilde{\mathbf{x}} = \mathbf{G}_e\mathbf{u} = \gamma_e\mathbf{F}_e\mathbf{u}, \tag{4.1}$$

where $\mathbf{G}_e$, $\mathbf{F}_e$ and γ_e identify the precoding matrix, precoding matrix without scaling and the scaling factor corresponding to the equivalent channel matrix $\mathbf{H}_e$, which is defined as

$$\mathbf{H}_e = \left[\underline{\mathbf{h}}_{1,e}, ..., \underline{\mathbf{h}}_{n,e}, ..., \underline{\mathbf{h}}_{N,e}\right]. \tag{4.2}$$

Here, the vector $\underline{\mathbf{h}}_{n,e}$ identifies the equivalent channel response corresponding to the n-th antenna and its entries can be either null, when the index n corresponds to a deactivated antenna, or equal to the channel response $\underline{\mathbf{h}}_n$, when corresponding to a selected antenna. Analytically

$$\underline{\mathbf{h}}_{n,e} = \begin{cases} \mathbf{0}^{M\times 1} & \forall n \notin \mathcal{N} \\ \underline{\mathbf{h}}_n & \forall n \in \mathcal{N}. \end{cases} \tag{4.3}$$

4.2 Proposed Constructive Interference Maximization Antenna Selection (CIM)

The proposed scheme combines low-complexity MF and AS to optimize the constructive interference at the receiver side, as defined according to the low-complexity metrics in (2.41). In Chapter 2, constructive interference for low-complexity metrics is defined according to the cross-correlation matrix $\mathbf{R} = \left(\mathbf{H}\mathbf{H}^H\right)$. More specifically, inter-channel interference for m-th user can be expressed to explicitly differentiate between constructive and destructive components as follows

$$ICI_m = \sum_{k=1,k\neq m}^{M} \rho_{m,k} u_k = C_m^{ICI} + D_m^{ICI} \tag{4.4}$$

where $\rho_{m,k}$ identifies the m-th element of the k-th column of $\mathbf{R}$ and C_m^{ICI}, D_m^{ICI} identify the constructive and destructive component of ICI.

Constructive and destructive ICI can be analytically expressed as

$$C_m^{ICI} = \sum_{k\in\mathcal{C}} \rho_{m,k} u_k \tag{4.5}$$

$$D_k^{ICI} = \sum_{k\in\mathcal{D}} \rho_{m,k} u_k. \tag{4.6}$$

where constructive and destructive subsets, i.e., $\mathcal{C}$ and $\mathcal{D}$, are defined in (2.42) and (2.43) for 2-PSK, (2.44) and (2.45) for 4-PSK and (2.46) and (2.47) for 8-PSK.

With the aim to exploit constructive interference energy, the transmitter can select the antenna subset that, within a channel realization, is characterized by the highest value of the minimum constructive interference. A straightforward application of AS would require to compute C_m^{ICI} for each user and select the minimum value for each of all the possible combinations of a subset of size N_{RF}. This simple approach becomes computationally prohibitive for systems with a high number of antennas and users, leading to $\binom{N}{N_{RF}} = \frac{N!}{N_{RF}!(N-N_{RF})!}$ possible subset combinations.

Accordingly, a low-complexity approach to interference-exploiting AS is proposed,

Algorithm 4.1 Constructive Interference Maximization for 2-PSK
Input: $\mathbf{H}$, $\mathbf{u}$, N_{RF}
Output: $\mathbf{H}_e$

- **for** $n = 1 \rightarrow N$
  - $\mathbf{R}_n = \underline{\mathbf{h}}_n \underline{\mathbf{h}}_n^H$
  - $[\phi_1, ..., \phi_m, ..., \phi_M]^T = \Re\left[\left(\mathbf{R}_n - diag\left\{\mathbf{R}_n\right\}\right)\mathbf{u}\right] \circ \mathbf{u}$
  - $\psi_n = \min\left\{\phi_1, ..., \phi_m, ..., \phi_M\right\}$
- **end**
- $\mathcal{N} = \arg\max_{N_{RF}} \left\{\psi_1, ..., \psi_n, ..., \psi_N\right\}$
- $\mathbf{H}_e = \left[\underline{\mathbf{h}}_{1,e}, ..., \underline{\mathbf{h}}_{n,e}, ..., \underline{\mathbf{h}}_{N,e}\right]$ as (4.3)

based on the property

$$\mathbf{H}\mathbf{H}^H = \sum_{n=1}^{N} \underline{\mathbf{h}}_n \underline{\mathbf{h}}_n^H = \sum_{n=1}^{N} \mathbf{R}_n, \tag{4.7}$$

where $\mathbf{R}_n$ identifies the n-th antenna cross-correlation and is computed according to n-th antenna channel response $\underline{\mathbf{h}}_n$.

Clearly, a symbol-by-symbol control of ICI is computationally prohibitive for highly populated scenarios, as it would require to compute constructive interference condition $M^2 - M$ times. In order to preserve a low computational complexity approach, the proposed AS scheme considers a new parameter ψ_n that defines the interference related to the n-th antenna. More specifically, for a 2-PSK modulated signal

$$\psi_n = \min\left\{\phi_m^{(n)}, \forall m\right\} = \min\left\{\Re\left[u_m\right]\Re\left[\sum_{k=1, k\neq m}^{M} \rho_{m,k}^{(n)} u_m\right], \forall m\right\} \tag{4.8}$$

where $\phi_m^{(n)} = \Re\left[u_m\right]\Re\left[\sum_{k=1,k\neq m}^{M} \rho_{m,k}^{(n)} u_k\right]$ is the decision metric for the n-th antenna and $\rho^{(n)}$ is used to identify the elements of $\mathbf{R}_n$. Finally, the algorithm proceeds to compute ψ_n for all the N available antennas, and selects the N_{RF} antennas that correspond to the highest values.

Algorithm 4.2 Constructive Interference Maximization for 4-PSK

Input: $\mathbf{H}$, $\mathbf{u}$, N_{RF}
Output: $\mathbf{H}_e$

- **for** $n = 1 \rightarrow N$
  - $\mathbf{R}_n = \underline{\mathbf{h}}_n \underline{\mathbf{h}}_n^H$
  - $\mathbf{t} = \left(\mathbf{R}_n - diag\left\{\mathbf{R}_n\right\}\right)\mathbf{u}$
  - $\left[\phi_1, ..., \phi_M\right]^T = \Re\left[\mathbf{u}\right] \circ \Re\left[\mathbf{t}\right] + \Im\left[\mathbf{u}\right] \circ \Im\left[\mathbf{t}\right]$
  - $\psi_n = \min\left\{\phi_1, ..., \phi_m, ..., \phi_M\right\}$
- **end**
- $\mathcal{N} = \arg\max_{N_{RF}} \left\{\psi_1, ..., \psi_n, ..., \psi_N\right\}$
- $\mathbf{H}_e = \left[\underline{\mathbf{h}}_{1,e}, ..., \underline{\mathbf{h}}_{n,e}, ..., \underline{\mathbf{h}}_{N,e}\right]$ as (4.3)

More specifically, the subset of selected antennas $\mathcal{N}$ can be defined as follows:

$$\begin{aligned} \mathcal{N} &= \arg\max_{N_{RF}} \left\{\min\left\{\Re\left[u_m\right] \Re\left[\sum_{k=1,k\neq m}^{M} \rho_{m,k}^{(n)} u_k\right], \forall m\right\}, \forall n\right\} \\ &= \arg\max_{N_{RF}} \left\{\min\left\{\phi_m^{(n)}, \forall m\right\}, \forall n\right\}. \end{aligned} \tag{4.9}$$

The selection technique is described analytically in Algorithm 4.1, where $\circ$ is used to identify the Hadamard product.

While (4.9) is specifically tailored for performing AS in a 2-PSK modulated scenario, constructive interference can also be used to enhance the received SINR of higher order PSK modulated transmissions. Considering the conditions for constructive ICI described in (2.44), the 4-PSK selection metric is defined as

$$\phi_{m,4PSK} = \Re\left[\left(\mathbf{R}_n - diag\left\{\mathbf{R}_n\right\}\right)\mathbf{u}\right] \circ \Re\left[\mathbf{u}\right] + \Im\left[\left(\mathbf{R}_n - diag\left\{\mathbf{R}_n\right\}\right)\mathbf{u}\right] \circ \Im\left[\mathbf{u}\right] \tag{4.10}$$

where the selected antennas subset $\mathcal{N}_{4PSK}$ is defined as

$$\mathcal{N}_{4PSK} = \arg\max_{N_{RF}} \left\{\min\left\{\phi_{m,4PSK}^{(n)}, \forall m\right\}, \forall n\right\}. \tag{4.11}$$

Selection for 4-PSK signaling is described analytically in Algorithm 4.2.

Unfortunately, because of the tightening on constructive interference conditions in (2.44), 4-PSK selection preserves part of the destructive interference components. Accordingly, this section introduces a hybrid approach that nullifies the remaining destructive interference components which could not be optimized through AS, while preserving the constructive interference benefits introduced by the selection algorithm. This is obtained via the definition of a constructive correlation matrix $\mathbf{R}_\phi$ whose entries can be analytically described as

$$\rho_\phi(n,m) = \begin{cases} \rho_{n,m} & \text{if } \rho_{n,m} \in \mathcal{C} \\ 0 & \text{if } \rho_{n,m} \notin \mathcal{C} \end{cases} \tag{4.12}$$

Hence, the equivalent precoding matrix is defined as [81]

$$\mathbf{G}_{e,HY} = \gamma_{e,HY} \mathbf{H}_e^H (\mathbf{H}_e \mathbf{H}_e^H)^{-1} \mathbf{R}_\phi \tag{4.13}$$

where $\mathbf{H}_e$ indicates the equivalent channel matrix after the AS and $\gamma_{e,HY} = \sqrt{1/tr\left[\mathbf{R}_\phi^H (\mathbf{H}_e^H \mathbf{H}_e)^{-1} \mathbf{R}_\phi\right]}$ represents the corresponding scaling factor [81].

4.3 System Computational Complexity

One of the effects brought by the use of hundreds of antennas in M-MIMO systems is a significant increase in computational costs, even when linear precoding techniques are involved in the transmission. This section studies the complexity of precoding and AS techniques of all the considered transceiving configurations in terms of floating-point operations per second (FLOPs), following the analysis in [114], based on the costs listed in the literature [115].

The proposed approaches are compared with several schemes where linear precoding is performed in cascade with AS algorithms from the literature. More specifically, in line with Chapter 2, the following algorithms are considered

- the low-complexity path gain maximization [40, 116] algorithm

- the recursive capacity maximization [38] algorithm
- a reduced complexity approach to the minimum eigenvalue [39] algorithm. Unfortunately, MEM, as proposed in [39] and described in Chapter 2, is computationally prohibitive for M-MIMO scenarios because of its exhaustive search-based approach. Accordingly, following the work in [117], a decremental approach to minimum eigenvalue maximization is considered, where the algorithm iteratively identifies the antenna whose deactivation leads to the intermediate subset with the largest smallest eigenvalue λ_{min}.

In particular, a thorough analysis of linear precoding techniques costs for systems that do not involve AS is first presented, then followed by a study of the computational burden of the schemes that involve the AS techniques presented in the chapter.

4.3.1 Precoding

The dominant costs of ZF precoding can be identified in the following steps:

- Compute the correlation matrix $\mathbf{R} = \mathbf{H}\mathbf{H}^H$
- Compute the inverse of $\mathbf{R}$
- Multiply $\mathbf{R}^{-1}$ by $\mathbf{H}^H$
- Apply the precoding matrix $\mathbf{G}_{ZF}$ to the data $\mathbf{u}$

The number of operations necessary for each step of the precoding procedure depends on the matrix size [115]. Matrix inversion is particularly expensive, as its computational complexity grows exponentially with the size $\frac{8}{3}M^3$, but it is computed only once per coherence time. At the same time, the precoding procedure in M-MIMO becomes significant for the complexity count. In fact, due to the size of the matrices involved, the costs of the precoding $\mathbf{G}_{ZF}\mathbf{u}$ become particularly relevant in the final computational count. Additionally, since the precoding operation is dependent on the desired symbols vector $\mathbf{u}$, it has to be performed on a symbol-by-symbol basis and is further characterized by a factor T_{DL}.

Full System with ZF		**Full System with MF**	
$\mathbf{R}$	$M(2M+1)(4N-1)$	$\mathbf{G}_{MF}$	MN
$\mathbf{R}^{-1}$	$\frac{8}{3}M^3$	$\mathbf{G}_{MF}\mathbf{u}$	$T_{DL}2N(4M-1)$
$\mathbf{G}_{ZF}$	$4MN(4M-1)$	–	–
$\mathbf{G}_{ZF}\mathbf{u}$	$T_{DL}2N(4M-1)$	–	–
Total	$2(M^2+M)(4N-1)+\frac{8}{3}M^3+$ $4MN(4M-1)+T_{DL}2N(4M-1)$	**Total**	$MN+T_{DL}2N(4M-1)$
PGM Ant. Sel. with ZF		**CIM Ant. Sel. with MF**	
$\mathbf{H}\mathbf{H}^H$	$N(2N+1)(4M-1)$	$\mathbf{R}_n$	$NM(2M+1)$
$\mathbf{H}_e$	N	ψ_n	2-PSK: $T_{DL}NM(2M-3)$
$\mathbf{R}$	$M(2M+1)(4N_{RF}-1)$		4-PSK: $2T_{DL}NM(2M-3)$
$\mathbf{R}^{-1}$	$\frac{8}{3}M^3$	$\mathbf{H}_e$	$T_{DL}N$
$\mathbf{G}_{ZF}$	$4MN_{RF}(4M-1)$	$\mathbf{G}_{MF}\mathbf{u}$	$T_{DL}2N_{RF}(4M-1)$
$\mathbf{G}_{ZF}\mathbf{u}$	$T_{DL}2N_{RF}(4M-1)$	–	–
Total	$(4M-1)(2N^2+N+4MN_{RF}+2N_{RF}T_{DL})+$ $(2M^2+M)(4N_{RF}-1)+\frac{8}{3}M^3+N$	**Total**	2-PSK: $NM(2M+1)+T_{DL}NM(2M-3)+$ $T_{DL}N+T_{DL}2N_{RF}(4M-1)$
CM Ant. Sel. with ZF			
$\mathbf{B}$	$M(2M+1)(4N-1)+2M+\frac{8}{3}M^3$		
$\mathbf{A}\mathbf{B}\mathbf{A}^H$	$\sum_{l=1}^{N-N_{RF}}[4(N-l)M(4M-1)+(N-l)[2(N-l)+1](4M-1)]$		
$\mathbf{B}$	$\sum_{l=1}^{N-N_{RF}}[2M(4M-1)+(4M-1)+4M(4M-1)+M^2]$		
$\mathbf{H}_e$	$\sum_{l=1}^{N-N_{RF}}(N-l)$		
$\mathbf{R}$	$M(2M+1)(4N_{RF}-1)$		
$\mathbf{R}^{-1}$	$\frac{8}{3}M^3$		
$\mathbf{G}_{ZF}$	$4MN_{RF}(4M-1)$		
$\mathbf{G}_{ZF}\mathbf{u}$	$T_{DL}2N_{RF}(4M-1)$		
Total	$\sum_{l=1}^{N-N_{RF}}[4(N-l)M(4M-1)+(N-l)[2(N-l)+1](4M-1)]+\frac{16}{3}M^3$		
	$\sum_{l=1}^{N-N_{RF}}[2M(4M-1)+(4M-1)+4M(4M-1)+M^2+(N-l)]+2M$		
	$(2M^2+M)(4N+4N_{RF}-2)+(4M-1)(4MN_{RF}+2N_{RF}T_{DL})$		
MEM Ant. Sel. with ZF			
$\mathbf{R}$	$\sum_{l=1}^{N-N_{RF}}M(2M+1)(4(N-l)-1)$		
λ_{min}	$\sum_{l=1}^{N-N_{RF}}[M+(N-l)(\frac{64}{3}M^3+4M^2)]$		
$\mathbf{H}_e$	$\sum_{l=1}^{N-N_{RF}}M$		
$\mathbf{R}$	$M(2M+1)(4N_{RF}-1)$		
$\mathbf{R}^{-1}$	$\frac{8}{3}M^3$		
$\mathbf{G}_{ZF}$	$4MN_{RF}(4M-1)$		
$\mathbf{G}_{ZF}\mathbf{u}$	$T_{DL}2N_{RF}(4M-1)$		
Total	$\sum_{l=1}^{N-N_{RF}}[M(2M+1)(4(N-l)-1)+2M+(N-l)(\frac{64}{3}M^3+4M^2)]+$ $(2M^2+M)(4N_{RF}-1)+\frac{8}{3}M^3+(4M-1)(4MN_{RF}+2N_{RF}T_{DL})$		

Table 4.1: Computational costs of different schemes in FLOPs

In opposition to zero forcing, MF precoding is based only on the computation of the Hermitian transpose of the channel matrix and its application to $\mathbf{u}$. As a consequence, main costs of MF reside in the application of precoding to the data signal vector $\mathbf{u}$.

4.3.2 Antenna Selection

4.3.2.1 PGM Antenna Selection

The PGM algorithm has low complexity, since it is characterized by two operations only: the computation of the antenna path gains from the diagonal of the matrix $\mathbf{H}^H\mathbf{H}$, and the identification of the N_{RF} highest values.

4.3.2.2 CM Antenna Selection

The CM algorithm has a very high complexity as its key operations are especially demanding. In particular, we need to: compute the matrix $\mathbf{B} = \left(\mathbf{I}_M + SNR \cdot \mathbf{H}\mathbf{H}^H\right)^{-1}$, select the minimum value of δ_n and, finally, update the matrix $\mathbf{B}$. Main costs reside in the iterative nature of this approach, as it leads to the need to repeat each of these steps $N - N_{RF}$ times. Since the sizes of the channel matrix at intermediate stages $\bar{\mathbf{H}}$ change at each iteration of CM, the computational costs of this technique require the use of a summation, whose elements are a function of the iteration number and N_{RF}.

4.3.2.3 MEM Antenna Selection

The MEM algorithm is affected by the highest computational costs as it requires to compute the eigenvalues of intermediate stages correlation matrices several times within a single iteration. More specifically, MEM is characterized by $N - N_{RF}$ iterations, each one characterized by the necessity to compute $N - l$ times the eigenvalues of $\bar{\mathbf{H}}^H\bar{\mathbf{H}}$, where l is the iteration step. In order to evaluate the computational burdens of MEM, a tridiagonal QR algorithm is assumed for the computation of the eigenvalues, with the assumption that $\mathbf{R}$ has been previously reduced to a tridiagonal form [118].

The costs of this approach are particularly high and nearly prohibitive for M-MIMO.

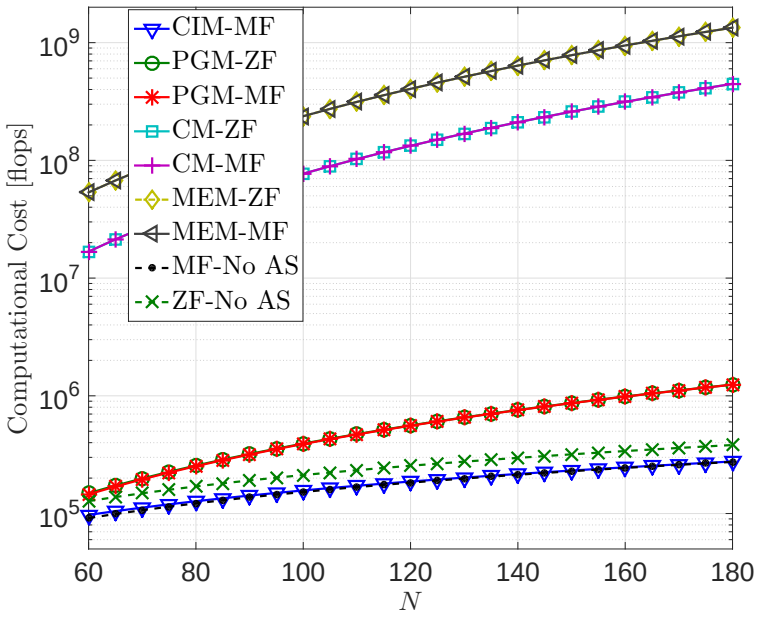

Figure 4.1: Computational costs as a function of the number of antennas at the transmitter N for a 2-PSK modulated system with $M = 5$, $N_{RF} = M$.

4.3.2.4 Proposed Constructive Interference Maximization (CIM) Antenna Selection

The computational costs for CIM can be identified mainly in the following steps:

- Compute the antenna cross-correlation matrix $\mathbf{R}_n = \underline{\mathbf{h}}_n \underline{\mathbf{h}}_n^H$
- Compute the decisional parameter ψ_n
- Identify maximum values of ψ_n

A detailed study of the computational burden of the proposed transceiving schemes, within a single T_{cohe}, is reported in Table 4.1, along with the total complexity of each of the AS schemes.

Table 4.1 does not include the computational studies for the MF precoding over PGM, CM and MEM selection for the sake of brevity, since they can be easily obtained by substituting the $\mathbf{R} \rightarrow \mathbf{G}_{ZF}\mathbf{u}$ steps with the $\mathbf{G}_{MF}\mathbf{u}$ step of the proposed scheme.

4.3.3 Transceiver Computational Costs Analysis

From Table 4.1 we can see that computational costs for linear precoding in a classical MIMO system reside mostly in the identification of the precoding matrix $\mathbf{G}$. In fact, costs for the application of data precoding in classic multiuser MIMO are less relevant because of the reduced sizes of the system. However, this is not true for M-MIMO, where the number of antennas is much larger than the number of users, hence leading to computational costs for precoding application that are directly proportional to N. This uncovers additional benefits brought by AS, as costs for precoding are strongly reduced. At the same time, it is important to highlight that the proposed AS is affected by the necessity to repeat the algorithm for each T_{DL} because of its data dependent nature. Nonetheless, the higher costs of data dependent AS over classical M-MIMO are mitigated by the higher T_{CSI} that characterizes such systems. It is important to stress that the values shown in Table 4.1 are computed for a single coherence time, while considering the renew frequency of data dependent operations. In fact, since precoding and the proposed AS have to be repeated at a symbol rate, they are characterized by a T_{DL} factor, typically on the order of 4 OFDM symbols for a fast-fading M-MIMO scenario [11]. On the other hand, the costs of classical AS algorithms are considered only once per coherence time, as they compute costly metrics that are dependent on the channel realization.

The selection metric of the proposed algorithm changes according to the constellation order used at the transmitter, leading to different complexities, as presented in Table 4.1. Nevertheless, as shown in Algorithm 4.2, we can note that the difference between 2-PSK and 4-PSK metric is identified only in the need to compute the interference metric for both real and imaginary part. In addition, the algebraic property in (4.7) is independent from the constellation used and its cost represents an important component of the global burden of the algorithm, significantly reducing the differences between the two cases.

The effects described can be observed in Fig. 4.1, which shows the computational costs in FLOPs as a function of the number of antennas at the BS N, when the number

of users is fixed to a specific value of M. In particular, Fig. 4.1 represents a fast fading scenario, i.e. T_{cohe} is shorter than a frame, with $M = 5$ users, subset size equal to the number of users $N_{RF} = 5$ and TDD is characterized by the parameters: $T_{cohe} = 100$, $\mu = 2$ and $\eta_{DL} = 50\%$. The values used correspond to a coherence time $t_{cohe} \approx 7ms$ when considering current LTE standards for frame time $t_f = 10ms$ and symbol time $t_s = 71.4\mu s$ [11] with a single carrier transmission scheme. This assumption is not uncommon in the study of energy efficient systems, as recent works over large-scale MIMO systems [119] showed the energy efficiency benefits of single-carrier transmission schemes. More specifically, [119] shows that multi-carrier OFDM modulation has a very high PAPR, which requires the RF power amplifiers to work within an operating regime where they have low efficiency. Toward this end, the use of CEP [18] for massive MIMO system has further shown the energy efficiency benefits of single carrier communications. In fact, as shown in Chapter 3, single carrier communications with CEP at the transmitter allow the use of energy efficient/non-linear RF components. From Fig. 4.1, we can see that previous selection techniques are characterized by high costs, due to the size of the system, leading to near overlapping curves for ZF and MF. It is interesting to notice that the proposed technique has always lower costs than all the other approaches and that the difference in costs increases as the number of antennas at the BS grows.

Note that the computational costs presented in Fig. 4.1 represent the overall FLOP count required by the systems described in the legend, including both the precoding costs and the AS costs, where applicable. Simple massive MIMO approaches, ZF - No AS and MF - No AS in the legend, are characterized only by zero forcing and matched filter precoding costs respectively, as they do not involve AS algorithms. On the other hand, the computational burden for AS systems include both precoding and selection algorithm. In fact, AS systems are identified in the legend according to the following notation: the first acronym for the AS algorithm, while the latter represents the precoding technique considered.

Given the data dependent/interference based nature of CIM selection, its performances in terms of computational costs are affected by the length of T_{cohe}. As we would expect, computational costs increase as the number of transmitted symbols per coher-

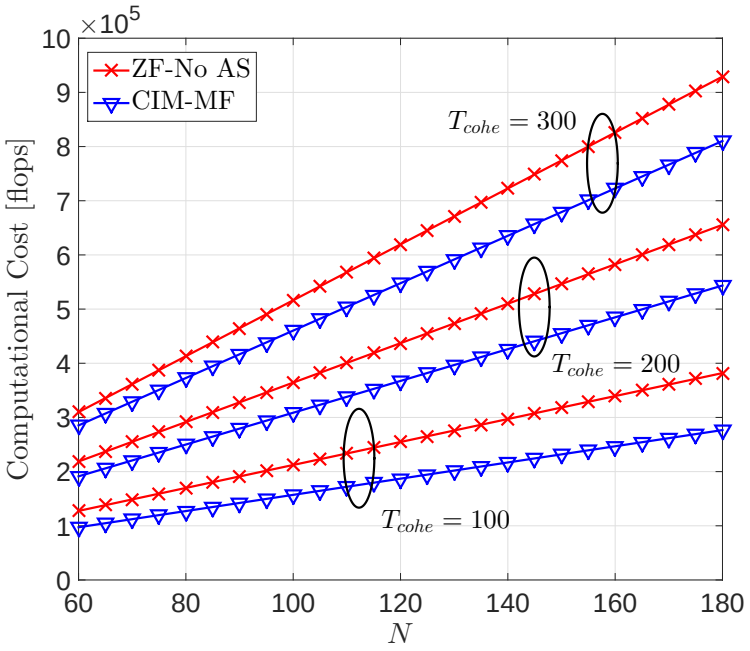

Figure 4.2: Computational costs as a function of T_{cohe} for a 2-PSK modulated system with $M = 5$, $N_{RF} = M$.

ence time becomes larger, but with a lower ratio than the classical MIMO approach with ZF. This effect is well described in Fig. 4.2, which shows the computational costs for different values of T_{cohe} for both approaches. In this figure, only the costs of CIM selection and the full system with ZF are considered, as results in Fig. 4.1 show that AS algorithms of the literature experience computational burdens that are one or more orders of magnitude higher than the proposed technique.

Note that the proposed AS algorithm requires a fast, symbol rate, RF switching. Due to the criticality of this element, it is important for the RF switching to be performed with low insertion losses. Toward this end, recent developments in hardware design show that GaN MMIC based switches by TriQuint [120] can achieve switching speeds on the order of ns, while offering promising performances in terms of insertion losses. In a similar manner, solid-state RF switches represent a widely used technology in modern communication systems and are able to provide switching speed inferior to $1\mu s$ [121].

In addition, it is important to state that fast symbol-rate RF switching schemes require time and bandwidth limited pulses [122] to tackle possible spectral regrowth. This cannot be realized through conventional shaping filters, such as the raised-cosine, as they

are bandwidth limited and time unlimited. The design of time-limited orthogonal shaping filters was first introduced for Ultra Wide Band (UWB) systems[123–125], showing that it is possible to achieve pulses which are limited in time and in frequency. It is important to stress that the algorithms proposed in [123–125] are not UWB-dependent, as they can be tuned to respect desired time and spectral constraints, as for the proposed scheme. More specifically, the authors in [123] present a pulse shaping methodology based on the Hermite functions, while [124] presents an algorithm based on the numerical solution of the convolution between pulse and filter responses. Finally, the study in [125] presents a convex optimization metric for a DSP based pulse shaping. In addition to these works, the recent study in [122] presents a thorough analysis of the performances of different time-limited shaping filters and applies the design to a multi-antenna system that employs symbol rate RF switching.

These critical advances have fuelled the interest over single RF-chains techniques [126], which require symbol rate switching, as for Spatial Modulation MIMO (SM-MIMO)[1] [127], Space Shift Keying (SSK)[2] [122] and electronically steerable parasitic array (ESPAR)[3] communications [128]. These techniques have been successfully implemented in real systems, in [129] for SM-MIMO and [130] for ESPAR, proving how transmission schemes with similar requirements can offer increased values of energy efficiency in modern communication systems.

[1]In Spatial Modulation MIMO, a single RF chain and an antenna array are used to simultaneously transmit multiple symbols. The RF chain switches among the antennas at symbol rate, in order to modulate the information symbols over a PSK/QAM symbol and over the antenna chosen for transmission.

[2]In SSK transmission, the information bits are mapped over the index of a single radiating transmit antenna. The system switches at a symbol rate between the available antennas according to the data to be transmitted, while all the other antennas radiate no power.

[3]Over ESPAR MIMO communications, it is possible to transmit multiple streams over a single RF chain by adaptively exploiting the beam pattern characteristics of the arrays involved at the transmitter side. In fact, while the ESPAR antenna explicitly transmits a PSK/QAM symbol, additional symbols are analogically modulated by the antenna pattern, which is modified by exploiting the mutual coupling.

4.4 Performance Analysis of CIM selection with MF precoding

In order to study the performances achieved by the proposed technique, the upper bound of the average SINR for a single user is derived. Consider the received signal for the m-th user when the base station employs CIM

$$y_m = \gamma_{e,MF} \mathbf{h}_m^T \mathbf{g}_{m,e} u_m + n_m \tag{4.14}$$

where $\mathbf{g}_{m,e}$ identifies m-th column of the equivalent $\mathbb{C}^{N \times M}$ precoding $\mathbf{G}_e$ and n_m is the m-th entry of the noise vector $\mathbf{n}$.

Theorem 4.4.1 *The received SINR of a downlink multiuser transmission under CIM selection with MF precoding is characterized by the following upperbound*

$$\widetilde{\xi_m} = \frac{M(M+1) + M(M-1)(1+\sqrt{M\pi} + (M-2)\pi/4)}{N_{RF} M N_0} \tag{4.15}$$

Proof of Theorem 4.4.1 The proof can be found in Appendix A.

The analysis of the received SINR can be used to derive a lower bound for the symbol error probability. This can be easily computed for the proposed scheme by substituting in (2.39) both the order modulation L and the final received SINR derived in (4.15).

4.5 Results

The performances obtained by the proposed AS technique are evaluated through Monte Carlo simulations over 50000 channel realizations. A single-cell downlink scenario with perfect CSI at the transmitter side is considered, where the BS is equipped with an antenna array of $N = 100$ elements and communicates with $M = 5$ single-antenna mobile users. The BS is assumed to possess a fixed number of RF chains N_{RF}, equal to the number of users M. In the simulations, both 2-PSK and 4-PSK modulations are employed.

All the schemes described in the figures are characterized by a cascade of AS and precoding at the transmitter, with the exception of simple massive MIMO approaches here used as performance references. Legends have been conventionally defined to first declare the AS performed: CIM to identify the proposed selection technique, PGM when the subset is defined according to the path gain, CM for the capacity maximization and MEM for the minimum eigenvalue maximization selection. Finally, precoding techniques are identified as follows: ZF and MF for zero forcing and matched filter precoding, respectively, and HY to identify the hybrid approach for 4-PSK transmissions. Precoding schemes followed by No AS identify classical massive MIMO approaches where the BS uses all the available antennas.

Fig. 4.3 and Fig. 4.4 show the SER performances as a function of the transmitted $SNR = 1/N_0$ for all the configurations described, with 2-PSK and 4-PSK signaling, respectively. Performances in terms of SER for both cases are higher when no AS at the transmitter is involved, but they are achieved thanks to a higher hardware complexity, as previously shown. All previous AS techniques with MF are characterized by strong losses in performances when N_{RF} equals the number of users.

It is interesting to notice how in Fig. 4.3, PGM selection is characterized by strong losses even with ZF precoding at the transmitter. Always in Fig. 4.3, we can see that MEM and CM approaches with ZF achieve good performances as the SNR grows, but at the expenses of high computational costs, which are nearly prohibitive for practical systems. On the other hand, the proposed scheme, CIM with MF, shows only minor losses in performances when compared to the full system with both ZF and MF, while using only M of the N antennas available at the transmitter.

Fig. 4.4 shows the performances of the proposed algorithm in a 4-PSK modulated scenario, when the antenna subset $N_{RF} = 10$ and $M = 5$. The performances achieved by the proposed scheme for 4-PSK are identified by the curve that corresponds to CIM-HY in the legend. As we can see, the proposed scheme follows similar performances to the previous and prohibitive AS techniques of the literature, showing a positive trade-off between complexity and performance. It is pivotal to highlight that the shown

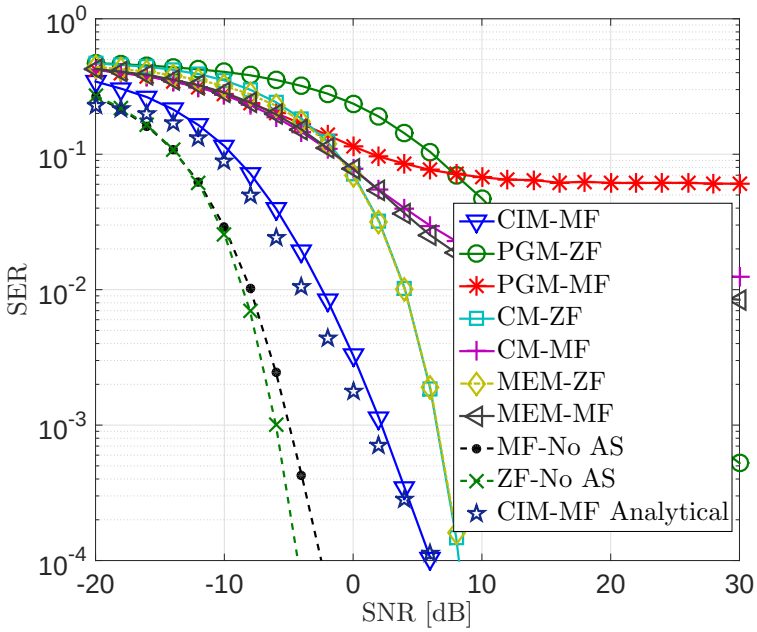

Figure 4.3: SER as a function of the transmitted SNR for 2-PSK modulation when $N = 100$, $M = 5$ and $N_{RF} = 5$.

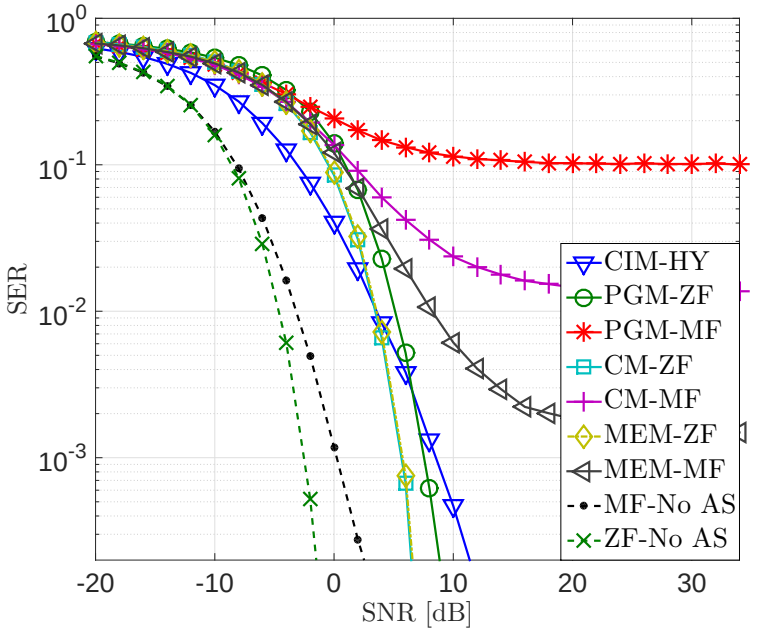

Figure 4.4: SER as a function of the transmitted SNR for 4-PSK modulation when $N = 100$, $M = 5$ and $N_{RF} = 10$.

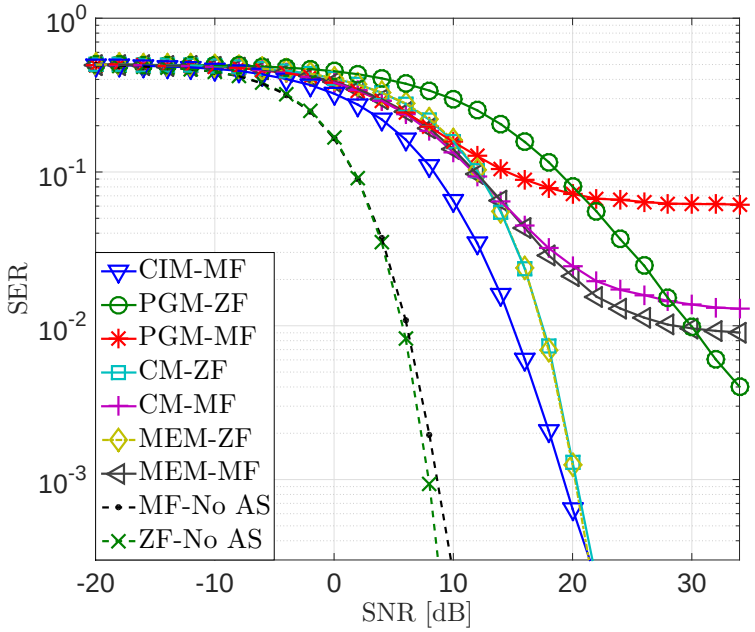

Figure 4.5: SER as a function of the transmitted SNR for 2-PSK modulation when $N = 100$, $M = 5$ and $N_{RF} = 5$ with imperfect CSI at the transmitter $\alpha = 10$.

performances for CIM-HY are achieved with significantly lower computational costs than CM or MEM, for both MF and ZF cases. In addition, we can see that previous AS systems that employ MF are affected by error floors. This behavior, distinctive for MF precoding and here kept for the sake of completeness, is caused by the inability of previous AS techniques to optimize the destructive effect of interference.

In Fig. 4.5 the proposed scheme is further characterized for the case where imperfect CSI is considered at the base station. During AS and precoding, the BS is assumed to be aware of an estimated channel matrix, defined analytically as follows [131]

$$\widehat{\mathbf{H}} = \mathbf{H} + \mathbf{E} \tag{4.16}$$

where $\mathbf{E} \sim \mathcal{CN}(0, \beta)$ is the error matrix, statistically independent from $\mathbf{H}$, and $\beta = \frac{\alpha}{SNR} = \alpha \cdot N_0$ is the variance of the estimation error for a TDD system, with α being an inverse proportionality coefficient [131]. Fig. 4.5 shows that for a system with $\alpha = 10$, the performances of the proposed technique are affected by the errors in the channel estimation. However, it is fundamental to highlight how the performance trend

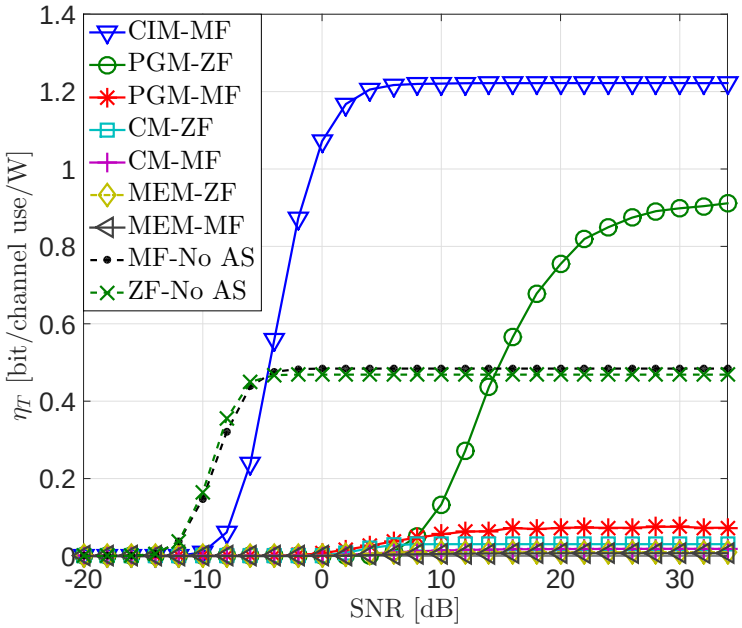

Figure 4.6: Energy efficiency over throughput as a function of the transmitted SNR for 2-PSK modulation when $N = 100$, $M = 5$ and $N_{RF} = 5$.

of the proposed scheme follows the one of a system when perfect CSI is available at the transmitter.

In order to better illustrate the benefits brought by the proposed scheme and the performance-complexity trade-off, we evaluate the achieved energy efficiency over throughput η_T, according to (2.21). When computing (2.21), we consider complexity values reported in Table 4.1 and we model hardware consumption from practical systems [45, 132], where $P_{amp} = P_t/\nu$ is defined as the power required by an amplifier with $\nu = 0.35$ efficiency in order to have a transmitted power $P_t = 30dBm$, $P_{RF} = 65.9mW$ and $P_{fpga} = 5.76mW/KFLOPs$.

Fig. 4.6 describes the results in terms of energy efficiency over throughput for a 2-PSK scenario, showing that the proposed approach is characterized by higher values of efficiency than all the other techniques, including the system without selection for both ZF and MF precoding. The higher energy efficiency of CIM-MF is supported by the lower hardware complexity it requires, which leads to reduced values of power at the denominator in (2.21), while achieving similar performances in terms of throughput. In addition to the computational savings, the proposed approach with CIM AS is able to

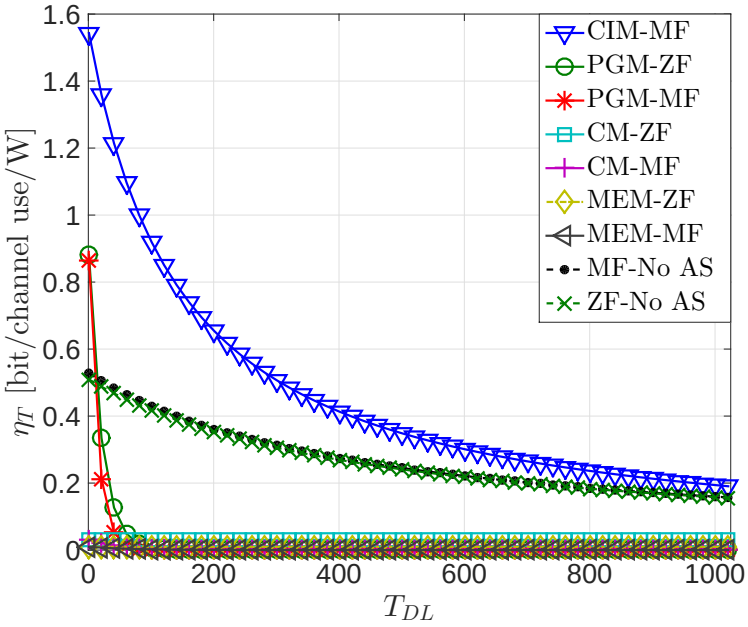

Figure 4.7: Energy efficiency over throughput as a function of the transmitted symbols T_{DL} when $SNR = 10dB$, $N = 100$ and $M = 5$.

achieve the shown performances with only 5% of the RF power required by full system BS, i.e., when no AS is involved. On the other hand, we can see that previous AS algorithms are characterized by very low energy efficiency because of the high computational burdens they are affected by. In fact, the increased power consumed by the FPGA is high enough to overcome the RF power savings.

Figure 4.7 presents the energy efficiency as a function of the number of single carrier symbols during the downlink T_{DL} when $SNR = 10dB$. As we can see from Fig. 4.7, the proposed technique CIM-MF maintains higher performances than the other approaches for increasing values of T_{DL}. The performance gap between CIM-MF and the systems without AS reduces as T_{DL} grows, however it is important to highlight that the proposed scheme keeps outperforming the classical MIMO approach until $T_{DL} \approx 1000$. These values of T_{DL} correspond to an OFDM modulated scenario with coherence time of 10 OFDM symbols with 256 sub-carriers. In fact, if we consider a $T_{cohe} = 10$ OFDM symbols and $T_{CSI} = 2$ OFDM symbols, we would have a $T_{DL} = 4$ OFDM symbols ($T_{DL} = 4 * 256$ sub-carriers roughly corresponds to $T_{DL} = 1000$ symbols). These values are often used when analyzing massive MIMO systems, as in the work by [51] where a

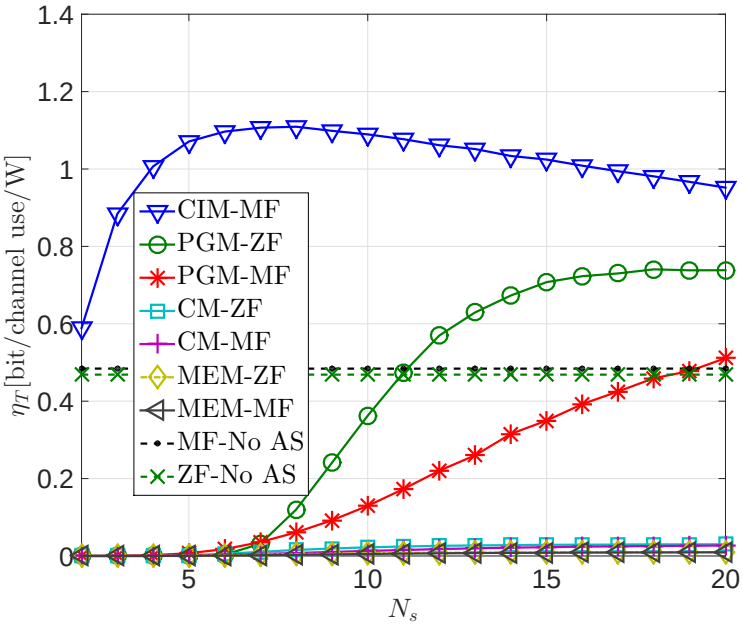

Figure 4.8: Energy efficiency over throughput as a function of the subset size N_{RF} when $SNR = 0dB$, $N = 100$ and $M = 5$.

coherence time with $T_{cohe} = 7$ OFDM symbols is considered.

In order to identify the subset size that optimizes the trade-off between complexity and performances, the energy efficiency is studied as a function of N_{RF}. As shown in Fig. 4.8, $N_{RF} = M$ proves to be a near optimal choice, as the CIM-MF curve presents a peak around $N_{RF} = 6/7$. Given the negligible efficiency gap between $N_{RF} = M = 5$ and $N_{RF} = 7$, the simple case where one transmit antenna is assigned to each user is considered. In addition, it is interesting to notice how the full system outperforms all the previous AS algorithms, with the exception of PGM, independently from the choice of N_{RF}. This is justified by the high complexity of MEM and CM, whose power consumptions overcome the savings introduced by the use of a subset of RF chains. To this end, Fig. 4.9 shows the power consumption of all the transmission schemes presented in the chapter. Circuit power values required by CM and MEM are characterized by very high consumptions, rapidly increasing towards the KW scale. On the other hand, the proposed technique shows low power consumption values which lie below the full system approaches, requiring $\sim 6.2W$ less than the MF without selection for the case studied by our simulations, i.e. when $N = 100$, $M = 5$ and $N_{RF} = 5$.

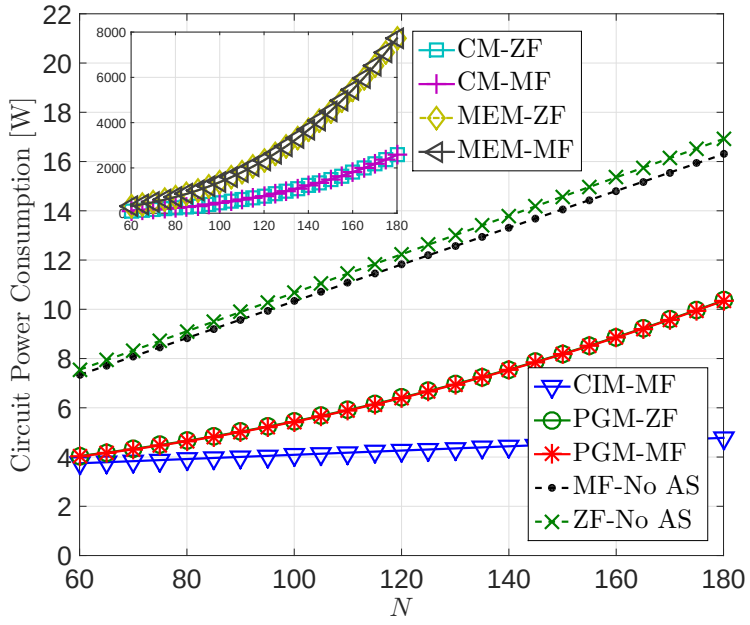

Figure 4.9: Circuit power consumption at the BS as a function of the arrays size N for a system with $M = 5$ mobile stations and $N_{RF} = 5$.

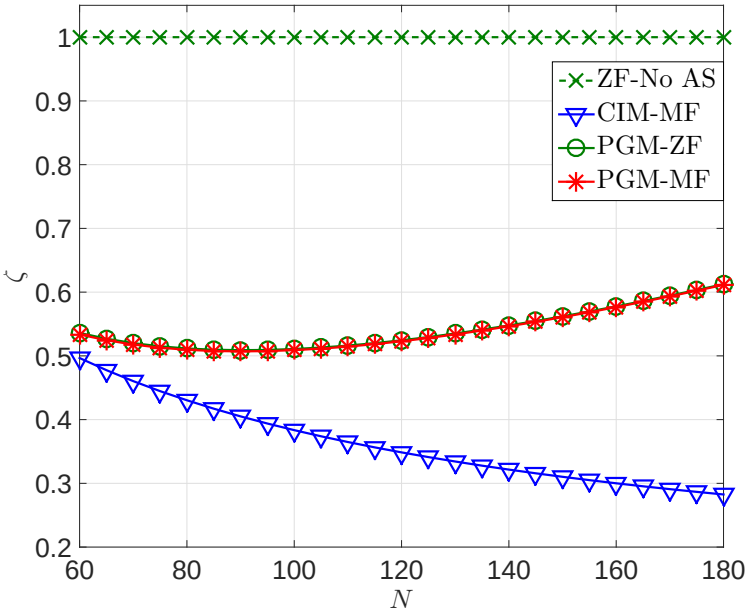

Figure 4.10: RF Power Savings ζ as a function of the arrays size N at the transmitter for a system with $M = 5$ mobile stations and $N_{RF} = 5$.

Fig. 4.10 is presented to clarify the benefits introduced by the proposed technique by showing the power savings $\zeta = P/P_{ZF}$ over a M-MIMO system that involves ZF, where P represents the power consumption of the studied technique and P_{ZF} is used to identify the power required by the full system with ZF. For the sake of simplicity the same scenario is considered, where $M = 5$, $N_{RF} = 5$ and the RF chains power values are modeled as in (2.21). From Fig. 4.10 it is clear that the proposed technique CIM-MF is less affected by the increased number of antennas at the transmitter because of the low complexity of the selection technique, since ζ decreases significantly as N increases. In particular, we can notice a power saving of $\zeta = 0.38$ for the scenario considered, where $N = 100$, $M = 5$ and $N_{RF} = 5$ with 2-PSK transmission, meaning that the performances are achieved with $\sim 62\%$ less power. At the same time, we can see how the other low-complexity approach PGM is characterized by increasing levels of power consumption at the base station, since the curves for both MF and ZF present values that grow towards the equal consumption $\zeta = 1$ threshold as the array size at the BS N increases.

4.6 Conclusions

This chapter proved that antenna selection and constructive inter-channel interference concepts can be jointly used to improve energy efficiency performances of M-MIMO. It was shown through analytical and numerical studies that constructive interference at the receiver side can be optimized by efficiently identifying a subset of antennas at the BS. Performances of the proposed algorithm have been evaluated in terms of symbol error rate and an energy efficiency metric that combines throughput and power requirements to analyze the trade-offs introduced. The presented system was further characterized by confirming the numerical results through the derivation of a closed form expression of the SER, when received SINR is considered equal to its analytical upper-bound.

Chapter 5

Large Scale Antenna Selection and Precoding for Interference Exploitation

The previous chapter showed that the hardware complexity deriving from the use of very large antenna arrays in M-MIMO can be tackled by means of TAS. Since a direct application of MU-MIMO AS techniques to massive systems can be impractical in terms of computational costs, see Chapter 4, recent works focused on AS algorithms precisely designed for M-MIMO systems [107, 108, 133, 134]. More specifically, the work in [110] presents an AS study under the perspective of energy efficiency, while the authors in [111] study a random selection approach. Finally, [112] and [133] proposed the use of Convex Optimization for M-MIMO AS systems, for a massively distributed antenna system and for channel capacity optimization, respectively.

Conventionally, TAS-based MU-MIMO systems approach selection and downlink precoding as two disjointed optimization problems. In fact, TAS systems are characterized by the definition of the antenna subset to be used for transmission and followed by either linear or nonlinear precoding [15,20,38,41,116,134], as described in Chapter 4 and shown in Fig. 5.1. This is mostly caused by the fact that conventional TAS algorithms and precoding designs are often based on different and disjointed metrics, hence leading

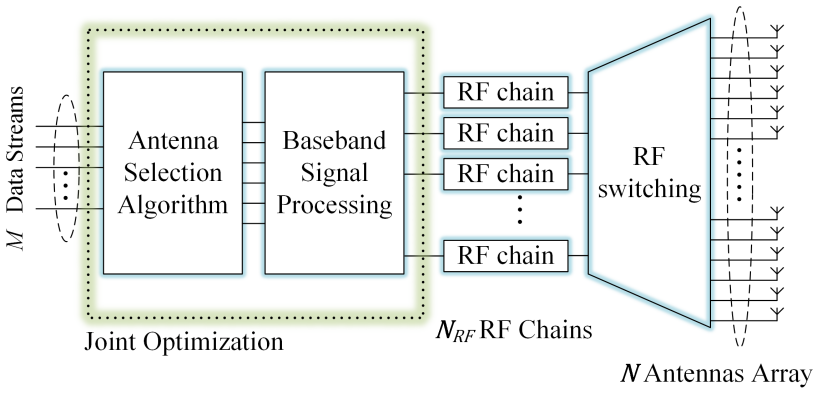

Figure 5.1: Conventional TAS block diagram.

to two separated optimization problems. In contrast to this, we propose a novel transmission approach where both TAS and precoding are jointly performed according to the same performance metric, so to achieve the highest benefits from both techniques. This key metric is based on the concept of interference exploitation [83, 84]. The deriving optimization is a Mixed-Integer Programming (MIP) problem and can be efficiently solved by commercial optimization solvers. In addition to the proposed MIP-based approach, three different heuristic solutions to the optimization problem are introduced and their performances are analyzed.

The algorithms here presented introduce a novel approach to M-MIMO TAS systems and are designed to fully exploit both constructive interference (CI) and the high diversity offered by very large arrays (VLAs) by jointly selecting a small subset of transmitting antennas and defining the precoded signal. The joint optimization enables to fully exploit the benefits of both TAS and precoding. In fact, the proposed joint TAS-precoding allows to greatly reduce the number of RF chains at the BS, hence achieving both a significant mitigation of hardware complexity and power consumption at the transmitter side, and an important reduction of the signal processing required.

The following list synthesizes the contributions presented in the chapter:

- Introduction of a novel transmission scheme for multiuser M-MIMO scenarios based on concepts of CI exploitation that jointly performs TAS and precoding;

- Definition of a MIP-based and three low-complexity heuristic approaches to effi-

ciently solve the proposed optimization problem. The optimality of these heuristic approaches is further discussed and analyzed;

- Study of the effects of imperfect CSI over the presented metrics and derivation of a CSI-robust approach for the proposed techniques;

- Evaluation of the performances obtained by the proposed schemes in terms of SER, Capacity and energy efficiency over throughput.

5.1 System Model and Benchmark Techniques

Similarly to previous chapters, we consider the application of the proposed schemes to the downlink transmission in a single-cell multiuser scenario, where the BS adopts a very large N-sized array to communicate with a population of M single-antenna users. Accordingly, the channel response is modeled as a $\mathbb{C}^{M\times N}$ matrix, whose entries are modeled as independent Rayleigh fading [99]. In line with the previous chapter on TAS, the BS is characterized by a total number of available RF chains $card\,(\mathcal{N}) = N_{RF} \leq N$.

Throughout the chapter, the proposed scheme is compared with classical TAS system approaches from the literature. More specifically, we consider a capacity-based TAS technique for M-MIMO where the selection is performed through convex optimization for multiuser scenarios [133] and PGM. With regards to the downlink beamforming techniques, we consider two main approaches based on SINR ratio metrics: TPM beamforming from [34], as described in (2.13), and the algorithmic SB beamforming from [35], as described in (2.14).

A convex approach to capacity-based TAS for M-MIMO has been recently proposed by [133], based on a relaxation of the binary constraints imposed over the diagonal of the selection matrix in (2.18). Accordingly, the new relaxed optimization problem for

Convex Capacity Maximization (CCM) can be defined as

$$\begin{aligned} \mathcal{P}_{CCM}: \quad & \underset{\mathbf{\Delta}}{\text{maximize}} \quad log_2\left[\det\left(\mathbf{I}_M + \rho\mathbf{H}\mathbf{\Delta}\mathbf{H}^H\right)\right] \\ & \text{subject to} \quad \Delta_{n,n} \in [0,1], \\ & \qquad\qquad \textstyle\sum_{n=1}^{N} \Delta_{n,n} = N_{RF}, \end{aligned} \tag{5.1}$$

which leads to the TAS subset definition

$$\mathcal{N} = \arg\max_{N_t} \left\{\Delta_{1,1}, ..., \Delta_{n,n}, ..., \Delta_{N,N}\right\}. \tag{5.2}$$

5.2 Proposed joint MIP Constructive Antenna Selection and Precoding (MIP-CASP)

In line with Chapter 3, CI conditions are imposed over the interfering signal for the m-th user t_m. Following the same notation, we defined the conditions for CI as

$$\omega_m \triangleq \Re\left(t_m \cdot e^{-j\phi_m}\right)\tan\Phi - \left|\Im\left(t_m \cdot e^{-j\phi_m}\right)\right| \geq 0, \tag{5.3}$$

Given the conditions for constructive interference in (5.3), it is possible to define a novel optimization problem that exploits the beneficial components of MUI by jointly performing TAS and precoding as

$$\begin{aligned} \mathcal{P}_{CASP}: \quad & \underset{\mathbf{a},\tilde{\mathbf{x}}}{\text{maximize}} \quad \min\left\{\Re\left(\mathbf{t}\circ\mathbf{u}^*\right)\tan\Phi - \left|\Im\left(\mathbf{t}\circ\mathbf{u}^*\right)\right|\right\} \\ & \text{subject to} \quad \mathbf{t} = \mathbf{H}\tilde{\mathbf{x}} - \mathbf{u}, \\ & \qquad\qquad \left\|\tilde{\mathbf{x}}\right\|^2 \leq 1, \\ & \qquad\qquad \left|\tilde{\mathbf{x}}\right| \preceq \mathbf{a}, \\ & \qquad\qquad \sum_{n=1}^{N} a_n = N_{RF}, \\ & \qquad\qquad a_n \in \{0,1\}, \end{aligned} \tag{5.4}$$

where the operator $\circ$ identifies the Hadamard product, $\mathbf{b} \preceq \mathbf{c}$ represents that inequality has to be respected for each element of both vectors (i.e.,$b_i \leq c_i, \forall i$) and $\mathbf{a}$ represents

the selection vector, whose entries are either one, when the corresponding antenna is to be connected to the RF chain for transmission, or null, when the corresponding antenna needs to be deactivated. Clearly, (5.4) jointly optimizes the precoded symbols through $\tilde{\mathbf{x}}$ and the TAS through $\mathbf{a}$, subject to power constraints in $\|\tilde{\mathbf{x}}\|^2 \leq 1$ (without loss of generality, the total power budget is assumed unitary for simplicity), and the typical antenna-number constraint also found in (5.1). Given its binary constraint, the optimization problem (5.4) is clearly non-convex, however it can be efficiently solved by means of commercial optimization tools such as MoSek. Still, it is important to highlight that its objective function is concave [84], since it can be deconstructed into the combination of two functions: a linear function $\Re\left(\mathbf{t} \circ \mathbf{u}^*\right)$ and a concave function $-\left|\Im\left(\mathbf{t} \circ \mathbf{u}^*\right)\right|$, as the extraction of the imaginary and real of a linear function preserves its linearity [84].

As we can see, $\mathcal{P}_{CASP}$ is designed in order to jointly perform the TAS (i.e., identifying the subset of transmitting antennas $\mathbf{a}$) and design the precoded signal $\tilde{\mathbf{x}}$. The joint optimization allows to fully exploit the beneficial components of MUI, achieving significant transmission benefits and a particularly interesting trade-off between system complexity and performances.

5.3 Heuristic Approaches to Joint Antenna Selection and Precoding

While the joint MIP-CASP approach effectively reduces the RF chains at the transmitter, the joint optimization of $\mathbf{a}$ and $\tilde{\mathbf{x}}$ involved introduces a significant computational burden. Accordingly, this section proposes three heuristic Successive Optimization (SO) approaches based on the decomposition of $\mathcal{P}_{CASP}$ into three different optimization problems. That is, $\mathcal{P}_{CASP}$ can be decomposed into the succession of three convex optimization problems, as follows:

- a full-system preliminary precoding, where the precoded signal $\mathbf{x}$ of the system with no TAS is derived via constructive beamforming (CBF)

- TAS, where the sub-set of transmitting antennas $\mathbf{a}$ is identified via CI AS (CAS)
- subset precoding, where the transmitted signal for the chosen N_{RF} transmitting antennas $\tilde{\mathbf{x}}$ is re-computed.

Towards reducing the involved computational complexity, the solution to the succession of these problems can be achieved through different approaches with decreasing computational complexities, here introduced and discussed. More specifically, the three following approaches with reducing computational complexity are presented:

- 3-step SO approach, namely CBF-CAS-CBF, involving CBF for the original precoding in the first step, CAS in the TAS step, and CBF in the final precoding step, where each one of the three aforementioned optimization problems is solved through convex optimization tools
- 2-step SO approach, namely MFCAS-CBF, where the first step is circumvented by employing a closed form MF precoder, while the remaining two problems are solved by means of convex optimization techniques
- 1-step SO approach, namely MFCAS, where the first and last steps are circumvented by employing the MF precoder and only the antenna optimization problem is solved by convex optimization.

The proposed schemes are described in details in the following subsections.

5.3.1 3-step Successive Optimization CBF-CAS-CBF

We identify as 3-step CBF-CAS-CBF the scheme based on the decomposition of $\mathcal{P}_{CASP}$ into three different convex problems to be solved in a sequential manner. In 3-step CBF-CAS-CBF, we first derive the precoded vector for the full-system $\mathbf{x} = [x_1, ..., x_N]^T$ by solving the CBF optimization problem

$$\begin{aligned} \mathcal{P}_{CASP3a}: \quad & \underset{\mathbf{x}}{\text{maximize}} \quad \min\left\{\Re\left(\mathbf{t}\circ\mathbf{u}^*\right)\tan\Phi - \left|\Im\left(\mathbf{t}\circ\mathbf{u}^*\right)\right|\right\} \\ & \text{subject to} \quad \mathbf{t} = \mathbf{H}\mathbf{x} - \mathbf{u}, \\ & \qquad\qquad \|\mathbf{x}\|^2 \leq 1. \end{aligned} \tag{5.5}$$

The optimization problem $\mathcal{P}_{CASP3a}$ can be cast as a Second-Order-Cone-Programming (SOCP) [102], since its objective function is concave [84]. Once the optimal precoded vector for the full N-antenna system $\mathbf{x}$ is achieved, the system proceeds to identify the antenna subset for transmission based on $\mathbf{a}$. The constructive TAS is performed according to the following CAS optimization problem

$$\begin{aligned} \mathcal{P}_{CASP3b}: \quad & \underset{\mathbf{a}}{\text{maximize}} \quad \min\left\{\Re\left(\mathbf{t}\circ\mathbf{u}^*\right)\tan\Phi - \left|\Im\left(\mathbf{t}\circ\mathbf{u}^*\right)\right|\right\} \\ & \text{subject to} \quad \mathbf{t} = \mathbf{H}\mathbf{x} - \mathbf{u}, \\ & \qquad\qquad\quad |\mathbf{x}| \preceq \mathbf{a}, \\ & \qquad\qquad\quad a_n \in [0,1], \forall n \in \{1,...,N\}, \\ & \qquad\qquad\quad \sum_{n=1}^{N} a_n = N_{RF}, \end{aligned} \tag{5.6}$$

where $\mathbf{a}$ represents the selection vector, following the same notation as for $\mathcal{P}_{CASP}$. The solution to $\mathcal{P}_{CASP3b}$ yields a vector with non-binary values of $\mathbf{a}$, which are achieved by selecting the N_{RF} largest elements with their indices representing the selected antennas. Finally, in order to achieve the final transmitted signal, the solution to $\mathcal{P}_{CASP3b}$ is used to identify the precoded vector $\tilde{\mathbf{x}}$ for the transmitting antennas subset $\mathcal{N}$ in the following

$$\begin{aligned} \mathcal{P}_{CASP3c}: \quad & \underset{\tilde{\mathbf{x}}}{\text{maximize}} \quad \min\left\{\Re\left(\mathbf{t}\circ\mathbf{u}^*\right)\tan\Phi - \left|\Im\left(\mathbf{t}\circ\mathbf{u}^*\right)\right|\right\} \\ & \text{subject to} \quad \mathbf{t} = \mathbf{H}\tilde{\mathbf{x}} - \mathbf{u}, \\ & \qquad\qquad\quad \|\tilde{\mathbf{x}}\|^2 \leq 1, \\ & \qquad\qquad\quad |\tilde{\mathbf{x}}| \preceq \mathbf{a}. \end{aligned} \tag{5.7}$$

5.3.2 2-step Successive Optimization MFCAS-CBF

While the previous approach is able to achieve near optimal performances, it is based on the derivation of the precoding vector for the full-size system $\mathbf{x}$, which is a computationally demanding step. Because of this, in order to further reduce the computational complexity of the signal processing at the BS, we propose an additional approach, called 2-step MFCAS-CBF, which leverages on the known property of asymptotic optimality for linear precoding in massive MIMO systems [11].

Thanks to this property, the computational burdens required by the convex precoding in $\mathcal{P}_{CASP3a}$ are greatly reduced, as they are replaced by a simple closed-form linear precoding approach. As it follows, the 2-step MFCAS-CBF approach can be synthesized in the following algorithm, where we first identify the subset of transmitting antennas based on the assumption of MF precoding

$$\begin{aligned} \mathcal{P}_{CASP2a}: \quad & \underset{\mathbf{\Delta}}{\text{maximize}} \quad \min\left\{\Re\left(\mathbf{c}\circ\mathbf{u}^*\right)\tan\Phi - \left|\Im\left(\mathbf{c}\circ\mathbf{u}^*\right)\right|\right\} \\ & \text{subject to} \quad \mathbf{c} = \mathbf{H}\mathbf{\Delta}\mathbf{H}^H\mathbf{u} - \mathbf{u}, \\ & \qquad\qquad \sum_{n=1}^{N}\Delta_{n,n} = N_{RF}, \\ & \qquad\qquad \Delta_{n,n}\in[0,1], \end{aligned} \tag{5.8}$$

where $\mathbf{\Delta}$ is the selection diagonal matrix, as in $\mathcal{P}_{CCM}$, and $\mathbf{c}$ identifies MUI interference under MF assumption $\mathbf{c} = \mathbf{H}\mathbf{\Delta}\mathbf{H}^H\mathbf{u} - \mathbf{u}$, i.e., $\mathbf{x} = \mathbf{H}^H\mathbf{u}$. After identifying the antenna subset $\mathbf{a} = diag(\mathbf{\Delta})$, we then proceed to derive the precoding vector $\tilde{\mathbf{x}}$ as a solution to the CBF problem

$$\begin{aligned} \mathcal{P}_{CASP2b}: \quad & \underset{\tilde{\mathbf{x}}}{\text{maximize}} \quad \min\left\{\Re\left(\mathbf{t}\circ\mathbf{u}^*\right)\tan\Phi - \left|\Im\left(\mathbf{t}\circ\mathbf{u}^*\right)\right|\right\} \\ & \text{subject to} \quad \mathbf{t} = \mathbf{H}\tilde{\mathbf{x}} - \mathbf{u}, \\ & \qquad\qquad \left\|\tilde{\mathbf{x}}\right\|^2 \le 1, \\ & \qquad\qquad \left|\tilde{\mathbf{x}}\right| \preceq \mathbf{a}, \end{aligned} \tag{5.9}$$

which can be efficiently solved by standard convex optimization techniques, as in (5.7).

5.3.3 1-step Successive Optimization MFCAS

In addition to the previous schemes, we propose a final approach to MUI exploiting AS-precoding where the computational burden is further reduced. Here, the antenna subset selection is the only problem that requires convex optimization in order to be solved, while precoding is performed by assuming only MF at the transmitter side.

Accordingly, we can define a new single-step optimization problem as follows

$$\begin{aligned} \mathcal{P}_{CASP1}: \quad & \underset{\mathbf{\Delta}}{\text{maximize}} \quad \min\left\{\Re\left(\mathbf{c}\circ\mathbf{u}^{*}\right)\tan\Phi-\left|\Im\left(\mathbf{c}\circ\mathbf{u}^{*}\right)\right|\right\} \\ & \text{subject to} \quad \mathbf{c}=\mathbf{H}\mathbf{\Delta}\mathbf{H}^{H}\mathbf{u}-\mathbf{u}, \\ & \qquad\qquad \sum_{n=1}^{N}\Delta_{n,n}=N_{_{RF}}, \\ & \qquad\qquad \Delta_{n,n}\in[0,1], \end{aligned} \tag{5.10}$$

After the transmitting subset $\mathcal{N}$ has been identified, we proceed to compute the transmitted signal $\tilde{\mathbf{x}}$, based on MF

$$\tilde{x}_n=\begin{cases} 1/\xi_n\sum\limits_{m=1}^{M}h_{m,n}u_m, & \forall \quad n\in\mathcal{N}, \\ 0 & \forall \quad n\notin\mathcal{N}, \end{cases} \tag{5.11}$$

where ξ_n is a scaling factor, which guarantees a unitary transmitted power $\sum\limits_{n=1}^{N}|x_n|^2=1$.

5.4 Optimality Evaluation

This section provides a further characterization of the proposed heuristic approaches by studying the impact that successive optimization and closed form approximations have over the achievable cost function values. In line with the literature [135], we define the figure of merit $\mathcal{M}$ as

$$\mathcal{M}=\frac{f}{f^{\star}_{MIP}}, \tag{5.12}$$

where f defines the objective function for which we want to measure the optimality. Clearly here

$$f=\min\left\{\Re\left(\mathbf{t}\circ\mathbf{u}^{*}\right)\tan\Phi-\left|\Im\left(\mathbf{t}\circ\mathbf{u}^{*}\right)\right|\right\}, \tag{5.13}$$

represents the cost function of the optimization problem $\mathcal{P}_{CASP}$ when the heuristic solutions are considered, i.e., the minimum CI achieved by successive optimization techniques, and $f^{\star}_{MIP}$ identifies the cost function evaluation when the optimal MIP-CASP solution is considered, i.e., when f is computed considering the $\tilde{\mathbf{x}}$ solution of $\mathcal{P}_{CASP}$. The defined metric represents a direct evaluation of the optimality of the proposed

heuristic approaches, as $f^{\star}_{MIP}$ represents the optimal and maximum value of minimum constructive interference achievable from a system. Clearly $\mathcal{M} = 1$ signifies that a MIP-equivalent solution is obtained.

Fig. 5.2 collects the cost function evaluation f for all the proposed approached with several modulation orders when considering increasing sub-set array sizes at the base station, i.e., increasing the number of transmitting antennas at the BS N_{RF}. Interestingly, we can notice that both the 3-step and the 2-step approaches are able to achieve near optimal solutions when compared to the optimal $f^{\star}_{MIP}$ for all the modulation orders. This result is particularly important, as it proves that SO-based approaches are able to efficiently approximate and solve the MIP equivalent formulation. On the other hand, we can see that the closed form single-step approach, 1-step MFCAS, is characterized by lower values of f when we increase the modulation order, because of its suboptimal approach when solving the precoding problem (i.e., MF linear precoding). Nevertheless, Fig. 5.2 shows that such approach can still represent an interesting alternative for low-order modulation and low-energy scenarios, as it is characterized by very low complexity and is still able to achieve acceptable performances for the 4-PSK and 8-PSK scenario.

These results are confirmed in Fig. 5.3, where the figure of merit $\mathcal{M}$ curves are presented for three different modulation orders. As we can see, these results confirm that both the 2-step and 3-step approaches are characterized by near optimal performances, as they rapidly and closely approach the optimality line, represented by the unitary value. On the other hand, the 1-step MFCAS approach proves to be a valuable alternative for low-power and low-modulation scenarios, thanks to its favorable trade-off between complexity and performances. Towards quantifying this trade-off, below we evaluate the computational complexity of each of the proposed schemes.

5.5 Computational Evaluation

This section analyzes the computational costs of the proposed schemes in terms of running time for different antenna array sizes at the transmitter side. In order to

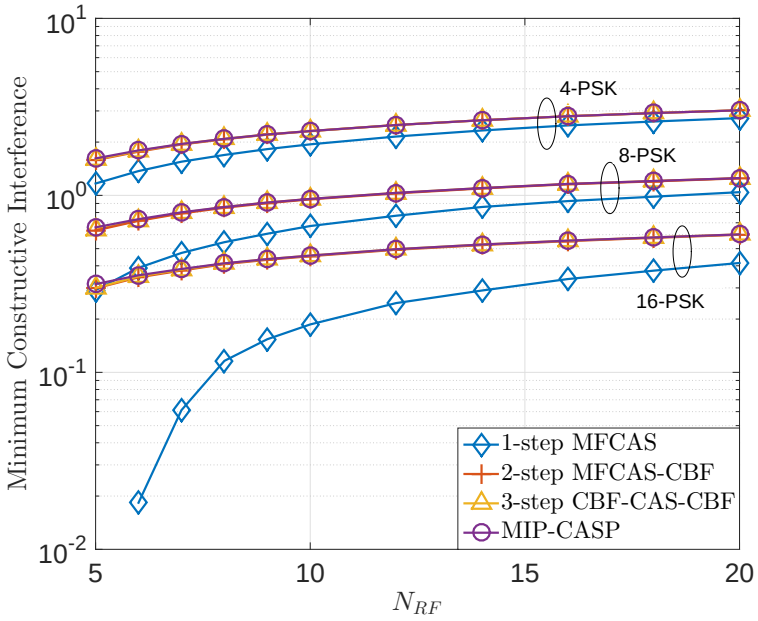

Figure 5.2: Minimum CI when $M = 5$ and $N = 100$.

perform a fair evaluation, we consider the running times in $[s]$ within a coherence time, i.e., for the number of frames where the CSI is assumed constant. This is due to the fact that the proposed schemes require a symbol-rate evaluation of TAS/precoding, while the conventional CCM scheme needs to be performed on a coherence time basis. With this regard, we consider a TDD scenario [51] with realistic values for a fast-fading scenario (i.e., where the proposed schemes are mostly suited for) where $T_{cohe} = 10$ symbols, in line with the work in [51]. More specifically, in reference to the notation used in (3.29), we consider a CSI acquisition time of $T_{CSI} = 5$ symbols (i.e., $\mu = 1$) in a DL dominant scenario with $T_{DL} = 4$ symbols dedicated to downlink transmission (i.e., $\eta_{DL} = 0.8$, with $T_{UL} = 1$).

As we can see in Fig. 5.4, the proposed schemes are overall affected by longer computational times over the length of the coherence time. This is due to the fact that the proposed schemes require a symbol-by-symbol update, in contrast with conventional TAS schemes from the literature. Nevertheless, it is interesting to notice that the proposed 1-step MFCAS scheme is characterized by running times that can be compared to the ones of the benchmark scheme. This strongly reaffirms that such approach represents a particularly appealing scheme for low-modulation scenarios, as it is able to achieve

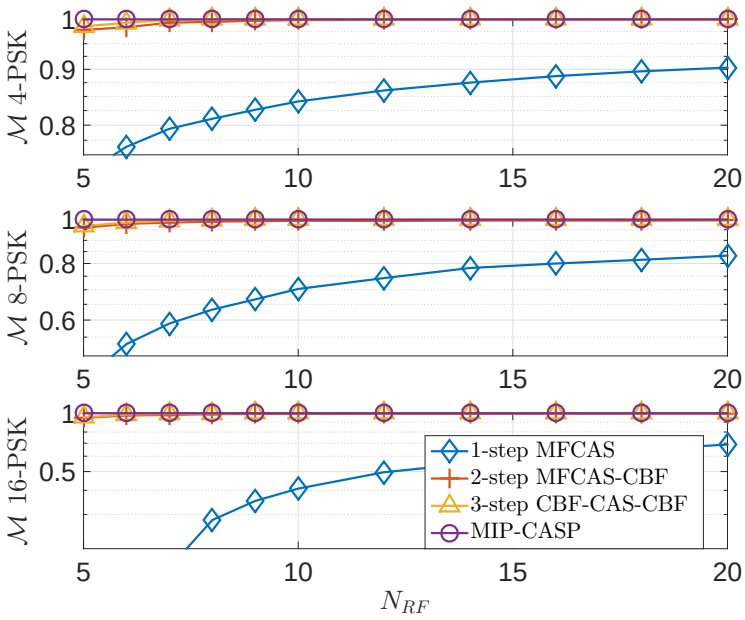

Figure 5.3: Figure of merit $\mathcal{M}$ when $M = 5$ and $N = 100$.

interesting performances with non-significant additional computational costs. On the other hand, it is important to notice how the proposed 2-step and 3-step schemes, are almost unaffected by the increase in array sizes, while the CCM-SB is instead characterized by increasing computational times as N grows. Accordingly, for very large systems, the proposed schemes are expected to be characterized by similar complexity, when compared to existing TAS schemes. On the other hand, we can see that the MIP-CASP approach is characterized by higher computational times, because of its trellis search-based solution.

Remark. It is important to highlight the fact that CCM-SB beamforming requires to equalize the received signal at the receiver side. This means that the BS is required to feed-forward the m-th mobile user with the product of the channel with the m-th precoding vector, i.e., $\mathbf{h}_m^T \mathbf{p}_m, \forall m$, in order to recover the data. For the CI precoding, as the received symbol resides in the constructive area of the constellation, there is no need to equalize the composite channel. Accordingly, such feedback is not required by the CI-exploiting approaches, where all complexity resides at the BS, which also makes them robust to the estimation and quantization errors that are involved in the feed-forwarding process for conventional beamformers.

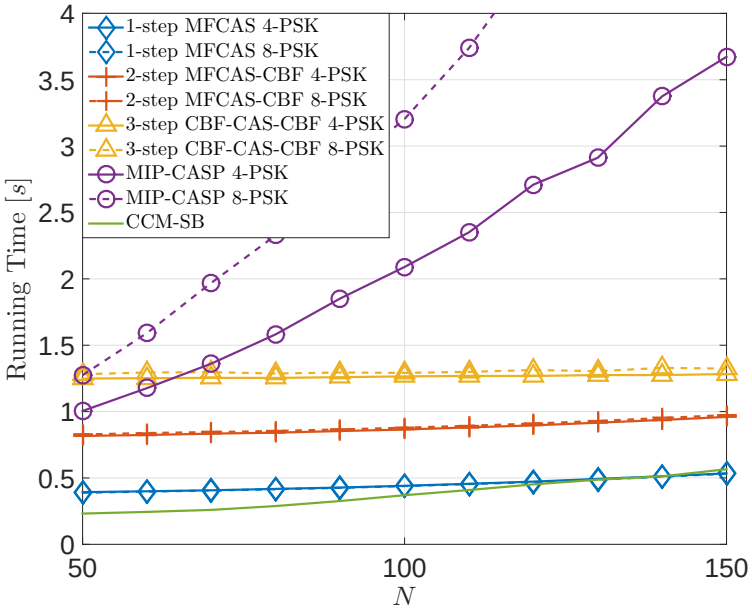

Figure 5.4: Frame Running time when $M = 5$, $N_{RF} = 5$ and $T_{DL} = 4$.

5.6 Channel Uncertainty and Robust Approach

In this section, the effects of imperfect CSI acquisition at the transmitter are analyzed and discussed. More specifically, we define the channel uncertainty model and derive a robust precoding technique to counteract the errors caused by imperfect CSI.

5.6.1 Model and Effects

In the following study, imperfect CSI at the transmitter side is modeled by adding a complex random component to the channel matrix $\mathbf{H}$. Without loss of generality, we consider the case where channel uncertainty amplitude is upper bounded by a specific value, i.e., CSI at the BS is affected by spherical noise [84].

Accordingly, the estimated channel gain between the n-th antenna and the m-th user is analytically defined as

$$\hat{h}_{m,n} = h_{m,n} + e_{m,n}, \forall n \in \{1, ..., N\}\,,\ \forall m \in \{1, ..., M\}\,, \tag{5.14}$$

where $\hat{h}_{m,n}$ represents the channel gain estimation available at the BS and $e_{m,n}$ repre-

sents the channel uncertainty, i.e., $\sum_{n=1}^{N} |e_{m,n}|^2 \leq \delta_m^2$ with δ_m being the uncertainty upper bound over the channel estimation for the m-th user.

Clearly, the presence of uncertainty over the available CSI at the BS has negative effects over the performances of a system. In fact, if the BS possesses imperfect CSI as modeled, the received signal in a noise free scenario becomes

$$\hat{r}_m = \sum_{n=1}^{N} \hat{h}_{m,n} x_n = \sum_{n=1}^{N} h_{m,n} x_n + \sum_{n=1}^{N} e_{m,n} x_n, \tag{5.15}$$

where the second term of the last equation explicitly represents effects of imperfect CSI at the transmitter side during signal processing.

In line with the standard approach [84,136], the BS is assumed to have no knowledge over the channel uncertainty $e_{m,n}, \forall n \in \{1, ..., N\}, m \in \{1, ..., M\}$ beside the upper bound δ_m related to the m-th user channel. This is a common assumption in the literature [84], and allows to derive a robust precoding design, which guarantees the downlink transmission to be resistant against all possible channel uncertainties within the upper bound δ_m^2.

In the following, we derive a CSI-robust TAS-precoding technique based on a common approach in robust precoding design where the aim is to minimize the overall transmitted power P_t required to respect the constraints imposed by the specific optimization.

5.6.2 MIP-CASP Robust Scheme

Given the MIP-based optimization in (5.4), we can identify a worst-case design for imperfect CSI scenarios as

$$\begin{aligned}
\mathcal{P}_{CASPR}: \quad & \underset{\mathbf{a},\tilde{\mathbf{x}}}{\text{minimize}} \quad \|\tilde{\mathbf{x}}\|^2 \\
& \text{subject to} \quad \min_{\|\mathbf{e}_m\|^2 \leq \delta_m^2, \forall m} \left\{ \Re\left(\hat{\mathbf{t}} \circ \mathbf{u}^*\right) \tan\Phi - \left| \Im\left(\hat{\mathbf{t}} \circ \mathbf{u}^*\right) \right| \right\} \succeq 0, \\
& \hat{\mathbf{t}} = \left(\hat{\mathbf{H}}\tilde{\mathbf{x}} - \mathbf{u}\right), \\
& \|\tilde{\mathbf{x}}\|^2 \leq 1, \\
& |\tilde{\mathbf{x}}| \preceq \mathbf{a}, \\
& \sum_{n=1}^{N} a_n = N_{RF}, \\
& a_n \in \{0,1\}.
\end{aligned} \tag{5.16}$$

Because of the infinite number of possible error values $e_{m,n}$, the first constraint in $\mathcal{P}_{CASPR}$ is intractable. However, by employing a worst-case approach, it is possible to derive a MIP-CASP robust design optimization for TAS-precoding with CI exploitation. In order to do so, we need to identify the equivalent constraint for a worst-case scenario, where the largest error is considered, as in Theorem 5.6.1.

Theorem 5.6.1 *The worst-case equivalent to the optimization problem $\mathcal{P}_{CASPR}$ can be defined as*

$$\begin{aligned}
\mathcal{P}^*_{CASPR}: \quad & \underset{\mathbf{a},\mathbf{w}_1,\mathbf{w}_2}{\text{minimize}} \quad \sum_{n}^{N_{RF}} \|\mathbf{w}_1\|^2 \\
& \text{subject to} \quad \text{Constraints (A.27) and (A.28)} \\
& \left\{ \left|\mathbf{w}_1^{(1:N)}\right|, \left|\mathbf{w}_1^{(N+1:2N)}\right| \right\} \preceq \mathbf{a}, \\
& \left\{ \left|\mathbf{w}_2^{(1:N)}\right|, \left|\mathbf{w}_2^{(N+1:2N)}\right| \right\} \preceq \mathbf{a}, \\
& \mathbf{w}_1 = \mathbf{\Pi}\mathbf{w}_2, \\
& \sum_{n=1}^{N} a_n = N_{RF}, \quad a_n \in \{0,1\},
\end{aligned} \tag{5.17}$$

Proof of Theorem 5.6.1 The proof can be found in Appendix B.

5.7 Results

In this section the performances of the proposed transmission schemes are presented and discussed. The shown results are evaluated through Monte Carlo simulations over 50000 channel realizations. In order to study the performances of the proposed schemes, we evaluate the SER at the receiver side, the achievable capacity and the energy efficiency of the system. More specifically, results are presented for both 4-PSK and 8-PSK, as the proposed transmission schemes can be directly applied to any PSK modulation order. Legends are characterized by the following notation:

- MIP-CASP identifies the CI exploitation transmission scheme based on MIP,
- 3-step CBF-CAS-CBF is used to represent the CI transmission based on the solution of $\mathcal{P}_{CASP3}$,
- 2-step MFCAS-CBF represents the 2-step TAS-precoding heuristic scheme,
- 1-step MFCAS is used to classify the single-step approach,
- CCM-SB stands for the literature approach where TAS is performed by CCM and precoding is performed through SINR balancing.

Moreover, the proposed schemes are compared with two low-complexity additional approaches from the literature: PGM-ZF, where ZF linear precoding is considered and TAS is performed via PGM, and CIM-HY from the previous Chapter for the 4-PSK scenarios, where hybrid linear precoding is considered (HY) and TAS is performed according to CIM. In the simulations, a single-cell downlink M-MIMO scenario is considered, where the BS possesses perfect CSI, employs a VLA of $N = 100$ antennas and communicates with $M = 5$ single-antenna mobile users, unless differently specified.

5.7.1 Symbol Error Rate

Fig. 5.5 collects the SER of the proposed and conventional approaches for the case of 4-PSK modulation. We can see that the proposed schemes greatly outperform all

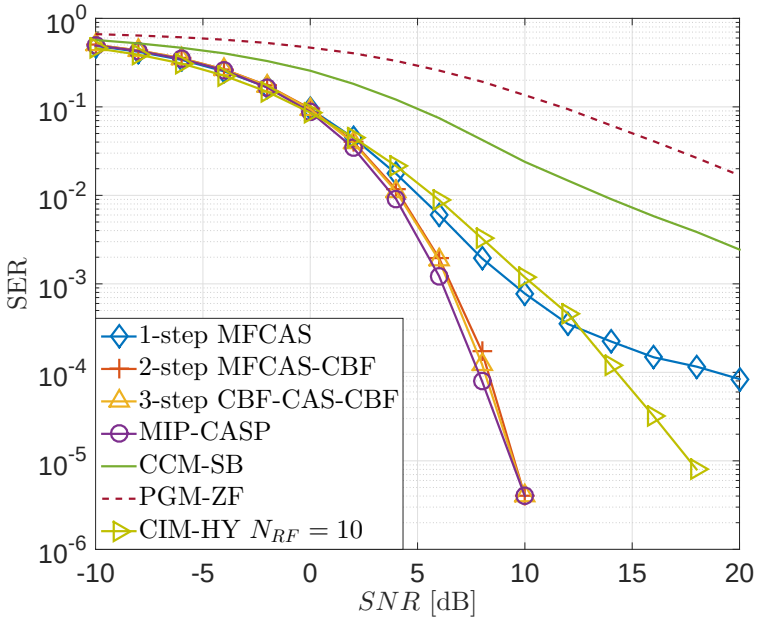

Figure 5.5: 4-PSK Symbol Error Rate when $M = 5$, $N = 100$ and $N_{RF} = 5$ with perfect CSI.

the benchmark techniques, including the CCM-SB scheme, which is characterized by a combination of CCM TAS [133] and SINR-balancing beamforming at the transmitter side [35]. At the same time, it is interesting to notice how both 2-step MFCAS-CBF and 3-step CBF-CAS-CBF are able to achieve near optimal performances when compared to the MIP-CASP approach. This is supported by the previous results in terms of $\mathcal{M}$, which showed how the two heuristic approaches were able to achieve similar performances to the MIP-based scheme. On the other hand, we can see that 1-step MFCAS obtains reasonable performance in the relatively low-to-mid SNR range, as the error-floor of the MF is reached when SER is lower than 10^{-4}. This is due to 4-PSK wider constructive interference regions, which allow a relative robustness against the inability of MF precoding to efficiently separate the stream between the users. However, such inability becomes the main cause for errors at high SNR and leads to the typical error-floor. This confirms our previous considerations regarding 1-step MFCAS as a valuable approach for the low-complexity and low-power scenarios.

In Fig. 5.6, the same set-up is explored for 8-PSK modulation. The performance trends for the proposed techniques are preserved. In fact, all the schemes based on

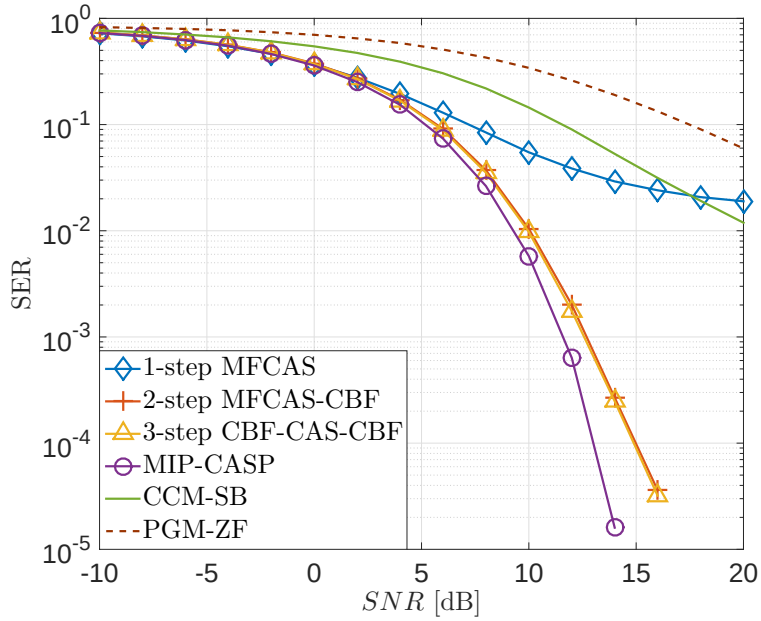

Figure 5.6: 8-PSK Symbol Error Rate when $M = 5$, $N = 100$ and $N_{RF} = 5$ with perfect CSI.

CI exploitation are able to outperform both the CCM-SB and the PGM-ZF schemes. At the same time, it is important to highlight how the error floor for the 1-step MF-CAS approach is higher than the one achieved in the 4-PSK case. This is due to the fact the final closed-form MF precoding is not able to correctly separate the different data-streams for different users, hence leading to uncontrolled inter-channel interference, whose effects are more visible in higher modulation orders.

5.7.2 Data Rate

As the conventional CCM approach is designed for capacity maximization, it is important to compare the rate performance of the proposed and conventional schemes. Accordingly, the throughput of the MIP-CASP scheme is compared with the capacity achievable when considering the CCM TAS scheme from the literature. The use of throughput instead of the ergodic capacity, i.e., $\sum_m log_2(1+\gamma_m)$, as a performance metric for the proposed MIP-CASP is justified by the fact that its assumption of a specific modulation, i.e., any PSK modulation order, does not allow to support the assumption of Gaussian signals. The throughput is defined as [83] $T = (1-BLER)\cdot l \cdot M$,

where $BLER$ is the block error rate, $l = \log_2(L)$ is the bit information per symbol and M is the number of users in the chosen scenario.

Performances are presented in Fig. 5.7, where the throughput of the proposed MIP-CASP approach for increasing modulation order is compared with the capacity of the full system and that of the CCM selection. The solid line with circular markers in the figure represents the peak-throughput trend for the proposed approach. We can see that the achieved throughput of the proposed scheme with increasing modulation orders outperforms the CCM selection from the literature. It is important to notice that the proposed scheme is able to achieve performances that are comparable to the ones of a full-system for low-to-mid SNR scenarios, where the gap with the CCM scheme from the literature is more pronounced.

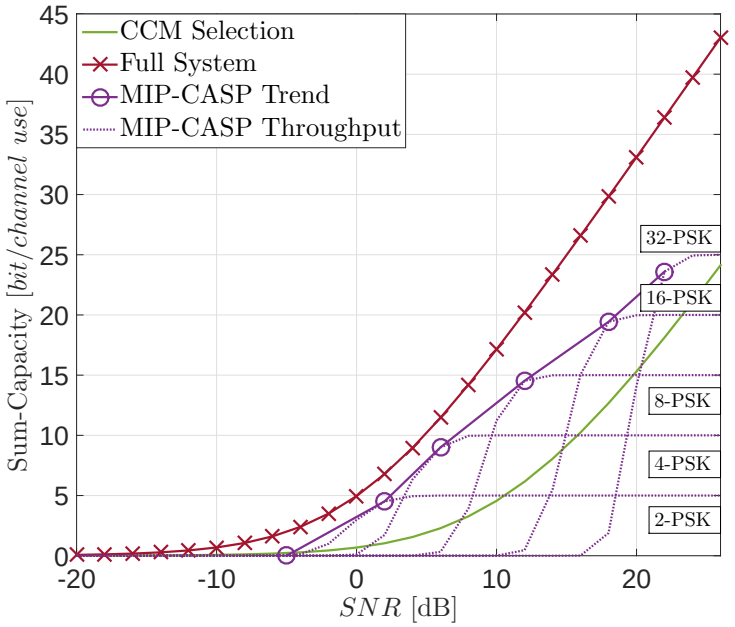

Figure 5.7: System Capacity comparison when $M = 5$, $N_{RF} = 5$ and $N = 100$.

5.7.3 Energy Efficiency

In order to better highlight benefits and trade-offs brought by the proposed schemes, we analyze the energy efficiency over throughput η_T, as defined in (2.22). In line with Chapter 4, we consider realistic power values from practical systems [132], where $P_{amp} =$

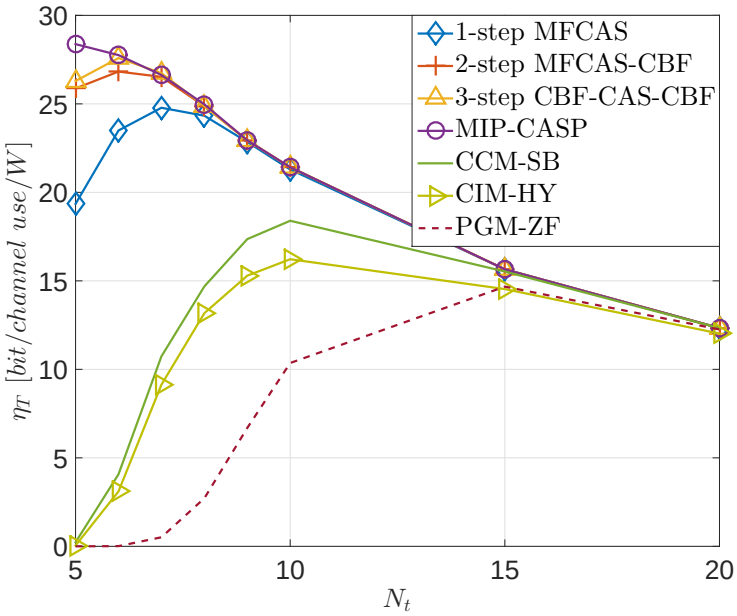

Figure 5.8: 4-PSK Energy Efficiency η_T when $M = 5$, $N = 100$ with perfect CSI and $SNR = 5dB$.

P_t/ν is defined as the power required by an amplifier with $\nu = 0.35$ efficiency and transmitted power $P_t = 30dBm$ and $P_{RF} = 65.9mW$. Performances are presented in Fig. 5.8 and Fig. 5.9 as a function of N_{RF} with $SNR = 5dB$ and $SNR = 10dB$, respectively. The proposed metric allows to better characterize the trade-off between power consumption at the transmitter and achieved throughput as a function of the variation over the subset size N_{RF}.

As already observed in the SER results, we can see that performance trends for both 4-PSK and 8-PSK are preserved. More specifically, we can see that the proposed schemes are all able to greatly outperform schemes from the literature for all the spectrum of N_{RF} values. At the same time, it is interesting to notice that the proposed schemes achieve their maximum energy efficiency between $N_{RF} = 6$ and $N_{RF} = 8$ for both 4-PSK and 8-PSK. This shows that systems with low numbers of active antennas can provide reasonable performance with a very positive trade-off between hardware complexity and power consumptions (i.e., when compared to the simplified chosen scenario where $N_{RF} = M$). For a direct performance-complexity comparison between the schemes, Table 5.1 collects the computational burdens required per frame to achieve the optimal

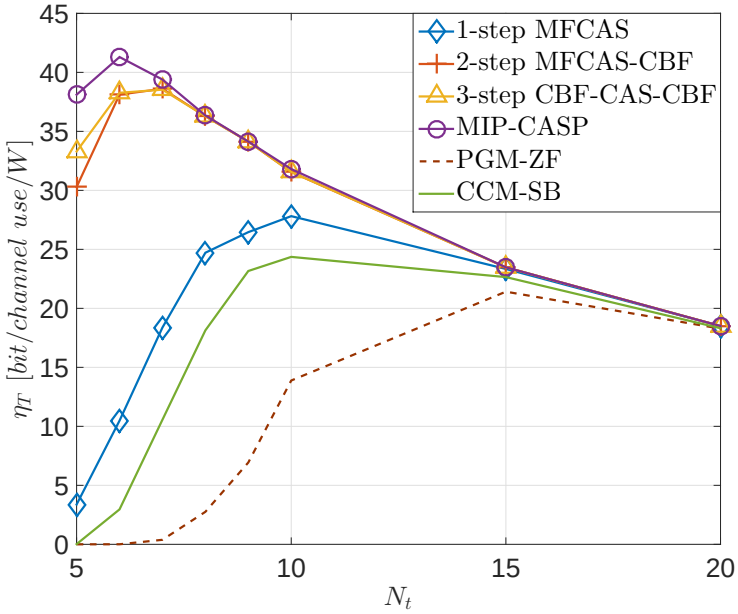

Figure 5.9: 8-PSK Energy Efficiency η_T when $M = 5$, $N = 100$ with perfect CSI and $SNR = 10dB$.

Table 5.1: Computational burdens for optimal Energy Efficiency points

Name	**Max** η_T $[bit/c.u./W]$	**Time** $[s]$	N_{RF}
1-step MFCAS	24.78	0.44	7
2-step MFCAS-CBF	26.83	0.85	6
3-step CBF-CAS-CBF	27.59	1.31	6
MIP-CASP	28.38	2	5
CCM-SB	18.4	0.55	10

value of energy efficiency shown in Fig. 5.8. There are evident complexity savings achieved by the heuristic schemes compared to the MIP approach, with little loss on the maximum energy efficiency. On the other hand their complexity is comparable to conventional CCM, with a more than 50% energy efficiency improvement and a ∼94% reduction in the RF chains required to achieve maximum PE.

5.7.4 Robustness to CSI

In order to characterize the performances of the proposed CSI-robust scheme, we introduce a conventional robust scheme from the literature, which will be used as a benchmark technique. In line with the previous approaches, when considering the benchmark scheme we assume a cascade of TAS, based on capacity, followed by a SINR metric-

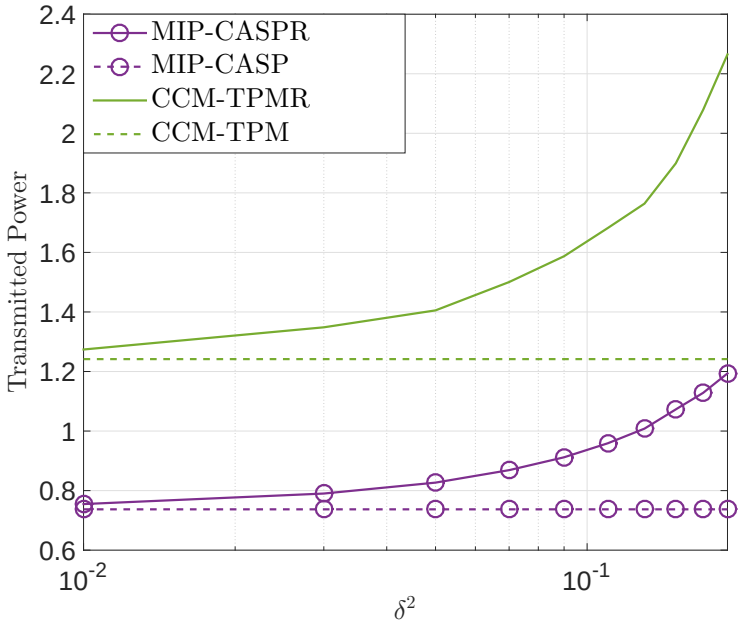

Figure 5.10: Transmitted power for 4-PSK transmission when $N = 100$, $M = 5$ and $N_{RF} = 5$.

based precoding. More specifically, when considering robust precoding, it is common to proceed to identify an optimization problem that aims to minimize the transmitted power required to overcome the worst-case scenario. Accordingly, Transmit Power Minimization Robust (TPMR) precoding can be defined as follows [136]

$$\begin{aligned} \mathcal{P}_{TPMR}: \quad & \underset{\mathbf{P}_m \geq \mathbf{0}, s_m \geq 0}{\text{minimize}} \quad \sum_{m=1}^{M} \text{tr}\left[\mathbf{P}_m\right] \\ & \text{subject to} \quad \begin{bmatrix} D_m & \hat{\mathbf{h}}_m^T \mathbf{Q}_m \\ \mathbf{Q}_m \hat{\mathbf{h}}_m^* & \mathbf{Q}_m + s_m \mathbf{I}_N \end{bmatrix} \geq \mathbf{0} \\ & D_m = \hat{\mathbf{h}}_m^T \mathbf{Q}_m \hat{\mathbf{h}}_m^* - \gamma_m N_0 - s_m \delta_m^2 \\ & \mathbf{Q}_m = \mathbf{p}_m \mathbf{p}_m^H - \gamma_m \sum_{i=1, i \neq m}^{M} \mathbf{p}_i \mathbf{p}_i^H \end{aligned} \tag{5.18}$$

where the notation $\mathbf{A} \geq \mathbf{0}$ is used to impose that the matrix $\mathbf{A}$ is semidefinite positive.

In Fig. 5.10 we can see a comparison between the two robust schemes in terms of transmitted power as a function of the error upper-bound $\delta_m = \delta, \forall m$. In addition to the robust schemes, the minimum transmitted power for the non-robust approaches is also presented. As shown, the proposed scheme is characterized by significantly lower

requirements in terms of transmitted power, when compared to both the robust and non-robust approach from the literature. Additionally, we can see that the CCM-TPMR scheme from the literature is affected by a faster growth rate as the channel uncertainty increases when compared to MIP-CASPR.

5.8 Conclusions

This chapter proved that antenna selection and precoding based on constructive multiuser interference concepts can be jointly used to greatly improve the energy efficiency of future M-MIMO systems. Analytical and numerical studies showed that constructive interference at the receiver side can be optimized by simultaneously identifying a subset of transmitting antennas and the precoded signal at the base station. The presented schemes have been characterized by analyzing the computational costs in terms of running time in comparison with state-of-the art algorithms. Performances have been evaluated in terms of symbol error rate, sum rate and energy efficiency to analyze the performance-complexity trade-offs introduced by the proposed scheme. Provided analyses and results have shown that the proposed approaches offer a favorable performance-complexity trade-off compared to conventional schemes, with a close-to-optimal performance.

Chapter 6

Beam Selection schemes for Millimeter-Wave Beamspace-MIMO Systems

Despite the great benefits introduced by the exploitation of mm-wave spectrum, energy efficient transceiver design for such frequencies still represents a key barrier to its implementation. In fact, a direct large or massive MIMO approach is considered prohibitive because of the high transceiver complexity [23, 137] deriving from the use of an extremely large number of antennas and RF chains in reduced physical spaces. In fact, recent studies [138] proved that systems with massive antenna arrays are particularly prone to RF chain imperfections, which lead to additional degradations in performance. Moreover it is understood that RF components may consume up to 70% of the total transceiver power consumption [139].

In order to exploit the favorable characteristics of mm-wave frequency communications, research is focusing on the development of new techniques that aim to reduce the hardware complexity of very high dimensional MIMO systems. Previous works on small-scale MIMO tackled the hardware complexity with antenna selection [15, 16, 20], amongst many others, but showed high degradation in performances compared to the full system. Nevertheless, since the high beamforming gains introduced by the use of

large number of antennas are fundamental to overcome the higher free space loss experienced in the mm-wave bands, such approaches are not viable at these frequencies [127].

As a consequence, research is regarding hybrid analog-digital transceivers, where analog beamformers in the RF domain are combined with a smaller number of digital beamformers in baseband, as a promising candidate for future mm-wave MIMO applications. This chapter focuses on a scheme that combines B-MIMO concepts [13] with DLA-based systems [14], where RF complexity reduction is approached by selecting a subset of transmitting beams, instead of antennas.

The following list summarizes the contributions presented in the chapter:

1. Introduction of a mm-wave transmission scheme based on beam selection for B-MIMO, able to achieve near-optimal performances with a reduced RF complexity transceiver, and presentation of 3 associated beam selection schemes,

2. Analytical evaluation of the computational complexity of the proposed beam selection schemes, with regards to conventional B-MIMO,

3. Analytical derivation of the capacity losses caused by beam selection, identifying an upper bound for the proposed techniques,

4. Analysis of the performances achieved by the proposed transmission schemes in terms of sum-rate and energy efficiency.

6.1 System Model

In this chapter, we consider a single-cell downlink scenario where the BS is equipped with a DLA and a simple linear ZF precoder to communicate with M single-antenna users [23], as in Fig. 6.1. DLAs can be analytically modeled as a critically sampled, i.e. $d = \frac{\lambda}{2}$ spaced, uniform linear array (ULA) of length L leading to a signal space

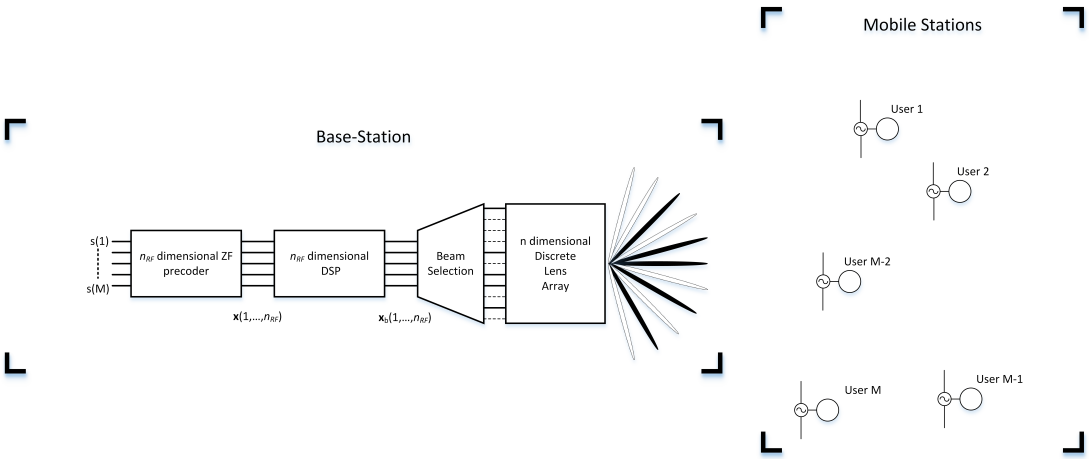

Figure 6.1: Block diagram of a mm-wave DLA-based transceiver scheme

dimension n that can be defined analytically as

$$n = \frac{2L}{\lambda}. \tag{6.1}$$

In DLA-based systems, the parameter n represents the maximum number of spatial modes that are supported in transmission/reception, i.e. the total number of orthogonal beams that are supported by the system[14].

Accordingly, the received symbol vector of a DLA-based linearly precoded transmission in the spatial domain can be expressed as

$$\mathbf{y} = \mathbf{Hx} + \mathbf{n} = \mathbf{HGu} + \mathbf{n}, \tag{6.2}$$

where $\mathbf{H} = [\mathbf{h}_1, ..., \mathbf{h}_M]^T$ is a $\mathbb{C}^{M \times n}$ matrix that collects the $\mathbb{C}^{n \times 1}$ channel response vectors $\mathbf{h}_1, .., \mathbf{h}_M$ of all the users, $\mathbf{x}$ is the $\mathbb{C}^{n \times 1}$ transmitted signal, $\mathbf{G}$ is the $\mathbb{C}^{n \times M}$ linear precoding matrix, $\mathbf{u}$ is the $\mathbb{C}^{M \times 1}$ vector that contains all the data symbols that have to be transmitted and $\mathbf{n}$ is the $\mathbb{C}^{M \times 1}$ additive white Gaussian noise (AWGN) vector.

It is pivotal to highlight that while the spatial domain channel model $\mathbf{H}$ for DLA can be analytically modeled and studied as a n sized ULA, the hardware complexity required by these approaches are profoundly different. In fact, as shown in Fig. 6.1,

a BS with DLA requires only a reduced set of n_{RF} RF chains and a beam selector to support n narrow beams. A classical MIMO approach instead, where the BS is equipped an equivalent n-dimensional linear array, requires one RF chain for each of the radiating elements, regardless of the number of streams to be transmitted.

In line with Chapter 2, the channel response for the m-th user in the spatial dimension for a mm-wave communications MIMO system can be modeled according to Rician fading, here briefly reported for the sake of ease of reading, as [10, 13]

$$\mathbf{h}_m = \mathbf{h}_m^{(LoS)} + \mathbf{h}_m^{(MP)} = \beta_0^{(m)} \mathbf{a}(\theta_0^{(m)}) + \sum_{i=1}^{N_p} \beta_i^{(m)} \mathbf{a}(\theta_i^{(m)}), \tag{6.3}$$

where $\mathbf{a}(\theta)$ is the $\mathbb{C}^{n\times 1}$ steering vector for the spatial direction θ.

Note that the spatial domain model described here implicitly includes the effects of transmit correlation. In fact, since the spatial domain for DLA is modeled as a critically sampled ULA, different degrees of correlation can be achieved by varying the angle spread [36].

However, a DLA-based system operates in the beamspace domain, defined by the beamforming matrix $\boldsymbol{\mathcal{U}}$ which represents the operation of a perfectly designed DLA [14]. The beamforming matrix is obtained by computing the steering vectors for n fixed spatial frequencies with uniform spacing [13, 140]. The beamforming matrix is defined analytically as follows

$$\boldsymbol{\mathcal{U}} = \frac{1}{\sqrt{n}} \left[\mathbf{a} \left(\Delta\theta_0 i \right) \right]_{i \in \mathcal{I}(n)}, \tag{6.4}$$

where $\mathcal{I}(n) = \{ i - (n-1)/2 : i = 0, 1, ...n-1 \}$ is a symmetric set of indices centered around 0, hence leading to a $\mathbb{C}^{n\times n}$ matrix where $\Delta\theta_0 = \frac{1}{n}$ is the uniform spacing used.

We can define the equation (6.2) in the beamspace domain as follows

$$\mathbf{y} = \boldsymbol{\mathcal{H}} \boldsymbol{x} + \mathbf{n} \tag{6.5}$$

where the channel matrix in the beamspace domain $\boldsymbol{\mathcal{H}}$ and the transmitted signal in

the beamspace domain $\boldsymbol{x}$ can be computed as

$$\boldsymbol{\mathcal{H}} = \mathbf{H}\boldsymbol{\mathcal{U}}^H, \ \boldsymbol{x} = \boldsymbol{\mathcal{U}}\mathbf{G}\mathbf{u} \tag{6.6}$$

It follows that the multiplication for the beamforming matrix $\boldsymbol{\mathcal{U}}$ represents a mapping of the signals for each mobile station in a new domain of orthogonal beams. In the angular or beamspace domain, each column of the channel model $\boldsymbol{\mathcal{H}}$ represents one of the n beams supported by the DLA. Such relationship between the channel in the angular-beamspace domain $\boldsymbol{\mathcal{H}}$ and the channel in the spatial domain $\mathbf{H}$ is well known. In fact, since the elements of $\boldsymbol{\mathcal{U}}$ are in the form $\frac{1}{\sqrt{n}}e^{-j2\pi ml/n}$, $\boldsymbol{\mathcal{H}}$ represents the inverse discrete Fourier transform of the channel matrix in the spatial domain $\mathbf{H}$ [10, 13].

Note that, given its analytical definition, the beamforming matrix defined in (6.4) is unitary, i.e., $\boldsymbol{\mathcal{U}}^H\boldsymbol{\mathcal{U}} = \boldsymbol{\mathcal{U}}\boldsymbol{\mathcal{U}}^H = \mathbf{I}$, hence leading to the following relationships between the spatial and the beamspace domain

$$\begin{aligned} \mathbf{x} &= \boldsymbol{\mathcal{U}}^H\boldsymbol{x}, \\ \mathbf{H} &= \boldsymbol{\mathcal{H}}\boldsymbol{\mathcal{U}}. \end{aligned} \tag{6.7}$$

6.1.1 Benchmark

As a consequence, the equivalent channel experienced by a DLA-based mm-wave transceiver has a very sparse nature, where few elements of the matrix have dominant values near the LoS direction of the users. Because of this, early works on DLA-based beamspace mm-wave MIMO proposed a simple beam selection scheme called Maximum Magnitude Beam Selection (MM-BS) [23], which proved to be able to take advantage of channel sparsity. This technique, here briefly reviewed for the sake of completeness, is based on the definition of a set of beam indices called sparsity masks.

Sparsity masks are used by the BS to identify the dominant beams to be selected for the transmission and are defined as follows

$$\mathcal{M}^{(m)} = \left\{ i \in \mathcal{I}(n) : |\mathfrak{h}_{m,i}|^2 \geq \xi^{(m)} \max_i |\mathfrak{h}_{m,i}|^2 \right\} \tag{6.8}$$

$$\mathcal{M} = \bigcup_{m=1,..,M} \mathcal{M}^{(m)} \tag{6.9}$$

where $\mathfrak{h}_{m,i}$ is the i-th element of the m-th user channel response, $\mathcal{M}^{(m)}$ is the sparsity mask for the m-th user and $\xi^{(m)} \in [0,1]$ is the threshold used to define it. We can see that in order to obtain a minimum number of beams for each user, the threshold $\xi^{(m)}$ is chosen independently for each user.

After the sparsity mask, we can define the equivalent channel after a subset of beams has been deactivated as

$$\boldsymbol{\mathcal{H}}_e = [\underline{\boldsymbol{h}}_l]_{l \in \mathcal{M}} \tag{6.10}$$

where the sizes $n_d \times M$ of the new channel matrix $\boldsymbol{\mathcal{H}}_e$ depend on the number of dominant beams $n_d = |\mathcal{M}|$ identified in the sparsity mask. From (6.9) we can see that the MM-BS algorithm leads to values of n_d which change according to the channel realization. In fact, the user-wise selection implemented by MM-BS often leads to multiple selections of the same beam for different users and therefore to a varying number of required RF chains for different channel realizations and user topologies. As a consequence, a direct application of MM-BS in practical systems, where the number of RF chains is fixed, is not viable. Note that, while MM-BS leads to a variable number of dominant beams n_d, it is still required to be lower or equal to the total number of available RF chains at the transmitter side, i.e., $n_d \leq n_{RF}$.

Since MM-BS selects the strongest channel paths, it can be seen that it is suboptimal in terms of achievable capacity in a multi-path scenario. In fact, MM-BS performance are strongly dependent on the assumption of a highly sparse channel, which is a valid assumption for channels where the multi-path component of (6.3) is negligible, but becomes questionable as we introduce additional paths to the model.

6.2 Proposed Beam Selection Techniques

With the aim to overcome the key drawbacks of MM-BS, i.e., the impossibility to have a fixed value of n_d and the strong dependence on the channel sparsity, this section

presents three different beam selection criteria. The use of DLA at the transmitter allows to apply the selection algorithm directly over the channel matrix in the beamspace domain, hence without affecting the beam-width nor the gain of the antenna pattern. As shown in Chapter 2, selection can be performed according to different parameters, such as path magnitude [23], SINR at the receiver [141], system capacity [21, 142] and minimum error rate [142]. Main focus resides on the application of selection criteria based on the first three metrics, since the proposed analysis mostly focuses on the capacity of the system.

6.2.1 SINR Maximization Beam Selection (SM-BS)

In the proposed technique, beams are chosen to maximize the SINR at the user side; this selection criterion is defined as SINR maximization beam selection (SM-BS). In order to identify the subset of beams used during data transmission, we need to define the SINR metric for the chosen model. The SINR for each user depends on the precoder used at the transmitter, identified by the precoding matrix in the angular domain $\boldsymbol{\mathcal{G}} = \gamma \boldsymbol{\mathcal{F}}$. More specifically, the received SINR of the m-th user is defined as [23]

$$SINR_m\left(\rho, \boldsymbol{\mathcal{G}} | \boldsymbol{\mathcal{H}}\right) = \frac{\frac{\rho|\gamma|^2}{M} |\boldsymbol{h}_m^T \boldsymbol{f}_m|^2}{\frac{\rho|\gamma|^2}{M} \sum\limits_{k \neq m} |\boldsymbol{h}_k^T \boldsymbol{f}_m|^2 + N_0} \tag{6.11}$$

where $\boldsymbol{h}_m^T$ is the transpose of the m-th user channel response, $\boldsymbol{f}_m$ is the m-th column of $\boldsymbol{\mathcal{F}}$, ρ is the transmitted power and N_0 is the noise power.

In this study, main focus resides on a practical case where the BS is equipped with a low-complexity ZF linear precoder, hence characterized by two important properties: null interference, i.e., $\sum_{k \neq m} |\boldsymbol{h}_k^T \boldsymbol{f}_m|^2 = 0$ and unitary gain, i.e., $|\boldsymbol{h}_m^T \boldsymbol{f}_m|^2 = 1$. Thanks to the properties of ZF precoding, the received SINR equation can be simplified to [36]

$$SINR_{m,ZF}\left(\nu, \boldsymbol{\mathcal{G}} | \boldsymbol{\mathcal{H}}\right) = \frac{\nu|\gamma|^2}{M} \tag{6.12}$$

where $\nu = \rho / N_0$ is the SNR. Accordingly, under the assumption of a ZF precoded BS, the SINR maximization selection at the transmitter can be directly achieved by maximizing

the scaling factor γ.

A direct application of SM-BS can be achieved by performing an exhaustive search of the SINR for all the possible combination of beam subsets and then choose the subset that leads to the highest value. While such approach leads to an optimal selection, it rapidly becomes computationally prohibitive because of its $\binom{n}{n_{RF}}$ possible combinations[1], where n_{RF} is the subset size. Accordingly, we derive a suboptimal decremental beam selection that identifies the beam subset with the minimum loss in terms of SINR, shown in Algorithm 6.1. Using (6.12), the SINR for the reduced system after the elimination of the l-th beam can be computed as

$$SINR_{m,ZF}^{(l)}\left(\nu, \boldsymbol{\mathcal{G}} | \boldsymbol{\mathcal{H}}_{(l)}\right) = \frac{\nu |\gamma^{(l)}|^2}{M} \tag{6.13}$$

with

$$\gamma^{(l)} = \sqrt{\frac{\rho}{tr(\boldsymbol{\mathcal{F}}_{(l)} \boldsymbol{\mathcal{F}}_{(l)}^H)}} \tag{6.14}$$

where $\boldsymbol{\mathcal{H}}_{(l)}$ represents the channel matrix whose l-th beam has been eliminated, $\boldsymbol{\mathcal{F}}_{(l)}$ is the precoding matrix obtained with the lower-dimensional channel matrix $\boldsymbol{\mathcal{H}}_{(l)}$ and $\gamma^{(l)}$ is the corresponding scaling factor[2]. Hence, we can identify the index of the beam to be disabled via the following maximization criterion

$$\delta = \arg\max_{l} \left\{ \frac{\nu |\gamma^{(l)}|^2}{M} \right\} \tag{6.15}$$

where δ is an element of the subset of disabled beams $\mathcal{D}$. Since ρ, M and N_0 are channel independent, the maximization criterion can be simplified to

$$\delta = \arg\max_{l} (|\gamma^{(l)}|^2). \tag{6.16}$$

[1] A scenario where $n = 81$ and $n_{RF} = 40$ leads to $\binom{81}{40} \approx 2 \cdot 10^{23}$ possible subsets, which is computationally prohibitive for a simulation evaluated study. However, previous works on antenna selection for low dimensional systems [117] showed that the performances of decremental approaches are close to the ones achieved by exhaustive search methods.

[2] Note that SM-BS does not affect the transmitted power constraint $E[\mathbf{x}\mathbf{x}^H] = 1$. In fact, the system deriving from the selection employs a ZF precoder, which is computed according to the low dimensional channel matrix $\boldsymbol{\mathcal{H}}_e$ obtained through SM-BS and uses a scaling factor to constrain the average transmit power.

Algorithm 6.1 SM-BS

Input: $\boldsymbol{\mathcal{H}}$

Output: $\boldsymbol{\mathcal{H}}_e$

- $\mathbf{C} := \boldsymbol{\mathcal{H}}$
- $\boldsymbol{\mathcal{F}} := \mathbf{C}(\mathbf{C}^H\mathbf{C})^{-1}$
- **for** $j = 1 \rightarrow n - n_{RF}$
  - **for** $l = 1 \rightarrow n - j$
    - $\boldsymbol{\mathcal{F}}_{(l)} = \mathbf{C}_{(l)}(\mathbf{C}_{(l)}^H\mathbf{C}_{(l)})^{-1}$
    - $\gamma^{(l)} = \sqrt{\rho / tr(\boldsymbol{\mathcal{F}}_{(l)}\boldsymbol{\mathcal{F}}_{(l)}^H)}$
  - **end**
  - $\delta_j = \arg\max_l \left\{|\gamma^{(l)}|^2\right\}$
  - $\mathcal{D} = \{\delta_1, ..., \delta_j\}$
  - $\mathbf{C} = [\underline{\boldsymbol{h}}_l]_{l \notin \mathcal{D}}$
- **end**
- $\boldsymbol{\mathcal{H}}_e = [\underline{\boldsymbol{h}}_l]_{l \notin \mathcal{D}}$

While the selection metric for SM-BS derived in (6.16) is obtained by exploiting the orthogonal properties of ZF precoding, the presented technique can be applied independently from the precoding involved at the BS. In fact, following the notation used in (6.11) and under a generic precoding assumption $\boldsymbol{\mathcal{G}}$, the SM-BS algorithm proceeds to maximize the SINR for the reduced system

$$SINR_m^{(l)} = SINR_m\left(\rho, \boldsymbol{\mathcal{G}}_{(l)} | \boldsymbol{\mathcal{H}}_{(l)}\right) \tag{6.17}$$

where $\boldsymbol{\mathcal{G}}_{(l)}$ represents the precoding matrix that corresponds to the reduced channel model $\boldsymbol{\mathcal{H}}_{(l)}$.

6.2.2 Capacity Maximization Beam Selection (CM-BS)

We define as Capacity Maximization Beam Selection (CM-BS) the algorithms that aim to identify the beam subset with the minimum capacity loss from the full system [21]. The CM-BS can be performed with two separate approaches:

- *Decremental*, where the algorithm recursively chooses the beams not to be used in transmission,

- *Incremental*, where the algorithm recursively chooses the beams to be used in transmission.

It is immediate to see that the difference between the two algorithms resides in the computational costs [21]. In fact, the incremental selection is faster when the number of beams to be included in the transmitting subset is lower than $n/2$, i.e., $n_{RF} \leq n/2$, while the decremental is to be preferred when the number of beams to be included in the transmitting subset is higher than $n/2$, i.e., $n_{RF} \geq n/2$.

6.2.2.1 Decremental CM-BS (DCM-BS)

The algorithm selects the beams whose elimination causes the minimum loss in terms of capacity. Given the full system capacity

$$C(\boldsymbol{\mathcal{H}}) = \log_2 \det(\mathbf{I} + \nu \boldsymbol{\mathcal{H}} \boldsymbol{\mathcal{H}}^H). \tag{6.18}$$

the capacity after the l-th beam has been disabled can be computed as [143]

$$C(\boldsymbol{\mathcal{H}}_{(l)}) = \log_2 \det(\mathbf{I} + \nu \boldsymbol{\mathcal{H}}_{(l)} \boldsymbol{\mathcal{H}}_{(l)}^H) \tag{6.19}$$

where the channel $\boldsymbol{\mathcal{H}}_{(l)}$ is related to the full system matrix according to the following equation

$$\boldsymbol{\mathcal{H}}_{(l)} \boldsymbol{\mathcal{H}}_{(l)}^H = \boldsymbol{\mathcal{H}} \boldsymbol{\mathcal{H}}^H - \underline{\boldsymbol{h}}_l \underline{\boldsymbol{h}}_l^H. \tag{6.20}$$

Substituting (6.20) in (6.19), we can show the relationship in terms of capacity between the two channels

$$C(\boldsymbol{\mathcal{H}}_{(l)}) = \log_2 \det(\mathbf{I} + \nu \boldsymbol{\mathcal{H}} \boldsymbol{\mathcal{H}}^H - \nu \underline{\boldsymbol{h}}_l \underline{\boldsymbol{h}}_l^H) \tag{6.21}$$

which can be rearranged to

$$C(\boldsymbol{\mathcal{H}}_l) = \log_2 \det(\mathbf{I}+\nu\boldsymbol{\mathcal{H}}\boldsymbol{\mathcal{H}}^H)+\log_2 \det(\mathbf{I}-(\mathbf{I}+\nu\boldsymbol{\mathcal{H}}\boldsymbol{\mathcal{H}}^H)^{-\frac{1}{2}}\nu\underline{\boldsymbol{h}}_l\underline{\boldsymbol{h}}_l^H(\mathbf{I}+\nu\boldsymbol{\mathcal{H}}\boldsymbol{\mathcal{H}}^H)^{-\frac{1}{2}}) \quad (6.22)$$

hence leading to [21]

$$C(\boldsymbol{\mathcal{H}}_{(l)}) = C(\boldsymbol{\mathcal{H}}) + \log_2\left[1 - \nu\underline{\boldsymbol{h}}_l^H(\mathbf{I} + \nu\boldsymbol{\mathcal{H}}\boldsymbol{\mathcal{H}}^H)^{-1}\underline{\boldsymbol{h}}_l\right]. \quad (6.23)$$

In particular (6.23) shows the relationship in terms of capacity between the full system and the system where a beam has been disabled. Here, it is clear that the second term on the right-hand side of the equation represents an analytical evaluation of the capacity loss caused by the l-th beam deactivation. Accordingly, the selection criterion for capacity maximization can be performed by minimizing such parameter and is described analytically as

$$\delta = \arg\min_l \left\{\underline{\boldsymbol{h}}_l^H(\mathbf{I} + \nu\boldsymbol{\mathcal{H}}\boldsymbol{\mathcal{H}}^H)^{-1}\underline{\boldsymbol{h}}_l\right\}. \quad (6.24)$$

Under the assumption of a fixed number of beams selected, the algorithm has to compute all the others $n - n_{RF}$ different beams to eliminate. The above selection is implemented using Algorithm 6.2.

6.2.2.2 Incremental CM-BS (ICM-BS)

The algorithm incrementally selects the beams with the highest capacity contribution. Using a similar notation as the previous one for the ICM-BS, it is possible to show how the capacity is affected when a new beam is added to a low-dimensional channel matrix as [21]

$$C\left(\bar{\boldsymbol{\mathcal{H}}}, \underline{\boldsymbol{h}}_l\right) = \log_2 \det\left[\mathbf{I}+\nu\left(\bar{\boldsymbol{\mathcal{H}}}\bar{\boldsymbol{\mathcal{H}}}^H + \underline{\boldsymbol{h}}_l\underline{\boldsymbol{h}}_l^H\right)\right] \quad (6.25)$$

where $\bar{\boldsymbol{\mathcal{H}}}$ represents the channel matrix formed by previously chosen beams and $\underline{\boldsymbol{h}}_l$ is the newly added beam. The equation (6.25) can be expressed as a function of the system

Algorithm 6.2 Decremental CM-BS

Input: $\boldsymbol{\mathcal{H}}$, ν

Output: $\boldsymbol{\mathcal{H}}_e$

- $\mathbf{K} := \boldsymbol{\mathcal{H}}$
- $\mathbf{B} := \left(\mathbf{I} + \nu \mathbf{K}\mathbf{K}^H\right)^{-1}$
- **for** $j = 1 \rightarrow n - n_{RF}$
  - **for** $l = 1 \rightarrow n - j$
    - $\Omega^{(l)} = \underline{\mathbf{k}}_l^H \mathbf{B} \underline{\mathbf{k}}_l$
  - **end**
  - $\delta_j = \arg\min_l \{\Omega^{(l)}\}$
  - $\mathcal{D} = \{\delta_1, \delta_2, ..., \delta_j\}$
  - $\mathbf{B} := \mathbf{B} + \mathbf{B}\underline{\mathbf{k}}_{\delta_j} \left(\nu^{-1} - \underline{\mathbf{k}}_{\delta_j}^H \mathbf{B} \underline{\mathbf{k}}_{\delta_j}\right)^{-1} \underline{\mathbf{k}}_{\delta_j}^H \mathbf{B}$
  - $\mathbf{K} := [\underline{\boldsymbol{h}}_l]_{l \notin \mathcal{D}}$
- **end**
- $\boldsymbol{\mathcal{H}}_e = [\underline{\boldsymbol{h}}_l]_{l \notin \mathcal{D}}$

channel $\bar{\boldsymbol{\mathcal{H}}}$ via the same procedure used for the DCM-BS, leading to

$$C\left(\bar{\boldsymbol{\mathcal{H}}}, \underline{\boldsymbol{h}}_l\right) = \log_2 \det\left(\mathbf{I} + \nu \bar{\boldsymbol{\mathcal{H}}} \bar{\boldsymbol{\mathcal{H}}}^H\right) + \log_2\left[1 + \nu \underline{\boldsymbol{h}}_l^H \left(\mathbf{I} + \nu \bar{\boldsymbol{\mathcal{H}}} \bar{\boldsymbol{\mathcal{H}}}^H\right)^{-1} \underline{\boldsymbol{h}}_l\right] \tag{6.26}$$

where the second term on the right-hand side of the equation represents the capacity contribution of the l-th beam and needs to be maximized with an exhaustive search through all the available beams. Accordingly, the selection criterion can be analytically expressed as

$$\epsilon = \arg\max_{l \notin \mathcal{E}} \left[\underline{\boldsymbol{h}}_l^H \left(\nu^{-1}\mathbf{I} + \bar{\boldsymbol{\mathcal{H}}} \bar{\boldsymbol{\mathcal{H}}}^H\right)^{-1} \underline{\boldsymbol{h}}_l\right] \tag{6.27}$$

where $\mathcal{E}$ represents the subset of enabled beams ϵ. This selection technique is presented analytically in Algorithm 6.3, where it uses a recursive update on the matrix inversion, based on the Sherman-Morrison-Woodbury Identity [144], see Appendix C.

Algorithm 6.3 Incremental CM-BS

Input: $\boldsymbol{\mathcal{H}}$, ν

Output: $\boldsymbol{\mathcal{H}}_e$

- $\mathbf{K} := \boldsymbol{\mathcal{H}}$
- $\mathbf{A} := \nu\mathbf{I}$
- $\epsilon_1 := \arg\max_l \|\underline{\mathbf{k}}_l\|^2$
- **for** $j = 1 \rightarrow N - 1$
  - $\mathbf{A} := \mathbf{A} - \mathbf{A}\underline{\mathbf{k}}_{\epsilon_j} \left(1 + \underline{\mathbf{k}}_{\epsilon_j}^H \mathbf{A} \underline{\mathbf{k}}_{\epsilon_j}\right)^{-1} \underline{\mathbf{k}}_{\epsilon_j}^H \mathbf{A}$
  - **for** $l = 1 \rightarrow n - j$
    - $\Omega^{(l)} = \underline{\mathbf{k}}_l^H \mathbf{A} \underline{\mathbf{k}}_l$
  - **end**
  - $\epsilon_{j+1} = \arg\max_l \{\Omega^{(l)}\}$
  - $\mathcal{E} = \{\epsilon_1, \epsilon_2, ..., \epsilon_j, \epsilon_{j+1}\}$
- **end**
- $\boldsymbol{\mathcal{H}}_e = [\underline{\boldsymbol{h}}_l]_{l \in \mathcal{E}}$

6.3 Computational Complexity Analysis

For the sake of a complete and fair comparison, this section evaluates and studies the computational complexity of each of the proposed algorithms. The computational complexity counts are listed in the Table 6.1 for all the algorithms, where the orders of magnitude of each operation are evaluated.

It is important to emphasize the distinction between digital signal processing (DSP) complexity, which is the focus of this section, and RF chain complexity. In fact DSP complexity involves the processor at the transmitter and its impact in power consumption is of the order of $5.76mW/KOps - 22.88mW/KOps$ as for the Virtex family from Xilinx [145], where values are expressed in watts per 10^3 operations. RF complexity, instead, derives by the number of chains used in the transmission. Each chain is characterized by a high number of elements, such as mixer, digital-analogic converter (DAC) and filters, whose values of power consumption are particularly significant. Typical values of power consumption for a single RF chain are of the order of $\sim 30mW$ as in [139],

leading to power consumptions in the order of watts, when the amplifier is included in the model.

The first column represents the MM-BS criterion as a reference, while the other columns collect the analysis of SM-BS, DCM-BS and ICM-BS respectively. In particular, n_b identifies the number of beams chosen per user by MM-BS and $n_{del} = n - n_{RF}$ represents the number of beams to be deactivated in decremental selections. We focus our analysis on the application of the algorithms within a channel realization and on the operations that dominate the complexity. Complexity order for each operation are considered in line with the literature [10, 146].

The table shows that the DSP complexity for the MM-BS is lower than the other algorithms, as the selection is based only on the amplitude of the paths. As a consequence, the beam selection algorithms presented in the other columns are affected by higher computational complexity. The higher costs are due to the necessity to compute additional elements, such as γ for the SM-BS or $\mathbf{A}$ and $\mathbf{B}$ for the DCM-BS and ICM-BS respectively. In order to highlight the differences between the DCM-BS and ICM-BS, the constant terms in the complexity computations are preserved in the computational count. Thanks to this notation, it is possible to confirm that DCM-BS is more efficient when $n_{del} \leq n/2$ while ICM-BS has to be chosen when $n_{RF} \leq n/2$. Since differences in performances are negligible, the results obtained by these techniques will be addressed as CM-BS from now on, without differentiating between incremental or decremental approach.

Finally, it is worth noticing that, even though the MM-BS has a lower computational time, it is affected by strong losses in performances in a realistic MP environment, as shown in the results that follow. This consideration makes the presented algorithms relevant in realistic applications, thanks to their appealing trade-off between computational costs and performances.

MM-BS	No.	**SM-BS**	No.
$\boldsymbol{\mathcal{H}} \circ \boldsymbol{\mathcal{H}}^*$	$O(Mn)$	$\boldsymbol{\mathcal{F}} = \mathbf{C}^H(\mathbf{C}\mathbf{C}^H)^{-1}$	$O(Mn^2)$
find	$O(n_b Mn)$	γ (n_{del})	$n_{del}O(n^3)$
		find (n_{del})	$n_{del}O(n)$
		$\boldsymbol{\mathcal{F}}(n_{del})$	$n_{del}O(Mn^2)$
Total	$O(Mn)+$ $n_b O(Mn)$	Total	$n_{del}O(n^3)+$ $(1+n_{del})O(Mn^2)$ $+n_{del}O(n)$
DCM-BS	No.	**ICM-BS**	No.
$\mathbf{B}$	$O(n^3)$	find	$O(n)$
$\underline{\mathbf{k}}_l^H \mathbf{B} \underline{\mathbf{k}}_l$ (n_{del})	$n_{del}O(n^2)$	$\mathbf{A}$	$O(n^3)$
find (n_{del})	$n_{del}O(n)$	$\mathbf{A}(n_{RF})$	$3n_{RF}O(n^2)$
$\mathbf{B}$ (n_{del})	$3n_{del}O(n^2)$	$\underline{\mathbf{k}}_l^H \mathbf{A} \underline{\mathbf{k}}_l (n_{RF})$	$n_{RF}O(n^2)$
		find (n_{RF})	$n_{RF}O(n)$
Total	$O(n^3)+$ $4n_{del}O(n^2)$ $+n_{del}O(n)$	Total	$O(n^3)+$ $4n_{RF}O(n^2)+$ $(n_{RF}+1)O(n)$

Table 6.1: Complexity in number of operations

6.4 Performance Analysis - Capacity Loss

This section is dedicated to the analysis of the capacity losses caused by the selection of a beam subset over the full system, providing an analytical study of the performances achieved by the proposed algorithms. The search of the best trade-off is a critical element of the system design, as the selection of a beam subset benefits from a hardware complexity simplification while suffering a degradation in performances.

The capacity achievable by a multiuser system can be defined as

$$C = \sum_{m=1}^{M} \log_2(1 + SINR_m). \tag{6.28}$$

As shown, under the assumption of ZF linear precoding, the received SINR in a multiuser scenario depends only on the scaling factor γ, and can be computed as [36]

$$SINR_{m,ZF} = \frac{\nu\rho}{M \cdot tr[(\boldsymbol{\mathcal{H}}^H \boldsymbol{\mathcal{H}})^{-1}]}. \tag{6.29}$$

Clearly, in this specific scenario, (6.29) leads to the same value of SINR for all the

users, hence allowing to simplify the capacity evaluation to

$$C = M \log_2(1 + SINR_{ZF}). \tag{6.30}$$

Capacity losses caused by the elimination of one beam can be defined as the difference between the performances achieved by the full system and by the system where one beam is eliminated as

$$\begin{aligned} \Psi^{(l)} &\triangleq M \log_2(1 + SINR_{ZF}) - M \log_2(1 + SINR_{ZF}^{(l)}) \\ &\triangleq M \log_2 \left(1 + \frac{\nu\rho/M}{tr[(\boldsymbol{\mathcal{H}}^H \boldsymbol{\mathcal{H}})^{-1}]}\right) - M \log_2 \left(1 + \frac{\nu\rho/M}{tr[(\boldsymbol{\mathcal{H}}_l^H \boldsymbol{\mathcal{H}}_l)^{-1}]}\right) \end{aligned} \tag{6.31}$$

where $SINR_{ZF}^{(l)}$ represents the SINR for the system without the l-th beam.

The equation (6.31) is particularly useful to study SM-BS optimality. In fact, the best trade-off between performances and hardware complexity corresponds to the case where capacity losses caused by the selection are minimized. Here, the first term in (6.31) does not depend on the selection because it represents the full system, while the second term depends on the criterion used to identify the l-th beam. Accordingly, the minimum loss $\Psi^{(l)}$ is obtained when the second term is maximized.

In particular, the second term of the equation can be rearranged by using the matrix properties showed in (6.20) and (A.32) as

$$M \log_2 \left(1 + \frac{\nu/M}{tr[\mathbf{R}^{-1} + \mathbf{R}^{-1}\underline{\boldsymbol{h}}_l(1 - \underline{\boldsymbol{h}}_l^H \mathbf{R}^{-1} \underline{\boldsymbol{h}}_l)^{-1} \underline{\boldsymbol{h}}_l^H \mathbf{R}^{-1}]}\right) \tag{6.32}$$

where $\mathbf{R} = \boldsymbol{\mathcal{H}}^H \boldsymbol{\mathcal{H}}$.

Hence, thanks to the properties of logarithms, equation (6.31) can be rearranged as

$$\Psi^{(l)} = M \log_2 \left(\frac{\left(1 + \frac{\nu/M}{tr(\mathbf{R}^{-1})}\right)}{\left(1 + \frac{\nu/M}{tr[\mathbf{R}^{-1} + \mathbf{R}^{-1}\underline{\boldsymbol{h}}_l(1 - \underline{\boldsymbol{h}}_l^H \mathbf{R}^{-1} \underline{\boldsymbol{h}}_l)^{-1} \underline{\boldsymbol{h}}_l^H \mathbf{R}^{-1}]}\right)} \right). \tag{6.33}$$

With some straightforward algebra, equation (6.33) can be simplified to the form

$$\Psi^{(l)} = M \log_2(1 + \iota) \tag{6.34}$$

where the parameter ι in the argument of the logarithm of (6.34) is

$$\iota = \frac{\frac{\nu}{M} tr(\mathbf{R}\underline{\boldsymbol{h}}_l(1 - \underline{\boldsymbol{h}}_l^H \mathbf{S}\underline{\boldsymbol{h}}_l)\underline{\boldsymbol{h}}_l^H \mathbf{S})}{tr(\mathbf{S})^2 + \frac{\nu}{M} tr(\mathbf{S}) + tr(\mathbf{S}) tr(\mathbf{S}\underline{\boldsymbol{h}}_l(1 - \underline{\boldsymbol{h}}_l^H \mathbf{S}\underline{\boldsymbol{h}}_l)^{-1}\underline{\boldsymbol{h}}_l^H \mathbf{S})} \tag{6.35}$$

where $\mathbf{S} = \mathbf{R}^{-1}$.

Results obtained in (6.34) (6.35) can be generalized to identify the global loss caused by the selection of a subset of beams as

$$\Psi = M \log_2 \left(1 + \frac{\frac{\nu}{M} tr(\mathbf{T}_{\mathcal{D}})}{tr(\mathbf{R}_{\mathcal{E}}^{-1})^2 + \frac{\nu}{M} tr(\mathbf{R}_{\mathcal{E}}^{-1}) + tr(\mathbf{R}_{\mathcal{E}}^{-1}) tr(\mathbf{T}_{\mathcal{D}})} \right) \tag{6.36}$$

where $\mathbf{R}_{\mathcal{E}} = \boldsymbol{\mathcal{H}}_{\mathcal{E}}^H \boldsymbol{\mathcal{H}}_{\mathcal{E}}$, $\mathbf{T}_{\mathcal{D}} = \mathbf{R}_{\mathcal{E}} \boldsymbol{\mathcal{H}}_{\mathcal{D}}^H (\mathbf{I} - \boldsymbol{\mathcal{H}}_{\mathcal{D}} \mathbf{R}_{\mathcal{E}}^{-1} \boldsymbol{\mathcal{H}}_{\mathcal{D}}^H)^{-1} \boldsymbol{\mathcal{H}}_{\mathcal{D}} \mathbf{R}_{\mathcal{E}}^{-1}$ and the subindices $\mathcal{E}$ and $\mathcal{D}$ represent the enabled and disabled subset of beams respectively. In particular $\boldsymbol{\mathcal{H}}_{\mathcal{D}} = [\underline{\boldsymbol{h}}_k]_{k \in \mathcal{D}}$ and $\boldsymbol{\mathcal{H}}_{\mathcal{E}} = [\underline{\boldsymbol{h}}_k]_{k \in \mathcal{E}}$.

Hence the loss Ψ is a function of ν and approaches an upper bound [117] as $\nu \to \infty$, defined in the following equation

$$\Psi \leq M \log_2 \left(1 + \frac{tr(\mathbf{T}_{\mathcal{D}})}{tr(\mathbf{R}_{\mathcal{E}}^{-1})} \right). \tag{6.37}$$

The analytical results of the loss are confirmed by simulations ($n = 81$ and $M = 40$ system), as shown in Fig. 6.2 for a MP scenario. In particular, the upperbounds derived through (6.37) are indicated in the legend as CM-BS $n_{RF} = 40$ Analytical and SM-BS $n_{RF} = 40$ Analytical for the selection over capacity and SINR respectively, while the numerical values are addressed as *Simulated* for all the selection techniques.

The MM-BS criterion is characterized by fluctuations in the size of the beam subset, leading to losses that are not limited by the upperbound defined in (6.37).

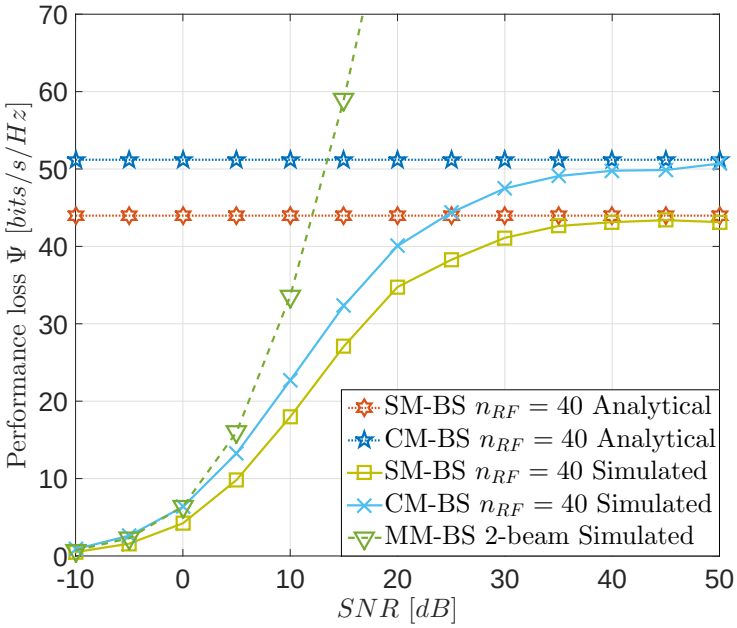

Figure 6.2: Comparison analytical and simulated Ψ for a $n = 81$ and $M = 40$ system

6.5 Numerical Results

This section presents the numerical results obtained through Monte Carlo simulations over 10000 channel realizations. In the simulations, the BS is assumed to be equipped with an DLA with $n = 81$ available beams and to communicate with $M = 40$ single-antenna users, in line with [23].

Two different channel scenarios are considered, both where perfect channel state information is available at the transmitter[3]: one with only the LOS component (2.37) in accordance to [23] and one with the additional MP components as in (2.38) with $N_P = 2$. Complex path gains are defined as

$$\beta_i = |\beta_i| \, e^{-j\psi_i} \tag{6.38}$$

[3]Perfect CSI is a common assumption in the literature [15] for systems that involve AS at the transmitter. Due to the sizes of the systems involved in mm-wave communications, the acquisition of channel state information represents a critical step. Recent works on M-MIMO approached the problem, with the aim to reduce the signal processing complexity [147] or the time [148] required for CSI acquisition. In the chosen scenario, to retain the benefit of reduced RF-chain operation, a trivial approach for the CSI provisioning would be by scheduled acquisition and RF switching, although more sophisticated and efficient approaches can be found in the literature.

where the MP component ($i \neq 0$) is set $|\beta_i|^2 = -10dB$ with ψ_i being uniformly distributed between 0 and 2π and the LoS component ($i = 0$) is characterized by $|\beta_0|^2 = 0dB$ and $\psi_0 = 0$. In order to have a simplified definition for the angles of arrival in the MP component, we consider a scenario where the distance between BS and users is wide enough so that $|\theta_m|$ is uniformly distributed between $\left[\Delta\theta - \frac{\Delta\theta}{4}, \Delta\theta + \frac{\Delta\theta}{4}\right]$ and $sign\,(\theta)$ is chosen randomly.

The algorithms are applied with two different approaches: one where the beam subset size is fixed to n_{RF} and one where beam selection is recursively applied in order to capture a certain percentage η of the total channel power σ_c^2. Accordingly, in the figures, the following notation is used: *Full System* to denote the performances obtained by the scheme without beam selection, *MM-BS 2-beam* to identify the performances obtained by magnitude selection with $n_b = 2$ in accordance to [23], $\eta = 95\%$ to classify the approach where the percentage of channel power captured by the subset of beams is fixed, $n_{RF} = 40$ and $n_{RF} = M$ to address the approach where the maximum number of beams is fixed at 40 or at the number of users M, respectively.

It is worth to notice that in practical systems the number of RF chains is generally fixed, making the MM-BS of [23] inapplicable and the $n_{RF} = \{40, M\}$ approaches shown here particularly relevant in realistic scenarios.

For the $\eta = 95\%$ approach, given the total channel power σ_c^2, we can compute the captured channel power ratio η as

$$\eta = \frac{tr\left(\boldsymbol{\mathcal{H}}_e \boldsymbol{\mathcal{H}}_e^H\right)}{\sigma_c^2} = \frac{tr\left(\boldsymbol{\mathcal{H}}_e \boldsymbol{\mathcal{H}}_e^H\right)}{tr\left(\boldsymbol{\mathcal{H}} \boldsymbol{\mathcal{H}}^H\right)}. \tag{6.39}$$

6.5.1 Capacity

This section evaluates the capacity achieved by the proposed selection algorithms when the transmitter is equipped with a ZF precoder. The proposed schemes are compared to the full system, i.e., where no selection is performed and $n_{RF} = n$, and to the MM-BS criterion from the literature [23].

Using the previous definition of SINR in (6.11), the capacity can be computed as

$$C(SINR, \boldsymbol{\mathcal{G}}|\boldsymbol{\mathcal{H}}) = \sum_{i=1}^{M} \log_2(1 + SINR_i(\gamma, \boldsymbol{\mathcal{G}}|\boldsymbol{\mathcal{H}})) \tag{6.40}$$

which considers the full channel model $\boldsymbol{\mathcal{H}}$, but it can be directly applied to the low-dimensional equivalent channel by replacing $\boldsymbol{\mathcal{H}}$ with $\boldsymbol{\mathcal{H}}_e$.

In Fig. 6.3 and Fig. 6.4 we can see the capacity as a function of the SNR for both fixed and variable beam subset size, i.e., $n_{RF} = 40$ and $\eta = 95\%$ in the legend, and both proposed algorithms,i.e., SM-BS and CM-BS in the legend. Since both incremental and decremental CM-BS achieve the same performances, DCM-BS has been used to obtain the shown results. When comparing the performances of CM-BS and SM-BS, we can see a gap in the low SNR region. This gap, beneficial for SM-BS, is justified by the different metrics used by the two algorithms. In fact, whilst CM-BS does not consider the precoding involved at the BS, the SM-BS algorithm maximizes the SINR at the receiver for the particular ZF precoding used, by maximizing the scaling factor γ. The impact of this difference over the received SINR is described analytically in (6.11), where the noise component of the denominator is inversely proportional to the scaling factor[4].

Beam selection losses in pure line-of-sight scenarios, i.e., $N_p = 0$, are almost negligible, as we can see in Fig. 6.3. In particular the figure shows that the $n_{RF} = 40$ approach is characterized by higher performance degradations in the low-SNR region, but it rapidly achieves similar or better performances than the MM-BS for $SNR \geq 10dB$ for both CM-BS and SM-BS. On the other hand, beam selection algorithms with a channel power-based approach show a significant performance increase for both CM-BS and SM-BS, with SM-BS nearly achieving full system optimal performances.

Fig. 6.4 shows the spectral efficiencies obtained in the MP environment. For the $n_{RF} = 40$ case we see that the CM-BS algorithm performs well as the SNR grows, while the SM-BS algorithm outperforms the previous MM-BS approach even in low SNR regions. When the beam subset size is defined according to the $\eta = 95\%$ approach instead,

[4]Hence, the gap between the two techniques is wider in the low-SNR region, since the dependence of the SINR over the scaling factor is more visible at high values of noise power.

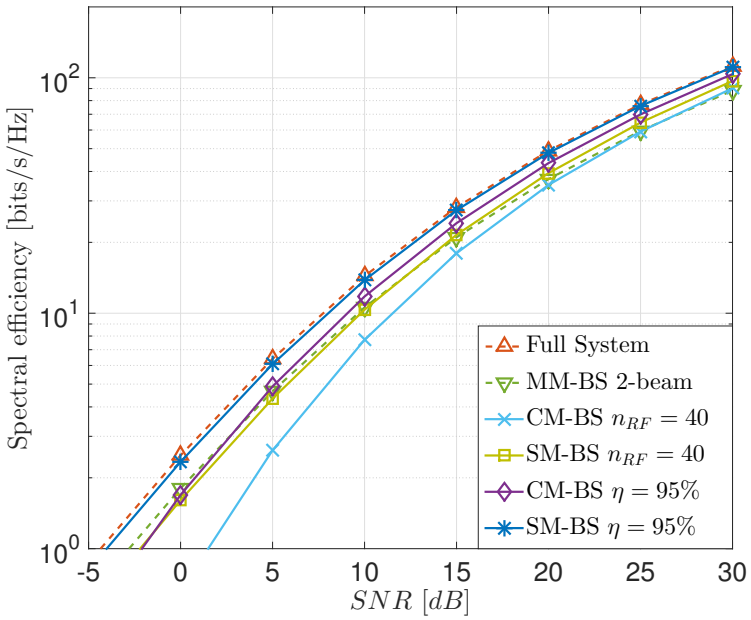

Figure 6.3: Capacity as a function of SNR[dB] in a line-of-sight scenario

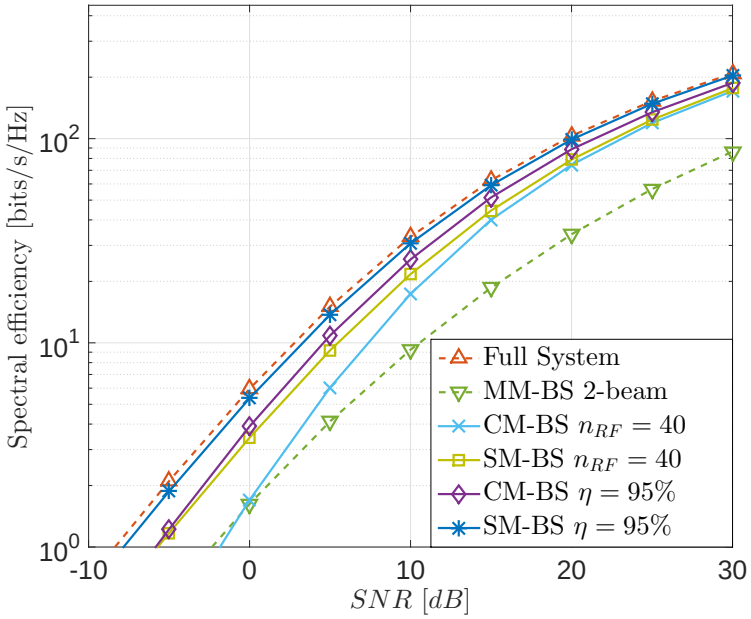

Figure 6.4: Capacity as a function of SNR[dB] in a multi-path scenario

we can see that both algorithms are able to achieve near optimal performances. In particular the SM-BS algorithm performs very closely to the full-system with a negligible degradation.

It is important to notice that the improvement in performances achieved by the $\eta = 95\%$ approach over the $n_{RF} = 40$ scheme resides in a larger beam subset size, as shown in the following section, which focuses on this aspect.

6.5.2 Mean number of beams

In this section we study the mean number of selected beams, i.e., the mean beam subset size, for both CM-BS and SM-BS as a function of the number of users M in the system. Beam usage represents a fundamental parameter for DLA-based schemes study, as it provides a direct evaluation of the RF complexity reduction achieved by beam selection at the transmitter. Clearly, the $n_{RF} = M$ scenario is characterized by a number of beams that is a linear function of the number of users M. This holds for both CM-BS and SM-BS and leads to matching results, presented in Fig. 6.5 and Fig. 6.6 with CM-BS $n_{RF} = M$ only.

In Fig. 6.5 we can see that MM-BS *2-beam* selects a number of beams that grows constantly and rapidly with the number of users in the scenario. In particular, it shows that the $n_{RF} = M$ approach achieves higher RF-complexity reductions than the other approaches in the region $20 \leq M \leq 46$. Additionally, for the $\eta = 95\%$ approach, CM-BS is characterized by a number of beams which is always lower than the MM-BS, except for $M = 20$, while SM-BS is affected by larger beam subset sizes than MM-BS but still provides an interesting complexity reduction.

In a more realistic multi-path scenario, see Fig. 6.6, the MM-BS technique uses a higher number of beams than the $n_{RF} = M$ approach for both CM-BS and SM-BS until the number of users $M \leq 50$. In particular, it is interesting to notice how this further complexity reduction is accomplished, while still providing higher spectral efficiencies. When CM-BS is applied with the power-based $\eta = 95\%$ approach, gains in terms of beam subset size are more visible in highly populated scenarios, i.e., where $M \geq 50$,

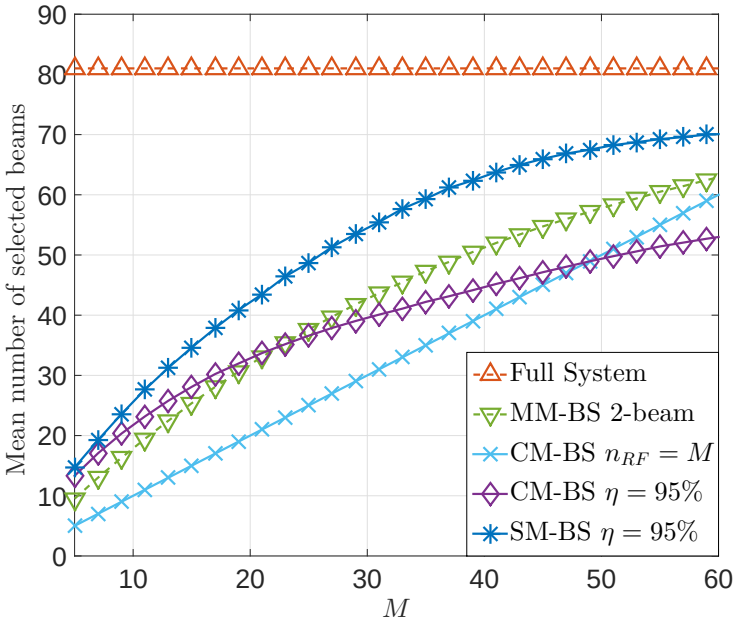

Figure 6.5: Mean number of beams (RF chains) used for transmission as a function of the number of users in a line-of-sight scenario

while the SM-BS is always characterized by larger subsets than MM-BS. For the case with $M = 40$ users, we can see that CM-BS selects in average only ~ 2 more beams than MM-BS and yet provides considerable benefits in terms of capacity, leading to a very advantageous trade-off. Finally, while power-based SM-BS is affected by a larger subset size than MM-BS or $n_{RF} = M$ approaches, it is able to provide near-optimal performances and significant complexity reduction when compared to the full system.

While both Fig. 6.5 and Fig. 6.6 are achieved for a $SNR = 15dB$ scenario, it is important to highlight that the effects of this assumption over the number of selected beams are negligible. In fact, selections with a fixed number of beams, MM-BS and power-based SM-BS are independent from the SNR, while CM-BS with the channel power approach showed imperceptible differences in a low SNR scenario.

6.5.3 Energy Efficiency

In order to better characterize the trade-off introduced by the proposed schemes, we compare the achievable energy efficiency of each scheme, according to the definition in (2.20). Practical values are assumed for $P_{RF} = 34.4mW$ [45], accounting for mixer,

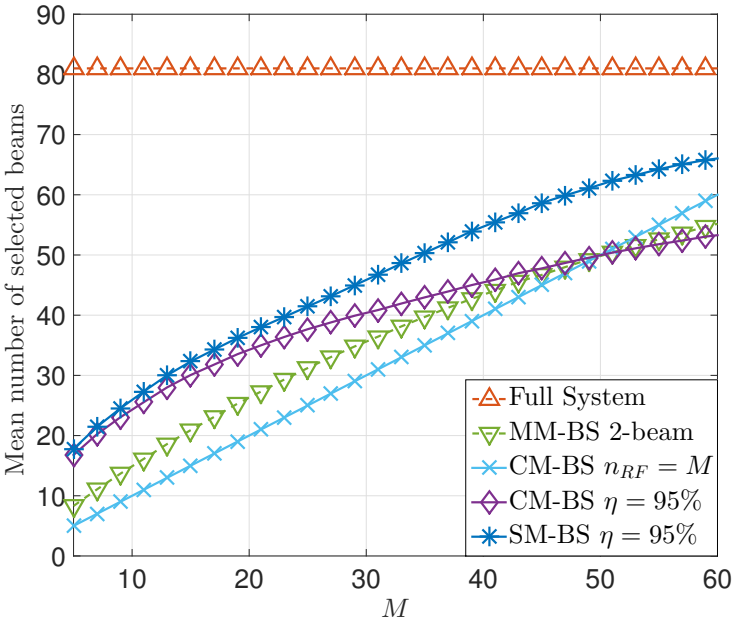

Figure 6.6: Mean number of beams (RF chains) used for transmission as a function of the number of users in a multi-path scenario with $N_p = 2$

DAC and filters, and $P_t = 15dBm$ [149], to model a small cell transmission. This metric is particularly useful for a direct evaluation of the joint effects caused by beam selection over the power needed by the system P_{BS}, and over the average capacity of the system C.

Fig. 6.7 illustrates how the $n_{RF} = M$ approach, with both the CM-BS and SM-BS, outperforms greatly all the others until the number of users $M \leq 31$. This is due to the fact that the number of beams, i.e., RF chains, is much smaller than other approaches, yielding a great reduction in power consumption. Power-based $\eta = 95\%$ approaches are characterized by lower energy efficiencies in low populated scenarios, due to the independence of the selection criterion from the number of users. However, as the number of users grows to $M \geq 35$, power-based CM-BS is able to outperform all the other techniques. In addition, CM-BS $\eta = 95\%$ shows an interesting behavior in highly populated scenarios, i.e. $M > 50$, where the values of energy efficiency start to increase. This behavior is caused by a phenomenon visible in Fig. 6.5, where the beam subset size of CM-BS $\eta = 95\%$ is lower than all the other approaches when $M > 50$, even lower than the number of users in the scenario. Consequently, the increasing capacity, combined

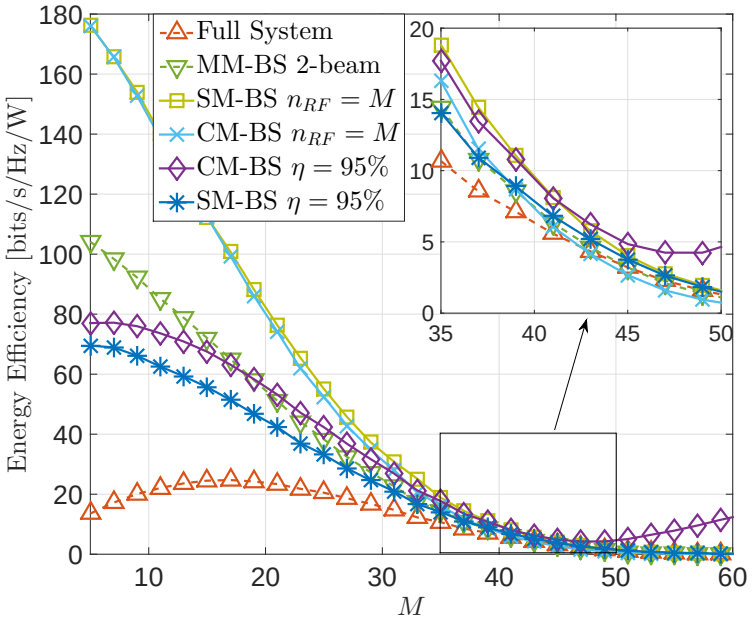

Figure 6.7: Energy efficiency as a function of M in a line-of-sight scenario with $P_t = 15dBm$

with lower power requirements, leads to an increase in terms of energy efficiency. Finally, for SM-BS $\eta = 95\%$, we can see that such approach is characterized by higher energy efficiency values than the MM-BS algorithm in $M \geq 36$ scenarios. This is due to the fact that the effects of a larger beam subset sizes are mitigated by near optimal capacity values.

In Fig. 6.8 we can see that the $n_{RF} = 40$ approaches are still preferable for systems with reduced populations. In particular, we can see that the both algorithms lead to similar energy efficiency values, with CM-BS being gradually outperformed by SM-BS as the number of users grows. This is due to the fact that the interference among users, which is optimized by SM-BS, becomes more relevant as the scenario gets more populated. When considering the $\eta = 95\%$ approach, we can see that CM-BS starts outperforming all other schemes as the number of users increases to $M \approx 35$. This is caused by the high capacity values CM-BS $\eta = 95\%$ leads to. Finally, it is worth noticing how the values of energy efficiency obtained by the MM-BS criterion rapidly decrease as M grows, because of the lower capacities obtained with such approach when the effects of scattering and multi-path increase.

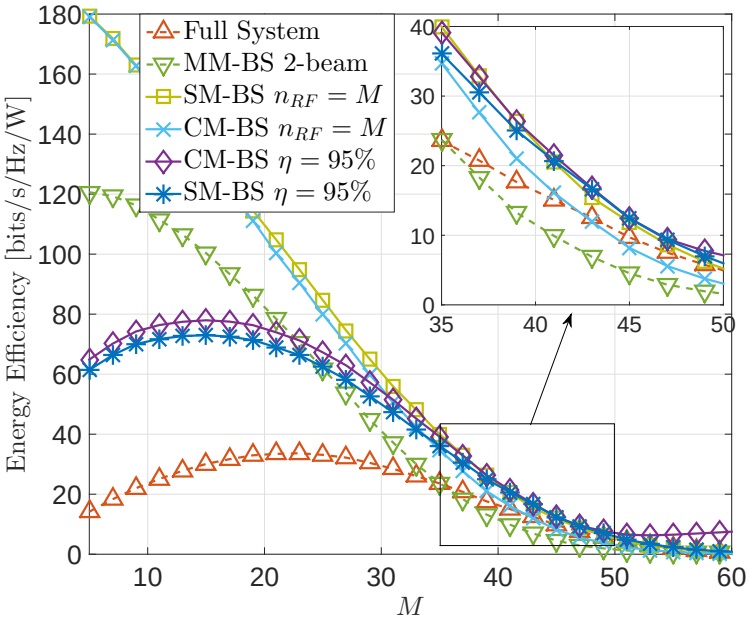

Figure 6.8: Energy efficiency as a function of M in a multi-path scenario with $N_p = 2$ and $P_t = 15dBm$

While Fig. 6.7 and Fig. 6.8 collect energy efficiency performances for the high SNR regime, i.e., where $SNR = 15dB$, we can infer that the benefits of the proposed schemes extend to low SNR scenarios. In fact, the capacity performance gap with the full system is narrow and hardware complexity savings are not affected by the SNR. Moreover, as shown in Fig. 6.2, the losses of the proposed techniques in comparison with the full system decrease together with the SNR. As a consequence, this suggests that the performance trends in terms of energy efficiency are not affected by the SNR.

In Fig. 6.9, energy efficiency is computed as a function of the transmitted power. In particular, we consider a scenario where $M = 40$ and $SNR = 15dB$. As in the previous figures, we can see that the CM-BS $\eta = 95\%$ is able to outperform all other schemes. Clearly, energy efficiency performances decrease as transmitted power grows, since the RF-chain term in (2.20) becomes less relevant. Additionally, we can see that MM-BS performs poorly in comparison with the proposed schemes because of the low values of capacity and larger beam subset size. The $n_{RF} = 40$ strategy provides better performances than the full system in the region where $P_t \leq 26dBm$ for CM-BS, and in the region where $P_t \leq 34dBm$ for SM-BS.

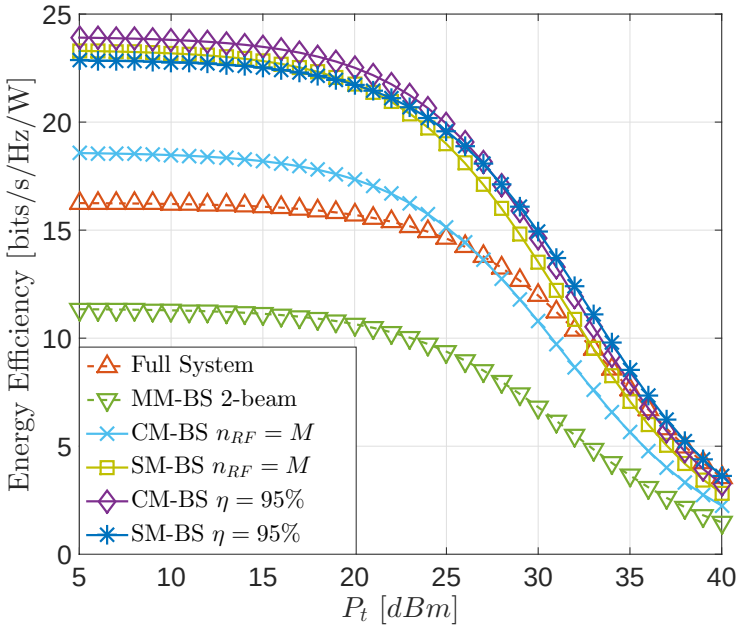

Figure 6.9: Energy efficiency as a function of P_t

6.6 Conclusions

This chapter introduced several beam selection techniques for DLA-based BS-MIMO, which allow to reduce the RF complexity of mm-wave transmitters while achieving near-optimal capacity performances, in both line-of-sight and multi-path environments. Shown results prove that the proposed transmission schemes are particularly promising for realistic implementations of mm-wave systems, where RF chain costs and power consumption are of crucial importance.

In particular, analytical and numerical results show that beam selection algorithms allow to achieve higher energy efficiencies than a full system, while reducing the transceiver RF complexity according to the number of users. It also demonstrated that beam selection algorithms with a channel power approach can lead to near-optimal performances in both line-of-sight and multi-path scenarios, while still achieving significant RF complexity reductions.

Chapter 7

Conclusions

This thesis showed how energy efficiency represents a fundamental evaluation metric for realistic implementation of future large-scale wireless communications systems. Since the employment of VLAs at the BS is envisaged as the necessary approach to satisfy the ever-growing spectral efficiency requirements, in this thesis we have discussed and proposed several transceiving schemes that aim at increasing the energy efficiency of M-MIMO in the downlink multiuser scenario for both the mm-wave and in the Ultra-High Frequency spectrum.

7.1 Summary and Conclusions of the Thesis

In this thesis, Chapter 2 presented a general overview of energy-efficient multiple antenna systems. Conventional precoding and detection schemes were first introduced for small-scale multiuser MIMO, followed by a description of general strategies for reducing the hardware complexity of multiple antenna systems. After highlighting the main shortcomings of these techniques, we proceeded to describe the main research contributions included in this thesis. More specifically:

- In Chapter 3, we aimed to increase the energy efficiency of large-scale MIMO by employing Constant Envelope Precoding in the multiuser downlink transmission. The combination of Constant Envelope Precoding with Constructive Interference

concepts was proven to be able to greatly outperform classical interference reduction approaches in terms of symbol error rate with gains in the order of 5 dB, when the desired constellation energy is considered unitary. In addition, a relaxation of the optimization region for the case of imperfect Channel-State Information was analytically derived, showing that a robust formulation of the proposed problem allows to increase the performances of its non-robust counterpart without the need to increase the transmitted power. The key contributions that can be identified in this chapter are:

C3.1. Constructive Interference can now be applied to Constant Envelope Precoding systems to further increase the power efficiency in large-scale MIMO communication systems. This allows to seamlessly optimize the transmitted constellation energy, without the need to solve additional optimization problems. The newly formulated non-convex optimization problem was solved via Cross-Entropy Optimization and a low-complexity Convex Optimization approach, based on an initial relaxation of the power constraints.

C3.2. The performance enhancements shown by the robust formulation of the proposed scheme proved that a relaxation on constructive interference constraints allows to achieve robustness against channel uncertainties, especially in the low-SNR region. However, excessive relaxation can lead to performance worsening in the high-SNR region.

- Low-Complexity Constructive Interference metrics were exploited in Chapter 4 for defining a highly power-efficient Transmit Antenna Selection algorithm in the massive multiuser downlink. The proposed algorithm demonstrated that modulation-specific metrics can be efficiently employed to achieve significant benefits while greatly reducing the hardware complexity of massive MIMO schemes. The proposed schemes employ 95% less RF chains than massive MIMO systems where no antenna selection is performed, yet they show reduced performance losses. The gains of the proposed schemes directly translate into energy efficiency improvements. These considerations suggest that the employment of very-large arrays at

the base station does not automatically imply the requirement for an equally large number of RF chains, as long as the subset of transmitting antennas is properly identified. The main observations included in this chapter are:

C4.1. Tailoring antenna selection algorithms for M-MIMO systems with Constructive Interference can be greatly beneficial for energy efficiency with 30% gains in the considered scenarios. Moreover, it was shown that state-of-the-art antenna selection for small-scale MIMO cannot be directly applied to large-scale systems, as their complexity is too high to attain any benefits.

C4.2. The proposed scheme is most useful in the low to mid SNR range for low-order modulations, where the proposed schemes are able to nearly triplicate the power-efficiency of large-scale MIMO system without antenna selection. However, at higher-order modulations, the proposed metrics appear to be less efficient in identifying the best transmitting antenna subset for exploiting interference.

- Considerations and results described in Chapters 3 and 4 motivated the definition of a novel transmission scheme in Chapter 5. Here, transmit antenna selection and downlink precoding are jointly performed to achieve the maximum benefits from both techniques. The use of a unified metric for both problems leads to the formulation of a Mixed-Integer Programming problem, hence non-convex. While a solution to the MIP formulation can be achieved through commercial solvers, three separate heuristic approaches are proposed and their optimality is studied. The main contributions of the chapter can be highlighted in the following list:

  C5.1. Jointly performing antenna selection and precoding under a unified metric allows to greatly enhance the performance from both techniques, allowing to reduce both hardware complexity and computational costs of systems where the two problems are solved separately. This is visible in the shown Symbol-Error Rate performances, where the proposed schemes are characterized by gains on the order of tens of dB when compared to state-of-the-art transmit antenna selection-based schemes.

C5.2. While the solution of the MIP-based approach is characterized by the highest performances, the optimality analysis of three heuristic schemes proved that the problem can be efficiently and near-optimally solved via successive optimization. More specifically, it was shown that the proposed successive optimization approaches are able to achieve increasing close-to-optimal performances as their complexity grows. Accordingly, the proposed scheme is able to offer a very high scalability with an always-positive adaptive trade-off between complexity and performances, which can be selected according to the specific requirements of the considered scenario.

- Chapter 6 proposed several beam selection schemes for DLA-based multiuser beamspace mm-wave MIMO systems. The proposed schemes showed that more sophisticated beam selection algorithms, based on antenna selection concepts, allow to jointly achieve a reduced hardware complexity and near-optimal performances in a multi-path scenario. However, these improvements come at the cost of an increased signal processing complexity. Main remarks from this chapter can be synthesized in the following:

  C6.1. The proposed algorithms allow to identify a fixed subset-size of transmitting beams, i.e., generally set equal to the number of users $n_{RF} = M$, differently from the conventional approaches from the literature.

  C6.2. When considering multi-path scenarios, the proposed schemes show higher robustness to additional paths with gains on the order of 5 dB in the high SNR scenarios. This justifies the employment of the proposed transceiving schemes in more realistic communication channels.

7.2 Future Work

The studies described in this thesis represent the foundation for future works which could focus on further developing novel techniques that aim at increasing the energetic efficiency of large-scale MIMO systems. We identify and discuss possible future lines of

work in this section. More specifically:

- **Characterization of the doughnut channel for multiuser large-scale Constant Envelope Precoding:** The results and conclusions derived in Chapter 3 motivate further research with the objective of identifying the bounds of the so-called doughnut channel for multiuser large-scale MIMO. As shown in [17], CEP in single-user scenarios leads to a doughnut shaped channel, where the minimum and maximum received constellation amplitude can be analytically derived. However, such derivations are not available for the multiuser scenario, hence not allowing to identify the optimal desired constellation amplitude for the considered channel. Therefore, the identification of the optimal desired constellation amplitude via a combination of constructive interference and doughnut channel concepts would allow to extend the benefits of interference exploiting CEP to other modulations, such as Quadrature Amplitude Modulation.

- **Low-Complexity Antenna selection for Quadrature Amplitude Modulation:** Chapter 4 showed that low-complexity constructive interference metrics can be applied to antenna selection for massive MIMO system under PSK transmission. More specifically, these results proved that such metrics allow to both reduce the computational complexity and the hardware requirements of large-scale systems. Nonetheless, these metrics are most efficient in lower modulations and for the specific case of PSK signaling. As a consequence, the possibility to extend these concepts to different modulations, such as Amplitude and Phase Shift Keying described in [150], definitely represents an interesting direction for future research developments.

- **Limited Connectivity in joint antenna selection and precoding:** The main shortcomings of the application of constructive interference concepts to antenna selection reside in the need to operate switching at a symbol-by-symbol rate. These issues, briefly addressed in Chapter 4, directly translate to the transceiving scheme presented in Chapter 5. Recent works [151] considered a switching network where each RF chain can be connected to a predefined subset of antennas in order to

reduce switching complexity in the VLAs. Therefore, in an effort to increase both energy efficiency and practicability of such schemes, the study of a combination of limited connectivity switching matrices with symbol level antenna selection metrics surely poses an appealing challenge for future research.

- **Employing the concepts of beamspace mm-wave MIMO onto spatial modulation:** The beam selection-based scheme developed in Chapter 6 allows to greatly reduce the hardware complexity of mm-wave systems, while preserving the high antenna gains required by higher frequencies. Accordingly, Discrete Lens Arrays (DLAs) could allow Spatial Modulation (SM) [127] to be applied in the mm-wave spectrum. In its simpler formulation, SM allows to convey two separate data streams while using only one transmitting antenna, hence one RF chain. This is performed by selecting a single transmitting antenna among a set of available antennas, each corresponding to a specific symbol or bit. Here, while assuming that the receiver is aware of the channel, it is possible to decode two separate data streams: one corresponding to the transmitted stream and one corresponding to the antenna used for transmission. As it follows, a direct and straightforward application of SM concepts to mm-wave frequencies is not viable because of their characteristic higher free loss attenuations. However, DLA-based schemes might suit the task, with future works aiming to characterize a beam modulation technique, where the beams can be selected according to the symbols to be transmitted.

Taking everything into consideration, this thesis presented and analyzed several energy-efficient designs for large-scale communication systems. The observations and conclusions derived from this thesis will be helpful for a more profound understanding of the challenges and practical issues involved in the employment of very large arrays in future wireless communication systems.

Appendices

Appendix A. Proof of Theorem 4.4.1

Generalize equation (4.14) to explicitly represent the effects of interference as

$$y_m = \gamma_{MF}|\rho_{m,m}|u_m + \gamma_{MF}\sum_{k\in\mathcal{C}}|\rho_{m,k}|u_k + \gamma_{MF}\sum_{k\in\mathcal{D}}|\rho_{m,k}|u_k + n_m. \tag{A.1}$$

Accordingly, we can define the received SINR for the m-th user as [81]

$$\xi_m = \frac{\gamma_{MF,e}^2|\rho_{m,m}|^2 + \gamma_{MF,e}^2\left(\sum_{k\in\mathcal{C}}|\rho_{m,k}|\right)^2}{N_0 + \gamma_{MF,e}^2\left(\sum_{k\in\mathcal{D}}|\rho_{m,k}|\right)^2}. \tag{A.2}$$

where the constructive interference that contributes to the signal power appears at the numerator and the destructive component of the interference is added to N_0 at the denominator, since it can be interpreted as an additional source of noise.

The received SINR is upper bounded by the condition where $D_m^{ICI} = 0$ with an optimal CIM antenna selection at the transmitter. Accordingly, a SINR upper bound can be derived as

$$\xi_m = \frac{\gamma_{MF,e}^2|\rho_{m,m}|^2 + \gamma_{MF,e}^2\left(\sum_{k\in\mathcal{C}}|\rho_{m,k}|\right)^2}{N_0} \tag{A.3}$$

which can be seen as a generalized form of SNR, as the interference is a constructive parameter. Since we are interested in the average value of the SINR, we can apply the

expectation over equation (A.3), leading to

$$\widetilde{\xi}_m = \frac{E\left\{\gamma^2_{MF,e}\left(\sum_{k=1}^{M}|\rho_{m,k}|\right)^2\right\}}{N_0} = \frac{E\left\{\gamma^2_{MF,e}\right\}E\left\{\left(\sum_{k=1}^{M}|\rho_{m,k}|\right)^2\right\}}{N_0}. \tag{A.4}$$

In this equation we consider $\gamma_{MF,e}$ to be data independent, even though the conditions used to perform the antenna selection do not support this assumption. This simplification is often performed and necessary to derive a closed form definition of $\widetilde{\xi_m}$.

In order to derive the expected value of the received SINR $\widetilde{\xi_m}$, we need to identify the statistical properties of the correlation matrix $\mathbf{R} = \mathbf{H}\mathbf{H}^H$ and its entries $\rho_{m,k}$. In an independent Rayleigh fading scenario where the entries of $\mathbf{H}$ are modelled as i.i.d Gaussian variables, the correlation matrix $\mathbf{R}$ is known to be a Wishart matrix, characterized by the following distribution function [47]

$$f_{\mathbf{R}}(\mathbf{A}) = \frac{\pi^{-M(M-1)/2}\det\mathbf{A}^{n-M}}{\det\mathbf{\Sigma}^n\prod_{k=1}^{M}(n-k)!}e^{-Tr[\mathbf{\Sigma}^{-1}\mathbf{A}]} \tag{A.5}$$

where the matrix $\mathbf{\Sigma}$ is the covariance matrix of the correlation matrix $\mathbf{R}$.

We can define the absolute value of the entries $\rho_{m,k}$ of the correlation matrix, related to the m-th user, as [152]

$$|\rho_{m,k}| = \sqrt{\left[\sum_{j=1}^{N_{RF}} h^R_{m,j}h^R_{k,j} + h^I_{m,j}h^I_{k,j}\right]^2 + \left[\sum_{j=1}^{N_{RF}} h^I_{m,j}h^R_{k,j} - h^R_{m,j}h^I_{k,j}\right]^2}, \tag{A.6}$$

where h^R and h^I are used to identify respectively the real and imaginary part of h. Thanks to the assumption of independent Rayleigh fading propagation, for $h^R_{m,j} \sim \mathcal{CN}(0, 1/2)$ we have

$$E\left\{\sum_{j=1}^{N_{RF}} h^R_{m,j}h^R_{k,j} + h^I_{m,j}h^I_{k,j}\right\} = 0, \forall j \in \{1, .., N_{RF}\} \tag{A.7}$$

$$var\left\{\sum_{j=1}^{N_{RF}} h_{m,j}^{R}h_{k,j}^{R} + h_{m,j}^{I}h_{k,j}^{I}\right\} = \frac{1}{2}, \forall j \in \{1,..,N_{RF}\} \tag{A.8}$$

where $var\{\cdot\}$ is used to identify the variance of the argument. These equations can be derived from $E\left\{h_{m,j}^{R}h_{k,j}^{R}\right\} = 0$ and $var\left\{h_{m,j}^{R}h_{k,j}^{R}\right\} = 1/4$, thanks to the linearity of $E\{\cdot\}$ and the uncorrelation of the entries of $\mathbf{H}$. Hence the variables $|\rho_{m,k}|$ can be distinguished between [152]:

- Rayleigh variables when $k \neq i$ with $E\{|\rho_{m,k}|\} = \frac{\sqrt{M\pi}}{2}$ and $E\left\{|\rho_{m,k}|^2\right\} = M$
- χ-squared variables when $m = k$ with $E\{|\rho_{m,k}|\} = M$ and $E\left\{|\rho_{m,k}|^2\right\} = M(M+1)$.

In order to complete the study of the upper bound received SINR for the proposed technique we need to identify the expected value of the scaling factor $E\left\{\gamma_{MF,e}^2\right\}$. Following (2.6), we have

$$E\left\{\gamma_{MF,e}^2\right\} = E\left\{tr\left[\mathbf{H}_e\mathbf{H}_e^H\right]^{-1}\right\}. \tag{A.9}$$

As previously stated, the statistical properties of the matrix $\mathbf{H}_e\mathbf{H}_e^H$ lead to [47]

$$E\left\{\gamma_{MF,e}^2\right\} = \frac{1}{N_{RF}M}. \tag{A.10}$$

Hence, we can evaluate the upper bound of the received SINR for the m-th user as

$$\widetilde{\xi}_m = \frac{E\left\{\left(\sum_{k=1}^{M}|\rho_{m,k}|^2\right)\right\} + E\left\{\left(\sum_{j\neq k}|\rho_{m,k}||\rho_{m,j}|\right)\right\}}{N_{RF}MN_0} \tag{A.11}$$

The first and second term on the numerator of (A.11) can be rearranged in order to exploit the statistical properties listed above. In particular, for the first term we have:

$$E\left\{|\rho_{m,m}|^2 + \sum_{k\neq m}|\rho_{m,k}|^2\right\} = M(M+1) + (M-1)M \tag{A.12}$$

and for the second term

$$E\left\{\sum_{j\neq m}|\rho_{m,m}||\rho_{m,j}|+\sum_{j\neq k,k\neq m}|\rho_{m,k}||\rho_{m,j}|\right\}=2(M-1)M\frac{\sqrt{M\pi}}{2}+(M-2)(M-1)\frac{M\pi}{4} \tag{A.13}$$

which is derived thanks to the independence of the random variables.

Hence, the equation (A.11) can be evaluated analytically as

$$\widetilde{\xi}_m=\frac{M(M+1)+M(M-1)(1+\sqrt{M\pi}+(M-2)\pi/4)}{N_{RF}MN_0} \tag{A.14}$$

which ends the proof.

Appendix B. Proof of Theorem 5.6.1

Consider an imperfect CSI and noiseless scenario, received symbols can be decomposed in order to explicitly show their real and imaginary part as follows

$$\begin{aligned}\hat{y}_m &= \sum_{n=1}^{N}\hat{h}_{m,n}x_n \\ &= \sum_{n=1}^{N}(\hat{h}^R_{m,n}x^R_n-\hat{h}^I_{m,n}x^I_n)+j(\hat{h}^R_{m,n}x^I_n+\hat{h}^I_{m,n}x^R_n),\end{aligned} \tag{A.15}$$

where real and imaginary part can be rearranged in order to explicitly identify the effects of imperfect CSI over the received symbols as

$$\Im\{\hat{y}_m\}=\sum_{n=1}^{N}(h^R_{m,n}x^R_n-h^I_{m,n}x^I_n)+(e^R_{m,n}x^R_n-e^I_{m,n}x^I_n) \tag{A.16}$$

$$\Re\{\hat{y}_m\}=\sum_{n=1}^{N}(h^R_{m,n}x^I_n+h^I_{m,n}x^R_n)+(e^R_{m,n}x^I_n+e^I_{m,n}x^R_n). \tag{A.17}$$

Both (A.16) and (A.17) can be presented in a more compact manner by exploiting auxiliary vectors, which lead to the following set of equations

$$\Im\{\hat{y}_m\}=\hat{\mathbf{f}}^T_m\mathbf{w}_1=\mathbf{f}^T_m\mathbf{w}_1+\bar{\mathbf{e}}^T_m\mathbf{w}_1 \tag{A.18}$$

$$\Re\left\{\hat{y}_m\right\} = \hat{\mathbf{f}}_m^T \mathbf{w}_2 = \mathbf{f}_m^T \mathbf{w}_2 + \bar{\mathbf{e}}_m^T \mathbf{w}_2, \tag{A.19}$$

where the vectors $\mathbf{f}_m = \left[\mathbf{h}_m^R, \mathbf{h}_m^I\right]^T$ and $\bar{\mathbf{e}}_m = \left[\mathbf{e}_m^R, \mathbf{e}_m^I\right]^T$ represent the real-valued channel response for the m-th user and the corresponding channel estimation error vector respectively, with $\hat{\mathbf{f}}_m = \mathbf{f} + \bar{\mathbf{e}}_m$. In a similar manner, $\mathbf{w}_1 = \left[\mathbf{x}^I, \mathbf{x}^R\right]^T$ and $\mathbf{w}_2 = \left[\mathbf{x}^R, -\mathbf{x}^I\right]^T$ are two auxiliary real-valued representations of the precoded vector.

Likewise, we can rewrite the first constraint of $\mathcal{P}_{CASPR}$ with the same notation

$$\Im\left(\hat{t}_m e^{-j\phi_m}\right) = \dot{\hat{\mathbf{f}}}^T \mathbf{w}_1 = \dot{\mathbf{f}}_m^T \mathbf{w}_1 + \dot{\mathbf{e}}^T \mathbf{w}_1 \tag{A.20}$$

$$\Re\left(\hat{t}_m e^{-j\phi_m}\right) = \dot{\hat{\mathbf{f}}}^T \mathbf{w}_2 = \dot{\mathbf{f}}_m^T \mathbf{w}_2 + \dot{\mathbf{e}}^T \mathbf{w}_2 - 1, \tag{A.21}$$

where

$$\dot{\mathbf{f}}_m = \left[(\mathbf{h}_m^I u_m^R - \mathbf{h}_m^R u_m^I), (\mathbf{h}_m^R u_m^R + \mathbf{h}_m^I u_m^I)\right]^T \tag{A.22}$$

$$\dot{\mathbf{e}}_m = \left[(\bar{\mathbf{e}}_m^I u_m^R - \bar{\mathbf{e}}_m^R u_m^I), (\bar{\mathbf{e}}_m^R u_m^R + \bar{\mathbf{e}}_m^I u_m^I)\right]^T \tag{A.23}$$

represent the real-valued channel vector and CSI error vector for the m-th user, whose representations have been modified in order to include the phase shift. Without loss of generality, for the sake of simplicity of notation, from now on we consider $\dot{\mathbf{e}}_m = \bar{\mathbf{e}}_m$. Accordingly, we can rewrite the first constraint of $\mathcal{P}_{CASPR}$, as

$$\min_{\|\mathbf{e}_m\|^2 \leq \delta_m^2} \left\{(\dot{\mathbf{f}}_m^T \mathbf{w}_2 + \bar{\mathbf{e}}_m^T \mathbf{w}_2 - 1)\tan\Phi - \left|\dot{\mathbf{f}}_m^T \mathbf{w}_1 + \bar{\mathbf{e}}_m^T \mathbf{w}_1\right|\right\} \geq 0. \tag{A.24}$$

which can be equivalently decomposed into two different constraints

$$\min_{\|\mathbf{e}_m\|^2 \leq \delta_m^2} \left\{(\dot{\mathbf{f}}_m^T \mathbf{w}_2 + \bar{\mathbf{e}}_m^T \mathbf{w}_2 - 1)\tan\Phi - (\dot{\mathbf{f}}_m^T \mathbf{w}_1 + \bar{\mathbf{e}}_m^T \mathbf{w}_1)\right\} \geq 0, \tag{A.25}$$

$$\min_{\|\mathbf{e}_m\|^2 \leq \delta_m^2} \left\{(\dot{\mathbf{f}}_m^T \mathbf{w}_2 + \bar{\mathbf{e}}_m^T \mathbf{w}_2 - 1)\tan\Phi + (\dot{\mathbf{f}}_m^T \mathbf{w}_1 + \bar{\mathbf{e}}_m^T \mathbf{w}_1)\right\} \geq 0. \tag{A.26}$$

The assumption of a spherical error over the CSI acquisition allows us to derive a robust formulation for (A.25) and (A.26). In fact, the worst-case scenario is characterized by the channel errors to be $\|\mathbf{e}_m\|^2 = \delta_m^2, \forall m$, hence causing the constraints to be lower-

bounded by the following equations

$$\left[(\dot{\mathbf{f}}_m^T\mathbf{w}_2 - 1)\tan\Phi - \dot{\mathbf{f}}_m^T\mathbf{w}_1\right] - \delta\left\|\mathbf{w}_1 - \mathbf{w}_2\tan\Phi\right\| \geq 0, \tag{A.27}$$

$$\left[(\dot{\mathbf{f}}_m^T\mathbf{w}_2 - 1)\tan\Phi + \dot{\mathbf{f}}_m^T\mathbf{w}_1\right] - \delta\left\|\mathbf{w}_1 + \mathbf{w}_2\tan\Phi)\right\| \geq 0. \tag{A.28}$$

Thanks to the new robust formulation for the constraints of $\mathcal{P}_{CASPR}$, we can derive a MIP representation of the worst-case design for imperfect CSI scenarios that can be efficiently solved by means of optimization tools as its non-robust counterpart. More specifically, the optimization problem $\mathcal{P}_{CASPR}$ in its MIP representation becomes

$$\begin{aligned}
\mathcal{P}^*_{CASPR}: \quad & \underset{\mathbf{a},\mathbf{w}_1,\mathbf{w}_2}{\text{minimize}} \quad \sum_{n}^{N_{RF}} \|\mathbf{w}_1\|^2 \\
& \text{subject to} \quad \text{Constraints (A.27) and (A.28)} \\
& \left\{\left|\mathbf{w}_1^{(1:N)}\right|, \left|\mathbf{w}_1^{(N+1:2N)}\right|\right\} \preceq \mathbf{a}, \\
& \left\{\left|\mathbf{w}_2^{(1:N)}\right|, \left|\mathbf{w}_2^{(N+1:2N)}\right|\right\} \preceq \mathbf{a}, \\
& \mathbf{w}_1 = \mathbf{\Pi}\mathbf{w}_2, \\
& \sum_{n=1}^{N} a_n = N_{RF}, \quad a_n \in \{0,1\},
\end{aligned} \tag{A.29}$$

where $\mathbf{\Pi} = [\mathbf{0}_N, -\mathbf{I}_N; \mathbf{I}_N, \mathbf{0}_N]$, $\mathbf{a}^{(1:N)}$ notation is used to identify the new vector $\mathbf{b} = [a_1, ..., a_N]$ and $\{\mathbf{a}, \mathbf{b}\} \preceq \mathbf{c}$ is used to impose the inequality to both vectors (i.e., $\mathbf{a} \preceq \mathbf{c}$ and $\mathbf{b} \preceq \mathbf{c}$).

Appendix C. Proof of Sherman-Morrison-Woodbury Identity

Sherman-Morrison-Woodbury Identity states that for an invertible matrix $\mathbf{A}$ and two or more non-invertible matrices $\mathbf{B}$,$\mathbf{C}$

$$\begin{aligned}
(\mathbf{A}+\mathbf{BC})^{-1} &= \left[\mathbf{A}(\mathbf{I}+\mathbf{A}^{-1}\mathbf{BC})\right]^{-1} \\
(\mathbf{A}+\mathbf{BC})^{-1} &= \left(\mathbf{I}+\mathbf{A}^{-1}\mathbf{BC}\right)^{-1}\mathbf{A}^{-1}
\end{aligned} \tag{A.30}$$

which, thanks to the identity $(\mathbf{I}+\mathbf{P})^{-1} = \mathbf{I} - (\mathbf{I}+\mathbf{P})^{-1}\,\mathbf{P}$, can be modified to

$$(\mathbf{A}+\mathbf{BC})^{-1} = \left[\mathbf{I} - \left(\mathbf{I}+\mathbf{A}^{-1}\mathbf{BC}\right)^{-1}\mathbf{A}^{-1}\mathbf{BC}\right]\mathbf{A}^{-1} \tag{A.31}$$

and rearranged with the identity $\mathbf{P}+\mathbf{PQP} = \mathbf{P}\,(\mathbf{I}+\mathbf{QP})^{-1}$ to

$$(\mathbf{A}+\mathbf{BC})^{-1} = \mathbf{A}^{-1} - \mathbf{A}^{-1}\mathbf{B}(1+\mathbf{CA}^{-1}\mathbf{B})^{-1}\mathbf{CA}^{-1}. \tag{A.32}$$

List of References

[1] S. Sesia, I. Toufik, and M. Baker, *LTE-the UMTS long term evolution.* Wiley Online Library, 2015.

[2] "Cisco Visual Networking Index : Global mobile data traffic forecast update," *White Paper*, pp. 2012–2017, 2013.

[3] Z. Hasan, H. Boostanimehr, and V. K. Bhargava, "Green cellular networks: A survey, some research issues and challenges," *IEEE Communications Surveys and Tutorials*, vol. 13, no. 4, pp. 524–540, April 2011.

[4] Deloitte, "Technology, media and telecommunications predictions 2012," *Media*, pp. 1–53, 2012.

[5] G. Y. Li, Z. Xu, C. Xiong, C. Yang, S. Zhang, Y. Chen, and S. Xu, "Energy-efficient wireless communications: tutorial, survey, and open issues," *IEEE Wireless Communications*, vol. 18, no. 6, pp. 28–35, December 2011.

[6] G. Fettweis and E. Zimmermann, "ICT energy consumption-trends and challenges," in *Proceedings of the 11th International Symposium on Wireless Personal Multimedia Communications*, vol. 2, no. 4. Lapland, 2008, p. 6.

[7] E. Björnson, L. Sanguinetti, J. Hoydis, and M. Debbah, "Optimal design of energy-efficient multi-user MIMO systems: Is massive MIMO the answer?" *IEEE Transactions on Wireless Communications*, vol. 14, no. 6, pp. 3059–3075, June 2015.

[8] Y. Chen, S. Zhang, S. Xu, and G. Y. Li, "Fundamental trade-offs on green wireless networks," *IEEE Communications Magazine*, vol. 49, no. 6, pp. 30–37, 2011.

[9] J. Wu, S. Rangan, and H. Zhang, *Green communications: theoretical fundamentals, algorithms and applications.* CRC Press, 2012.

[10] D. Tse and P. Viswanath, *Fundamentals of Wireless Communication.* Cambridge University Press, 2005.

[11] T. L. Marzetta, "Noncooperative cellular wireless with unlimited numbers of base station antennas," *IEEE Transactions on Wireless Communications*, vol. 9, no. 11, pp. 3590–3600, November 2010.

[12] E. Larsson, O. Edfors, F. Tufvesson, and T. L. Marzetta, "Massive MIMO for next generation wireless systems," *IEEE Communications Magazine*, vol. 52, no. 2, pp. 186–195, February 2014.

[13] A. Sayeed, "Deconstructing multiantenna fading channels," *IEEE Transactions on Signal Processing*, vol. 50, no. 10, pp. 2563–2579, 2002.

[14] J. Brady, N. Behdad, and A. M. Sayeed, "Beamspace MIMO for millimeter-wave communications: System architecture, modeling, analysis, and measurements," *IEEE Transactions on Antennas and Propagation*, vol. 61, no. 7, pp. 3814–3827, July 2013.

[15] S. Sanayei and A. Nosratinia, "Antenna selection in mimo systems," *IEEE Communications Magazine*, vol. 42, no. 10, pp. 68–73, October 2004.

[16] ——, "Capacity of MIMO channels with antenna selection," *IEEE Transactions on Information Theory*, vol. 53, no. 11, pp. 4356–4362, November 2007.

[17] S. Mohammed and E. Larsson, "Single-User beamforming in Large-Scale MISO systems with Per-Antenna Constant-Envelope constraints: The doughnut channel," *IEEE Transactions on Wireless Communications*, vol. 11, no. 11, pp. 3992–4005, November 2012.

[18] ——, "Per-Antenna constant envelope precoding for large Multi-User MIMO systems," *IEEE Transactions on Communications*, vol. 61, no. 3, pp. 1059–1071, March 2013.

[19] A. Molisch, M. Win, and J. Winters, "Capacity of mimo systems with antenna selection," *IEEE International Conference on Communications*, vol. 2, pp. 570–574, 2001.

[20] A. Molisch and M. Win, "MIMO Systems with antenna selection," *IEEE Microwave Magazine*, vol. 5, pp. 46–56, March 2004.

[21] A. Gorokhov, D. Gore, and A. Paulraj, "Receive antenna selection for MIMO flat-fading channels: theory and algorithms," *IEEE Transactions on Information Theory*, vol. 49, no. 10, pp. 203–206, October 2003.

[22] A. Sayeed and N. Behdad, "Continuous Aperture Phased MIMO: A new architecture for optimum line-of-sight links," *IEEE APSURSI*, pp. 293–296, July 2011.

[23] A. M. Sayeed and J. Brady, "Beamspace MIMO for high-dimensional multiuser communication at millimeter-wave frequencies," in *GLOBECOM 2013*, 2013, pp. 3784–3789.

[24] T. S. Rappaport, F. Gutierrez, E. Ben-Dor, J. N. Murdock, Y. Qiao, and J. I. Tamir, "Broadband millimeter-wave propagation measurements and models using adaptive-beam antennas for outdoor urban cellular communications," *IEEE transactions on antennas and propagation*, vol. 61, no. 4, pp. 1850–1859, April 2013.

[25] Q. Spencer, C. Peel, A. Swindlehurst, and M. Haardt, "An introduction to the multi-user MIMO downlink," *IEEE Communications Magazine*, vol. 42, no. 10, pp. 60–67, October 2004.

[26] E. Telatar, "Capacity of Multi-antenna Gaussian Channels," *European transactions on telecommunications*, vol. 10, no. 6, pp. 585–595, November 1999.

[27] A. H. Mehana and A. Nosratinia, "Diversity of MIMO linear precoding," *IEEE Transactions on Information Theory*, vol. 60, no. 2, pp. 1019–1038, February 2014.

[28] M. Joham, W. Utschick, and J. Nossek, "Linear transmit processing in MIMO communications systems," *IEEE Transactions on Signal Processing*, vol. 53, no. 8, pp. 2700–2712, August 2005.

[29] C. Peel, B. Hochwald, and A. Swindlehurst, "A vector-perturbation technique for near-capacity multiantenna multiuser communication - Part I: Channel inversion and regularization," *IEEE Transactions on Communications*, vol. 53, no. 1, pp. 195–202, January 2005.

[30] V. Nguyen and J. Evans, "Multiuser transmit beamforming via regularized channel inversion: A large system analysis," *IEEE GLOBECOM*, pp. 1–4, 2008.

[31] M. Costa, "Writing on dirty paper," *IEEE Transactions on Information Theory*, vol. 29, no. 3, pp. 439–441, May 1983.

[32] B. M. Hochwald, C. B. Peel, and A. L. Swindlehurst, "A Vector-Perturbation technique for Near-Capacity multiantenna multiuser communication - Part II: Perturbation," *IEEE Transactions on Communications*, vol. 53, no. 3, pp. 537–544, March 2005.

[33] C. Windpassinger, R. F. H. Fischer, T. Vencel, and J. B. Huber, "Precoding in multiantenna and multiuser communications," *IEEE Transactions on Wireless Communications*, vol. 3, no. 4, pp. 1305–1316, July 2004.

[34] A. B. Gershman, N. D. Sidiropoulos, S. Shahbazpanahi, M. Bengtsson, and B. Ottersten, "Convex optimization-based beamforming," *IEEE Signal Processing Magazine*, vol. 27, no. 3, pp. 62–75, May 2010.

[35] M. Schubert and H. Boche, "Solution of the multiuser downlink beamforming problem with individual SINR constraints," *IEEE Transactions on Vehicular Technology*, vol. 53, no. 1, pp. 18–28, January 2004.

[36] C. Masouros, M. Sellathurai, and T. Ratnarajah, "Large-Scale MIMO transmitters in fixed physical spaces: The effect of transmit correlation and mutual coupling," *IEEE Transactions on Communications*, vol. 61, no. 7, pp. 2794–2804, July 2013.

[37] ——, "Interference optimization for transmit power reduction in Tomlinson-Harashima precoded MIMO downlinks," *IEEE Transactions on Signal Processing*, vol. 60, no. 5, pp. 2470–2841, May 2012.

[38] A. Gorokhov, D. Gore, and A. Paulraj, "Receive antenna selection for MIMO spatial multiplexing: Theory and algorithms," *IEEE Transactions on Signal Processing*, vol. 51, no. 11, pp. 2796–2807, November 2003.

[39] R. Chen, R. W. Heath, and J. G. Andrews, "Transmit selection diversity for unitary precoded multiuser spatial multiplexing systems with linear receivers," *IEEE Transactions on Signal Processing*, vol. 55, no. 3, pp. 1159–1171, March 2007.

[40] Z. Chen, J. Yuan, and B. Vucetic, "Analysis of transmit antenna selection/maximal-ratio combining in Rayleigh fading channels," *IEEE Transactions on Vehicular Technology*, vol. 54, no. 4, pp. 1312–1321, July 2005.

[41] R. Heath and A. Paulraj, "Antenna selection for spatial multiplexing systems based on minimum error rate," *IEEE International Conference on Communications (ICC)*, vol. 7, pp. 2276–2280, 2001.

[42] T. Eng, N. Kong, and L. B. Milstein, "Comparison of diversity combining techniques for Rayleigh-fading channels," *IEEE Transactions on Communications*, vol. 44, no. 9, pp. 1117–1129, September 1996.

[43] M. Z. Win and J. H. Winters, "Analysis of hybrid selection/maximal-ratio combining in Rayleigh fading," in *Communications, 1999. ICC'99. 1999 IEEE International Conference on*, vol. 1. IEEE, 1999, pp. 6–10.

[44] D. A. Gore, R. U. Nabar, and A. Paulraj, "Selecting an optimal set of transmit antennas for a low rank matrix channel," in *Acoustics, Speech, and Signal Processing, 2000. ICASSP'00. Proceedings. 2000 IEEE International Conference on*, vol. 5. IEEE, 2000, pp. 2785–2788.

[45] C. Masouros, M. Sellathurai, and T. Ratnarajah, "Computationally efficient vector perturbation using thresholded optimization," *IEEE Transactions on Communications*, vol. 61, no. 5, pp. 1880–1890, May 2013.

[46] S. Cui, A. J. Goldsmith, and A. Bahai, "Energy-constrained modulation optimization," *IEEE Transactions on Wireless Communications*, vol. 4, no. 5, pp. 2349–2360, September 2005.

[47] A. M. Tulino and S. Verdu, "Random matrix theory and wireless communications," *Foundations and Trends in Communications and Information Theory*, vol. 1, no. 1, pp. 1–182, June 2004.

[48] F. Rusek, D. Persson, B. K. Lau, E. Larsson, T. Marzetta, O. Edfors, and F. Tufvesson, "Scaling up MIMO: Opportunities and challenges with Very Large Arrays," *IEEE Signal Processing Magazine*, vol. 30, no. 1, pp. 40–60, January 2013.

[49] A. Adhikary, J. Nam, J.-Y. Ahn, and G. Caire, "Joint spatial division and multiplexing - The large-scale array regime," *IEEE transactions on information theory*, vol. 59, no. 10, pp. 6441–6463, October 2013.

[50] J. Hoydis, S. ten Brink, and M. Debbah, "Massive MIMO in the UL/DL of cellular networks: How many antennas do we need?" *IEEE Journal on Selected Areas in Communications*, vol. 31, no. 2, pp. 160–171, February 2013.

[51] T. L. Marzetta, "How much training is required for multiuser MIMO?" *Asilomar Conference on Signals, Systems and Computers (ACSSC)*, pp. 359–363, October 2006.

[52] Y. Li, Y.-H. Nam, B. L. Ng, and J. Zhang, "A non-asymptotic throughput for massive MIMO cellular uplink with pilot reuse," in *Global Communications Conference (GLOBECOM), 2012 IEEE*. IEEE, 2012, pp. 4500–4504.

[53] K. Appaiah, A. Ashikhmin, and T. L. Marzetta, "Pilot contamination reduction in multi-user TDD systems," in *Communications (ICC), 2010 IEEE International Conference on*. IEEE, 2010, pp. 1–5.

[54] F. Fernandes, A. Ashikhmin, and T. L. Marzetta, "Inter-cell interference in noncooperative tdd large scale antenna systems," *IEEE Journal on Selected Areas in Communications*, vol. 31, no. 2, pp. 192–201, February 2013.

[55] J. Jose, A. Ashikhmin, T. L. Marzetta, and S. Vishwanath, "Pilot contamination and precoding in multi-cell TDD systems," *IEEE Transactions on Wireless Communications*, vol. 10, no. 8, pp. 2640–2651, August 2011.

[56] H. Huh, S.-H. Moon, Y.-T. Kim, I. Lee, and G. Caire, "Multi-cell MIMO downlink with cell cooperation and fair scheduling: A large-system limit analysis," *IEEE Transactions on Information Theory*, vol. 57, no. 12, pp. 7771–7786, December 2011.

[57] H. Huh, A. M. Tulino, and G. Caire, "Network MIMO with linear zero-forcing beamforming: Large system analysis, impact of channel estimation, and reduced-complexity scheduling," *IEEE Transactions on Information Theory*, vol. 58, no. 5, pp. 2911–2934, May 2012.

[58] H. Q. Ngo and E. G. Larsson, "EVD-based channel estimation in multicell multiuser MIMO systems with very large antenna arrays," in *2012 IEEE International Conference on Acoustics, Speech and Signal Processing (ICASSP)*. IEEE, 2012, pp. 3249–3252.

[59] E. Björnson, J. Hoydis, M. Kountouris, and M. Debbah, "Massive MIMO systems with non-ideal hardware: Energy efficiency, estimation, and capacity limits," *IEEE Transactions on Information Theory*, vol. 60, no. 11, pp. 7112–7139, November 2014.

[60] T. Schenk, *RF imperfections in high-rate wireless systems: Impact and digital compensation*. Springer Science & Business Media, 2008.

[61] C. Masouros and M. Matthaiou, "Space-Constrained Massive MIMO: Hitting the wall of favorable propagation," *IEEE Communications Letters*, vol. 19, no. 5, pp. 771–774, May 2015.

[62] Z. Pi and F. Khan, "An introduction to millimeter-wave mobile broadband systems," *IEEE Communications Magazine*, vol. 49, no. 6, pp. 101–107, June 2011.

[63] *Millimeter Wave Propagation : Spectrum Management Implications*. Federal Communications Commission. Office Of Engineering and Technology, 1997, no. 70.

[64] T. Rappaport, S. Sun, R. Mayzus, H. Zhao, Y. Azar, K. Wang, J. K. Wong, G. N.and Schulz, M. Samimi, and F. Gutierrez, "Millimeter wave mobile communications for 5G cellular: It will work!" *IEEE Access*, vol. 1, pp. 335–349, 2013.

[65] D. M. Pozar, *Microwave engineering*. John Wiley & Sons, 2009.

[66] A. V. Alejos, M. G. Sánchez, and I. Cuiñas, "Measurement and analysis of propagation mechanisms at 40 GHz: Viability of site shielding forced by obstacles," *IEEE Transactions on Vehicular Technology*, vol. 57, no. 6, pp. 3369–3380, November 2008.

[67] M. Samimi, K. Wang, Y. Azar, G. N. Wong, R. Mayzus, H. Zhao, J. K. Schulz, S. Sun, F. Gutierrez, and T. S. Rappaport, "28 GHz angle of arrival and angle of departure analysis for outdoor cellular communications using steerable beam antennas in New York City," in *Vehicular Technology Conference (VTC Spring), 2013 IEEE 77th*. IEEE, 2013, pp. 1–6.

[68] T. S. Rappaport, R. W. Heath Jr, R. C. Daniels, and J. N. Murdock, *Millimeter wave wireless communications*. Pearson Education, 2014.

[69] X. Zhang, A. F. Molisch, and S.-Y. Kung, "Variable-phase-shift-based RF-baseband codesign for MIMO antenna selection," *IEEE Transactions on Signal Processing*, vol. 53, no. 11, pp. 4091–4103, November 2005.

[70] R. W. Heath, N. Gonzalez-Prelcic, S. Rangan, W. Roh, and A. M. Sayeed, "An overview of signal processing techniques for millimeter wave MIMO systems," *IEEE Journal of Selected Topics in Signal Processing*, vol. 10, no. 3, pp. 436–453, April 2016.

[71] V. Venkateswaran and A.-J. van der Veen, "Analog beamforming in MIMO communications with phase shift networks and online channel estimation," *IEEE Transactions on Signal Processing*, vol. 58, no. 8, pp. 4131–4143, August 2010.

[72] A. Alkhateeb, O. El Ayach, G. Leus, and R. W. Heath, "Channel estimation and hybrid precoding for millimeter wave cellular systems," *IEEE Journal of Selected Topics in Signal Processing*, vol. 8, no. 5, pp. 831–846, October 2014.

[73] A. Alkhateeb, G. Leus, and R. W. Heath, "Limited feedback hybrid precoding for multi-user millimeter wave systems," *IEEE Transactions on Wireless Communications*, vol. 14, no. 11, pp. 6481–6494, November 2015.

[74] X. Gao, L. Dai, S. Han, I. Chih-Lin, and R. W. Heath, "Energy-efficient hybrid analog and digital precoding for mmWave MIMO systems with large antenna arrays," *IEEE Journal on Selected Areas in Communications*, vol. 34, no. 4, pp. 998–1009, April 2016.

[75] L. Liang, W. Xu, and X. Dong, "Low-complexity hybrid precoding in massive multiuser MIMO systems," *IEEE Wireless Communications Letters*, vol. 3, no. 6, pp. 653–656, December 2014.

[76] A. Garcia-Rodriguez and C. Masouros, "Exploiting the increasing correlation of space constrained massive MIMO for CSI relaxation," *IEEE Transactions on Communications*, vol. 64, no. 4, pp. 1572–1587, April 2016.

[77] Y. Zeng and R. Zhang, "Millimeter wave MIMO with lens antenna array: A new path division multiplexing paradigm," *IEEE Transactions on Communications*, vol. 64, no. 4, pp. 1557–1571, April 2016.

[78] X. Gao, L. Dai, Z. Chen, Z. Wang, and Z. Zhang, "Near-Optimal Beam Selection for Beamspace MmWave Massive MIMO Systems," *IEEE Communications Letters*, vol. 20, no. 5, pp. 1054–1057, May 2016.

[79] L. Yang, Y. Zeng, and R. Zhang, "Efficient channel estimation for millimeter wave MIMO with limited RF chains," in *Communications (ICC), 2016 IEEE International Conference on*. IEEE, 2016, pp. 1–6.

[80] C. Masouros, T. Ratnarajah, M. Sellathurai, C. Papadias, and A. Shukla, "Known interference in the cellular downlink: A performance limiting factor or a source of green signal power?" *IEEE Communications Magazine*, vol. 51, no. 10, pp. 162–171, October 2013.

[81] C. Masouros and E. Alsusa, "Two-Stage transmitter precoding based on data-driven code hopping and partial zero forcing beamforming for MC-DCMA communications," *IEEE Transactions on Wireless Communications*, vol. 8, no. 7, pp. 3634–3645, July 2009.

[82] ——, "Soft linear precoding for the downlink of DS/CDMA communication systems," *IEEE Transactions on Vehicular Technology*, vol. 59, no. 1, pp. 203–215, January 2010.

[83] C. Masouros, "Correlation rotation linear precoding for MIMO broadcast communications," *IEEE Transactions on Signal Processing*, vol. 59, no. 1, pp. 252–262, January 2011.

[84] C. Masouros and G. Zheng, "Exploiting known interference as green signal power for downlink beamforming optimization," *IEEE Transactions on Signal Processing*, vol. 63, no. 14, pp. 3628–3640, July 2015.

[85] M. Alodeh, S. Chatzinotas, and B. Ottersten, "Constructive multiuser interference in symbol level precoding for the MISO Downlink channel," *IEEE Transactions on Signal Processing*, vol. 63, no. 9, pp. 2239–2252, May 2015.

[86] ——, "Energy-efficient symbol-level precoding in multiuser miso based on relaxed detection region," *IEEE Transactions on Wireless Communications*, vol. 15, no. 5, pp. 3755–3767, May 2016.

[87] A. Li and C. Masouros, "Exploiting constructive mutual coupling in P2P MIMO by Analog-Digital phase alignment," *IEEE Transactions on Wireless Communications*, In Press.

[88] K. L. Law, C. Masouros, K. K. Wong, and G. Zheng, "Constructive interference exploitation for Outage-Probability constrained downlink precoding optimization," *IEEE Transactions on Signal Processing*, In Press.

[89] A. Kalantari, M. Soltanalian, S. Maleki, S. Chatzinotas, and B. Ottersten, "Directional modulation via symbol-level precoding: A way to enhance security," *arXiv preprint arXiv:1606.04488*, 2016.

[90] M. P. Daly and J. T. Bernhard, "Directional modulation technique for phased arrays," *IEEE Transactions on Antennas and Propagation*, vol. 57, no. 9, September 2009.

[91] C. Masouros and E. Alsusa, "Dynamic Linear Precoding for the Exploitation of Known Interference in MIMO Broadcast Systems," *IEEE Transactions on Wireless Communications*, vol. 8, no. 3, pp. 1396–1404, March 2009.

[92] V. Mancuso and S. Alouf, "Reducing costs and pollution in cellular networks," *IEEE Communications Magazine*, vol. 49, no. 8, pp. 63–71, August 2011.

[93] S. H. Han and J. H. Lee, "An overview of Peak-to-Average power ratio reduction techniques for multicarrier transmission," *IEEE Wireless Communications Magazine*, vol. 12, no. 2, pp. 56–65, April 2005.

[94] C. Studer and E. Larsson, "PAR-Aware Large-Scale Multi-User MIMO-OFDM downlink," *IEEE Journal on Selected Areas in Communications*, vol. 31, no. 2, pp. 303–313, February 2013.

[95] S. Mohammed and E. Larsson, "Constant-Envelope Multi-User precoding for Frequency-Selective massive MIMO systems," *IEEE Wireless Communications Letters*, vol. 2, no. 5, pp. 547–550, October 2013.

[96] S. Mukherjee and S. K. Mohammed, "Constant-envelope precoding with time-variation constraint on the transmitted phase angles," *IEEE Wireless Communications Letters*, vol. 4, no. 2, pp. 221–224, April 2015.

[97] J. C. Chen, C. K. Wen, and K. K. Wong, "Improved constant envelope multiuser precoding for massive MIMO systems," *IEEE Communications Letters*, vol. 18, no. 8, pp. 1311–1314, August 2014.

[98] *Evolved Universal Terrestrial Radio Access (E-UTRA); Physical Channels and Modulation,.* 3GPP TS 36.211, V8.2.0 (2008-03), Release 8.

[99] H. Yang and T. L. Marzetta, "Performance of conjugate and zero-forcing beamforming in Large-Scale Antenna systems," *IEEE Journal on Selected Areas in Communications*, vol. 31, no. 2, pp. 172–179, February 2013.

[100] P. T. De Boer, D. P. Kroese, S. Mannor, and R. Y. Rubinstein, "A tutorial on the cross-entropy method," *Annals of operations research*, vol. 134, no. 1, pp. 19–67, 2005.

[101] R. Rubinstein and D. Kroese, *The Cross-Entropy Method: A Unified Approach to Combinatorial Optimization, Monte-Carlo Simulation and Machine Learning*, ser. Information Science and Statistics. Springer New York, 2011.

[102] S. Boyd and L. Vandenberghe, *Convex Optimization*. Cambridge University Press, 2010.

[103] N. Vucic and H. Boche, "Robust QoS-Constrained optimization of downlink multiuser MISO systems," *IEEE Transactions on Signal Processing*, vol. 57, no. 2, pp. 714–725, February 2009.

[104] B. Chalise, S. Shahbaz Panahi, A. Czylwik, and A. Gershman, "Robust downlink beamforming based on outage probability specifications," *IEEE Transactions on Wireless Communications*, vol. 6, no. 10, pp. 3498–3503, October 2007.

[105] L. Correia, D. Zeller, O. Blume, D. Ferling, Y. Jading, I. Godor, G. Auer, and L. Van der Perre, "Challenges and enabling technologies for energy aware mobile radio networks," *IEEE Communications Magazine*, vol. 48, no. 11, pp. 66–72, November 2010.

[106] T. Gucluoglu and T. Duman, "Performance analysis of transmit and receive antenna selection over flat fading channels," *Wireless Communications, IEEE Transactions on*, vol. 7, no. 8, pp. 3056–3065, August 2008.

[107] K. Dong, N. Prasad, X. Wang, and S. Zhu, "Adaptive antenna selection and Tx/Rx beamforming for large-scale MIMO systems in 60 GHz channels," *EURASIP Journal on Wireless Communications*, vol. 2011, no. 59, August 2011.

[108] B. Tae-Won and J. Bang Chul, "A practical antenna selection technique in multiuser massive MIMO networks," *IEICE Transactions on Communications*, vol. E96.B, no. 11, pp. 2901–2905, 2013.

[109] X. Gao, O. Edfors, J. Liu, and F. Tufvesson, "Antenna selection in measured massive MIMO channels using convex optimization," *2013 IEEE Globecom Workshops (GLOBECOM)*, pp. 129–134, 2013.

[110] H. Li, L. Song, and M. Debbah, "Energy efficiency of large-scale multiple antenna systems with transmit antenna selection," *IEEE Transactions on Communications*, vol. 62, no. 2, pp. 638–647, February 2014.

[111] B. M. Lee, J. Choi, J. Bang, and B.-C. Kang, "An energy efficient antenna selection for large scale green mimo systems," *IEEE International Symposium on Circuits and Systems (ISCAS)*, pp. 950–953, May 2013.

[112] S. Mahboob, R. Ruby, and V. Leung, "Transmit antenna selection for downlink transmission in a massively distributed antenna system using convex optimization," *International Conference on Broadband, Wireless Computing, Communication and Applications (BWCCA)*, pp. 228–233, November 2012.

[113] G. Zheng, I. Krikidis, C. Masouros, S. Timotheou, D. A. Toumpakaris, and Z. Ding, "Rethinking the role of interference in wireless networks," *IEEE Communications Magazine*, vol. 52, no. 11, pp. 152–158, November 2014.

[114] A. Müller, A. Kammoun, E. Björnson, and M. Debbah, "Linear precoding based on polynomial expansion : Reducing complexity in massive MIMO," *IEEE Transactions on Information Theory*, 2014, Submitted.

[115] S. Boyd and L. Vandenberghe, *Convex optimization*. Cambridge University Press, 2004.

[116] Z. Chen, J. Yuan, B. Vucetic, and Z. Zhou, "Performance of alamouti scheme with transmit antenna selection," *Electronics Letters*, vol. 39, no. 23, pp. 1666–1668, November 2003.

[117] P.-H. Lin and S.-H. Tsai, "Performance analysis and algorithm designs for transmit antenna selection in linearly precoded multiuser MIMO systems," *IEEE Transactions on Vehicular Technology*, vol. 61, no. 4, pp. 1698–1708, May 2012.

[118] J. W. Demmel, *Applied numerical linear algebra*. Society for Industrial and Applied Mathematics, 1997.

[119] A. Pitarokoilis, S. Mohammed, and E. Larsson, "On the optimality of single-carrier transmission in Large-Scale Antenna systems," *IEEE Wireless Communications Letters*, vol. 1, no. 4, pp. 276–279, August 2012.

[120] C. Campbell and D. Dumka, "Wideband high power gan on sic spdt switch mmics," *IEEE MTT-S International Microwave Symposium Digest (MTT)*, pp. 1–1, May 2010.

[121] "Agilent solid state switches (White paper)," *Application Note*, 2010.

[122] M. Di Renzo, D. De Leonardis, F. Graziosi, and H. Haas, "Space Shift Keying (SSK) MIMO with practical channel estimates," *IEEE Transactions on Communications*, vol. 60, no. 4, pp. 998–1012, April 2012.

[123] J. Ney da Silva and M. de Campos, "Spectrally efficient UWB pulse shaping with application in orthogonal PSM," *IEEE Transactions on Communications*, vol. 55, no. 2, pp. 313–322, February 2007.

[124] B. Parr, B. Cho, K. Wallace, and Z. Ding, "A novel ultra-wideband pulse design algorithm," *IEEE Communications Letters*, vol. 7, no. 5, pp. 219–221, May 2003.

[125] X. Wu, Z. Tian, T. Davidson, and G. Giannakis, "Optimal waveform design for UWB radios," *IEEE Transactions on Signal Processing*, vol. 54, no. 6, pp. 2009–2021, June 2006.

[126] A. Mohammadi and F. Ghannouchi, "Single RF front-end MIMO transceivers," *IEEE Communications Magazine*, vol. 49, no. 12, pp. 104–109, December 2011.

[127] M. Di Renzo, H. Haas, A. Ghrayeb, S. Sugiura, and L. Hanzo, "Spatial Modulation for generalized MIMO: Challenges, opportunities, and implementation," *Proceedings of the IEEE*, vol. 102, no. 1, pp. 56–103, January 2014.

[128] O. N. Alrabadi, C. B. Papadias, A. Kalis, and R. Prasad, "A universal encoding scheme for mimo transmission using a single active element for psk modulation schemes," *IEEE Transactions on Wireless Communications*, vol. 8, no. 10, pp. 5133–5142, September 2009.

[129] N. Serafimovski, A. Younis, R. Mesleh, P. Chambers, M. Di Renzo, C.-X. Wang, P. Grant, M. Beach, and H. Haas, "Practical implementation of spatial modulation," *IEEE Transactions on Vehicular Technologies*, vol. 62, no. 9, pp. 4511–4523, November 2013.

[130] J. Perruisseau-Carrier, O. Alrabadi, and A. Kalis, "Implementation of a reconfigurable parasitic antenna for beam-space bpsk transmissions," *European Microwave Conference (EuMC)*, pp. 644–647, September 2010.

[131] C. Masouros, M. Sellathurai, and T. Ratnarajah, "Vector perturbation based on symbol scaling for limited feedback MISO downlinks," *IEEE Transactions on Signal Processing*, vol. 62, no. 3, pp. 562–571, February 2014.

[132] D. Ha, K. Lee, and J. Kang, "Energy efficiency analysis with circuit power consumption in massive MIMO systems," *IEEE 24th International Symposium on Personal Indoor and Mobile Radio Communications (PIMRC)*, pp. 938–942, September 2013.

[133] X. Gao, O. Edfors, F. Tufvesson, and E. G. Larsson, "Massive mimo in real propagation environments: Do all antennas contribute equally?" *IEEE Transactions on Communications*, vol. 63, no. 11, pp. 3917–3928, November 2015.

[134] P. V. Amadori and C. Masouros, "Interference driven antenna selection for Massive Multi-User MIMO," *IEEE Transactions on Vehicular Technology*, vol. PP, no. 99, pp. 1–1, 2015.

[135] A. Garcia-Rodriguez, C. Masouros, and L. Hanzo, "Pre-Scaling optimization for Space Shift Keying based on Semidefinite Relaxation," *IEEE Transactions on Communications*, vol. 63, no. 11, pp. 4231–4243, November 2015.

[136] G. Zheng, K.-K. Wong, and T.-S. Ng, "Robust linear mimo in the downlink: A worst-case optimization with ellipsoidal uncertainty regions," *EURASIP Journal on Advances in Signal Processing.*, 2008.

[137] F. Rusek, D. Persson, B. K. Lau, E. Larsson, T. Marzetta, O. Edfors, and F. Tufvesson, "Scaling up MIMO: Opportunities and challenges with very large arrays," *IEEE Signal Processing Magazine*, vol. 30, no. 1, pp. 40–60, January 2013.

[138] A. Hakkarainen, J. Werner, K. R. Dandekar, and M. Valkama, "Widely-linear beamforming and RF impairment suppression in massive antenna arrays," *Journal of Communications and Networks*, vol. 15, no. 4, pp. 383–397, August 2013.

[139] S. Cui, A. J. Goldsmith, and A. Bahai, "Energy-efficiency of MIMO and cooperative MIMO techniques in sensor networks," *IEEE Journal on Selected Areas in Communications*, vol. 22, no. 6, pp. 1089–1098, August 2004.

[140] A. S. Y. Poon, R. W. Brodersen, and D. Tse, "Degrees of freedom in multiple-antenna channels: A signal space approach," *IEEE Transactions on Information Theory*, vol. 51, no. 2, pp. 523–536, February 2005.

[141] M. Sadek, A. Tarighat, and A. H. Sayed, "Active antenna selection in multiuser MIMO communications," *IEEE Transactions on Signal Processing*, vol. 55, no. 4, pp. 1498–1510, April 2007.

[142] I. Berenguer, X. Wang, and V. Krishnamurthy, "Adaptive MIMO antenna selection via discrete stochastic optimization," *IEEE Transactions on Signal Processing*, vol. 53, no. 11, pp. 4315–4329, November 2005.

[143] A. Gorokhov, "Antenna selection algorithms for MEA transmission systems," *IEEE ICASSP*, vol. 3, no. 2, pp. 2857–2860, May 2002.

[144] H. Henderson and S. Searle, "On deriving the inverse of a sum of matrices," *Siam Review*, vol. 23, no. 1, pp. 53–60, January 1981.

[145] D. Curd, "Power consumption in 65 nm FPGAs," *Xilinx White Paper*, February 2007.

[146] R. Hunger, *Floating point operations in matrix-vector calculus.* Munich University of Technology, Inst. for Circuit Theory and Signal Processing Munich, 2005.

[147] H. Prabhu, J. Rodrigues, O. Edfors, and F. Rusek, "Approximative matrix inverse computations for very-large mimo and applications to linear pre-coding systems," *IEEE Wireless Communications and Networking Conference (WCNC)*, pp. 2710–2715, April 2013.

[148] S. L. H. Nguyen and A. Ghrayeb, "Compressive sensing-based channel estimation for massive multiuser mimo systems," *IEEE Wireless Communications and Networking Conference (WCNC)*, pp. 2890–2895, April 2013.

[149] T. S. Rappaport, J. N. Murdock, and F. Gutierrez, "State of the art in 60-ghz integrated circuits and systems for wireless communications," *Proceedings of the IEEE*, vol. 99, no. 8, August 2011.

[150] M. Alodeh, S. Chatzinotas, and B. Ottersten, "Symbol-Level Multiuser MISO Precoding for Multi-level Adaptive Modulation: A Multicast View," *arXiv:1601.02788.*, 2016.

[151] R. Méndez-Rial, C. Rusu, N. González-Prelcic, A. Alkhateeb, and R. W. Heath, "Hybrid MIMO architectures for millimeter wave communications: Phase shifters or switches?" *IEEE Access*, vol. 4, pp. 247–267, 2016.

[152] S. M. Razavi, T. Ratnarajah, and C. Masouros, "Transmit-power efficient linear precoding utilizing known interference for the multiantenna downlink," *IEEE Transactions on Vehicular Technology*, vol. 63, no. 9, pp. 4383 – 4394, November 2014.